Università degli Studi di Padova

Department of Physics and Astronomy
"Galileo Galilei"

Master degree in Astronomy

MCCXXII

Master Thesis in Astronomy

Equilibrium models of rotating compact stars: an application to the post-merger phase of GW170817

Supervisor: Roberto Turolla

Co-supervisors: Alessandro Drago, Giuseppe Pagliara,
Prasanta Char
(Department of Physics and Earth Sciences, Ferrara)

Master Candidate: Andrea Pavan

Academic year 2018-2019

07/03/2019

Une intelligence qui pour un instant donné, connaîtrait toutes les forces dont la nature est animée, et la situation respective des êtres qui la composent, si d'ailleurs elle était assez vaste pour soumettre ces données à l'analyse, embrasserait dans la même formule les mouvements des plus grands corps de l'univers et ceux du plus léger atome: rien ne serait incertain pour elle, et l'avenir comme le passé, serait présent à ses yeux. L'esprit humain offre, dans la perfection qu'il a su donner à l'Astronomie, une faible esquisse de cette intelligence.

Un'intelligenza che, per un'istante dato, potesse conoscere tutte le forze da cui la natura è animata, e la situazione rispettiva degli esseri che la compongono e che inoltre fosse abbastanza grande da sottomettere questi dati all'analisi, abbraccerebbe nella stessa formula i movimenti dei più grandi corpi dell'universo e quelli dell'atomo più leggero. Nulla le risulterebbe incerto, l'avvenire come il passato sarebbe presente ai suoi occhi. L'ingegno umano offre un debole abbozzo di tale intelligenza nella perfezione che ha saputo dare all'Astronomia.

Laplace Pierre Simon, Essai philosophique sur les probabilités (1825)

Abstract

The topic of this thesis is the role of the rotation in relativistic stars. Equilibrium models of static, uniformly and differentially rotating compact stars are numerically computed applying several realistic equations of state and probing the so-called "two-families scenario". The work provides a differentially rotating quark star as a possible solution for the post-merger phase of GW170817.

L'argomento di questa tesi è il ruolo della rotazione nelle stelle relativistiche. Modelli di equilibrio di stelle compatte statiche, a rotazione uniforme e differenziale vengono calcolati numericamente applicando diverse realistiche equazioni di stato ed esaminando il cosiddetto "scenario a due famiglie". La tesi propone come possibile soluzione della fase di post-merger di GW170817 una stella di quark a rotazione differenziale.

Contents

Introduction

The event of August 17, 2017, has represented the first observation of gravitational waves (GW) generated by the merger of two neutron stars. It has been particularly relevant because it has been also associated with an electromagnetic counterpart, spanning from the X-rays, to optical and near infrared wavelengths, to the radio band.

The evidence of the so-called "Kilonova" signal has indicated that there was not a direct collapse to a black hole immediately after the merger but that instead a rapidly and differentially rotating compact object was formed. However, the absence of an extend emission in the electromagnetic signal has suggested the collapse within timescales ranging from a few tens of milliseconds up to about one second, compatible with the damping time of the differential rotation.

Very recently, two papers have discussed possible evidences of a long-lived remnant [1, 2]. In particular, [1] has suggested the existence of a post-merger GW emission lasting about 6-7 s, while [2] has identified an X-ray feature 155 days after the coalescence and possibly associated with the activity of a neutron star. Nevertheless, it is important to remark that in [3] no evidence of a post-merger GW emission has been found.

In this thesis we discuss a possible scenario for the post-merger phase, trying to interpret the signal suggested in [1]. While the evidence of such a signal is quite weak, our scheme could be useful to describe future detections of a post-merger emission. An interpretative scheme compatible with what proposed in [1] needs to solve three problems: the origin of the extended GW emission; the origin of the high energy electromagnetic emission (i.e. the engine of GRB170817A); the dissipation of the rotational kinetic energy of the remnant, compatible with the upper limits on the energy deposited in the environment by the electromagnetic emission.

This work is organized as follows. In Chapter1 we summarize state-of-the-art knowledge concerning masses, radii and spin frequencies of neutron stars. A short background on rotating stars in classical physics is also reported here, just to introduce fundamental results and physical quantities needed by our analysis. Therefore, in Chapter2 we focus on the theoretical overview about rotating compact stars in relativity, which is necessary in order to probe a possible differentially rotating outcome of a double-NS merger. In this chapter we also treat in details some numerical approaches usually applied to compute models of rotating neutron stars. In Chapter3 some of the most relevant equations of state describing dense matter are discussed. In Chapter4 the phenomenology of GW170817/GRB170817A/AT2017gfo is summarized. Finally, in Chapter5 we illustrate our suggested scenario for the post-merger phase of the event of August, 2017.

Chapter 1

Neutron Stars

Nowadays lots of physical research aim to probe what kind of picture seems to be the most appropriate to describe the *Beginning* of the Universe. An interesting result of these investigations is the remarkable tendency of all the branches of physics towards a "great" unification when the time *zero* is approached. Both of the two current standard models developed by theoretical physicists and cosmologists to describe the whole nature of the Universe point out that the *Theory of Everything* is hidden somewhere in the past. But, what about the *Ending*? It's surprising that the same kind of things seem to happen when one looks in the opposite sense. Clearly it is not possible to see the future of the Universe, nevertheless we can study the ultimate stages of the evolution of astrophysical objects. We can probe what happens when a star dies. We can deal with neutron stars.

> *Neutron stars are superdense objects; superfast rotators; superfluid and superconducting inside; superaccelerators of high-energy particles; sources of superstrong magnetic fields; superprecise timers; superglitching objects; superrich in the range of physics involved. Neutron stars are related to many branches of contemporary physics and astrophysics, particularly to nuclear physics; particle physics; condensed matter physics; plasma physics; general theory of relativity; hydrodynamics; quantum electrodynamics in superstrong magnetic fields; quantum chromodynamics; radio-, optical-, X-ray and gamma-ray astronomy; neutrino astronomy; gravitational-wave astronomy; physics of stellar structure and evolution, etc.*[4]

1.1 State of the art

Neutron stars (NSs) represent the end point of the life of stars whose initial mass belongs to a range of $[8, 20-25]M_\odot$. At the last stages of the evolution of these stars, when the Si-burning and the formation of iron nuclei in their core is completed, the inner nuclear fuel is exhausted. This is due to the binding energy of iron nuclei, which is the more high among all the others nuclei. Therefore, no further energy can be released by nuclear fusion. When this happens the progenitor leaves its hydrostatic equilibrium state. Because of the lack of an internal energy source, the gravity pressure triggers the dynamical collapse of the star. This generates a violent and catastrophic explosion that we call ”Supernova”. It is an astrophysical object consisting in a sudden powerful burst in luminosity, sometimes capable of outshining the luminosity of an entire galaxy. If observed in our Galaxy, it should be visible in daylight and for weeks thereafter. Baade and Zwicky[5] suggested that the source of such a magnitude must be gravitational binding energy. The luminosity of supernovae ($\sim 10^{53}$ ergs^{-1}) is mainly due to neutrinos emission[6] ($\sim 10^{51}$ ergs^{-1}), which carry away lots of the gravitational energy associated to the collapse, the remaining small fraction can be released either mechanically or by emission of gravitational waves (GWs). Baade and Zwicky also stated that that supernovae would actually represent the transition of an ordinary star to a neutron star. This is true only if the mass of the progenitor belongs to the previous range. In the case of more high initial masses the outcome of a supernova should be a black hole. Instead, if the progenitor is not so massive, there is the possibility that the hydrostatic equilibrium of the collapsed object is restored at a certain point during the supernova explosion. The gravitational collapse makes the star so dense that in its inner regions the repulsive component of the strong interactions becomes evident. The hydrostatic equilibrium is restored thanks to several components which act against the gravity. Mainly the strong repulsion between atomic nuclei but also the degeneracy pressure of neutrons, protons and electrons generates by the Pauli principle. The thermal pressure also is relevant in order to stop the collapse. When the equilibrium is restored a neutron star is born.

After the discovery of the first pulsar[1][7] lot of work has been done in order to understand the physical properties of neutron stars as well as their origin and evolution. During the last dozen of years our knowledge about these objects has improved considerably. Countless theoretical studies on spacetimes, microphysics and high energy astrophysics have been performed together with a remarkable progress in computational sciences. We are now able to model these peculiar objects with high accuracy numerical codes. However, although the great improvement on theoretical physics over the years, the major advances mainly came from astrophysical observations. Nowadays terrestrial experiments are not able to approach high densities like those inside NSs cores, i.e. significantly higher than the nuclear mass density at the saturation ($\rho_0 = 2.7 \cdot 10^{14}$ gcm^{-3}[8]). These extreme physical regimes can be investigated only by space surveys. Thanks to the new generation X-ray and γ-ray telescopes, large and high quality datasets have been obtained. Awesome improvements were due to the application of different observational techniques applied to all the wavelengths of the electromagnetic spectrum, from the radio to gamma rays. Moreover, after the first observation of GWs coming from a binary NS merger together with a short-duration gamma-ray burst[9] a new multi-messenger era for the Astrophysics has begun: we are now able to detect the gravitational counterpart of the signal emitted by NSs probing new and weird features of these objects. Up today $\sim$3000 NSs have been observed and a complicated picture turned out. There is a great variety of possibly distinct observational classes of compact stars, like an intricate zoo: rotation-powered pulsars, millisecond pulsars, isolated neutron stars,

---

[1] A pulsar is a highly magnetized rotating neutron star that emits a beam of electromagnetic radiation which can be observed only when the beam of emission is pointing toward Earth. This emission is seen periodically in the form of ”pulses”.

magnetars and others types of have been catalogued. Some interesting ideas for grand unification are emerging; for instance, models of magneto-thermal evolution have been suggested[10]. Observationally we are not able to probe directly the deep interior of these stars. However, severe constraints on the properties of ultra dense and cold nuclear matter can be put through NSs masses and radii measurements together with theoretical investigations. Given a particular equation of state, one can solve equations of structure within the framework of general relativity computing at first static and spherical stellar models and mapping them into mass-radius diagrams. Different equations of state allow to different maximum masses of NSs. A measurement of the mass, even without a simultaneous estimation of the radius, can be very useful to constrain the equation of state: candidates yielding models with maximum masses of nonrotating stars below the observational limits must be ruled out. Several types of equations of state have already been excluded, in particular thanks to the latest mass measurements[11, 12]. This led to new theoretical investigations concerning nuclear matter at larger densities. Several scenarios have been suggested taking account the possibility of different families of NSs[13] (we will discuss them very deeply in the next chapters).

The value of the maximum mass of neutron stars is regularly discussed in the literature[14, 15, 16, 17] because its fundamental role in defining the nature of the compact object itself: beyond an upper mass limit the prompt collapse to a black hole cannot be avoided. The understanding about this is so important not only for the aim of probing new regimes of nuclear physics but also for several astrophysical phenomena related to it, like the outcomes of supernova explosions or even of CO-CO mergers, the signal emitted by them and their characteristic evolutionary timescales. In order to realize a stable hydrostatic configuration, masses beyond a lower limit are also required. The minimum neutron star mass is rather well established because of its really weak dependence on the equation of state of nuclear matter: $\approx 0.1 M_{\odot}$[18]. We now know precise masses for ∼35 CSs spanning the range from 1.17 to 2.00 $M_{\odot}$[19]. The most precise measurements have been performed detecting the radio signal associated with rotation-powered pulsars. About 2250 of them are isolated NSs and the remaining 250 are located in binary systems. Only for the latter ones accurate estimations are possible by applying timing techniques and evaluating the system orbital parameters in which relativistic corrections are needful. Most of them are "recycled" pulsars: a great mass transfer from the companion to the NS happened at a certain point of the dynamical evolution. Double-NS binary systems have been also discovered. The first of them was PSR B1913+16[20], the latest mass estimates yielding $M_{PSR} = 1.4398 M_{\odot}$ and $M_c = 1.3886 M_{\odot}$ (the companion mass). Its discovery was of great importance since it consisted in the first indirect observation of gravitational radiation[21]. By applying relativistic calculations, it was possible to explain the revealed orbital decay of the system as a dissipation mechanism in which the orbital energy is gradually converted in gravitational waves. A number of others double-NS systems have since been observed. These provided lots of stringent tests for general relativity proving its extraordinary precision in the description of compact objects and thus ruling out several families of others gravity theories. J0737-3039 is the only double-pulsar system known among them[22, 23]; all the post-Keplerian parameters have been measured independently for each of the two stars and they were completely consistent with relativistic predictions[24]. This peculiar system has been well investigated because of its precious information about the formation and the coalescence of double-NS systems, which are prime targets for GW detectors on Earth. By combining radio and X-ray observations also pulsars heavily recycled by a long-lived accretion phase in a low-mass X-ray binary have been detected. These are characterized by a 10^{-3}s absolutely stable rotational period and a remarkable X-ray emission generated by the accretion mechanism. They also exhibit strong pulsed high energy γ-ray emissions[25]. The first detected "millisecond pulsar" (MSPs) was B1937+21[26]. Their number has since increased very rapidly. Various searches have revealed a total of 255 MSPs[27]; about $\sim$20% of them are isolated CSs and most of the remaining have WD companions. Pulsar-WD systems have well been investigated through Shapiro delay measurements. Among these, PSR J1614-2230 represented definitely the most impressive one. Its more recently estimated mass is about $1.928 M_\odot$[28]. This allowed to fix relevant constraints on the neutron stars equation of state as well as their mass distribution. Moreover for some of the millisecond pulsars optically emissions from the companion were detected. Spectroscopic investigations of the Balmer lines produced by hydrogen in the WD atmospheres have provided important measurements, in particular the masses of the pulsar-WD system PSR J0348+0432[12]: $M_{PSR} = 2.01 M_\odot$ and $M_c = 0.172 M_\odot$. This ensured that NSs can reach masses around $2M_\odot$. Neutron stars in high-mass X-ray binary systems have also been discovered by observing eclipse phenomena and optical emissions. In Figure 1.1 the recent mass measurements of several categories of NSs are shown.

The determination of the radius of NSs of known masses would allow to reveal the equation of state of nuclear matter at ultra density regimes. However this would require very small uncertainties in the measurements. Up today the precise evaluation of NSs radii represents a challenge for observers. Several observational methods have been developed over the years. Currently, two main approaches are applied: one involves spectro-photometric analysis and the other timing techniques. Their goal is to detect the atmospheric thermal emission of the neutron star or the effects of spacetime on this emission to obtain information about the star radius. As for Newtonian stars, the spectroscopic method measures the observed radius of the star (R_{obs}) by the estimate of the bolometric thermal flux (F_{bol}), the effective temperature (T_{eff}) and the luminosity distance (D). Assuming thermal emission from the surface of the star we have that:

$$\begin{cases} L_{bol} = 4\pi\sigma_{SB} R_{obs}^2 T_{eff}^4 \\ L_{bol} = F_{bol} 4\pi D^2 \end{cases} \tag{1.1}$$

where σ_{SB} is the Stefan-Boltzmann constant. Thus, the NS radius is given by:

$$R_{obs} = D\Big(\frac{F_{bol}}{\sigma_{SB} T_{eff}^4}\Big)^{1/2} \tag{1.2}$$

However, numbers of complications come out in this estimation. Firstly, unlike Newtonian stars, there is a relativistic mass-dependent correction in eq.1.2 due to the spacetime curvature. For instance, in the case of a static-spherically symmetric

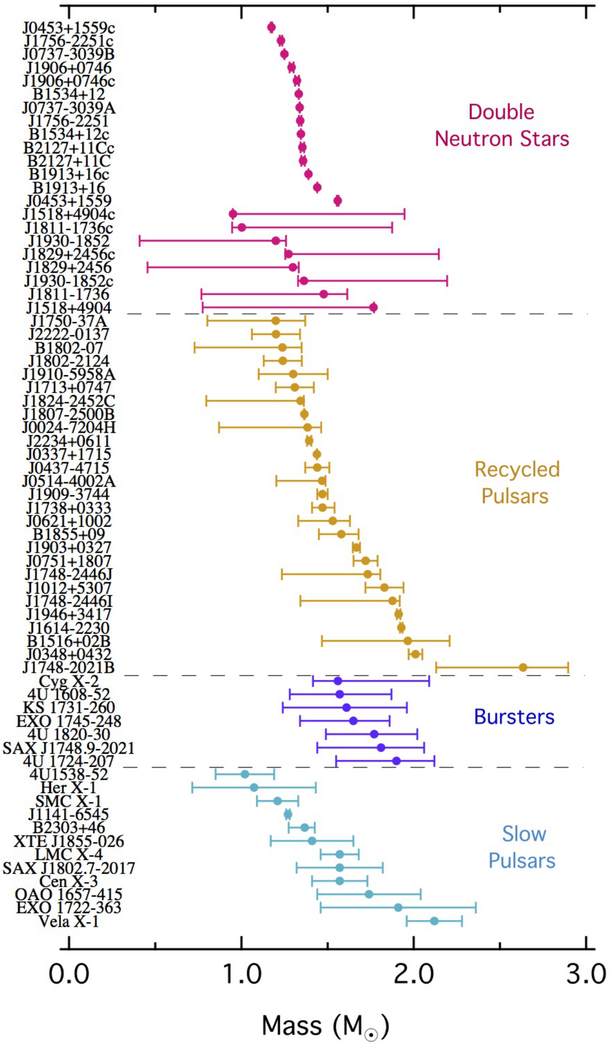

Figure 1.1: Current measurements of compact star masses. Several classes are reported here with different colors: Double NSs (magenta), Recycled Pulsars (gold), Bursters (purple) and Slow Pulsars (cyan). Reference: *Ozel & Freire 2016, Annual Reviews of Astronomy and Astrophysics.*

Schwarzschild spacetime the proper radius R of the NS is related to R_{obs} by:

$$R_{obs} = \left(1 - \frac{2GM}{Rc^2}\right)^{-1/2} R \tag{1.3}$$

where G is the gravitational constant, c the speed of light and M the gravitational mass of the star (we will define it later). Thus a mass measurement is needed to estimate the radius. The situation even becomes more complex when considering rotating NSs, for which the spacetime cannot be described with a Schwarzschild metric and the gravitational mass and the radius are both affected by the spin[29] (also this will be discussed later in this thesis), or also when non-thermal emissions or strong magnetic fields on the surface are considered. The chemical composition of the atmosphere also affects the results[30]. Moreover, it's very difficult to obtain accurate evaluations of the NS luminosity distance. Lots of radius measurements concern

NSs located in globular clusters whose distances are quite known. However in some cases the uncertainties on the distance can be as large as 25%[31], especially when one considers also the effects of the interstellar absorption[30]. Detailed theoretical modeling of emission from neutron stars in general relativity have been developed during the last decades in order to overcome these problems[8, 19]. Essentially these models have been applied to three types of objects: quiescent X-ray transients (QXTs), bursting NSs (BNSs) and rotation-powered radio millisecond pulsars (RP-MPS).

The first ones are NSs belonging to a binary system observed when the accretion process is stopped or is continuing at a very low level. This allows observations of the surface thermal emission powered by the re-radiation of the heat stored in the deep crust during the accretion phases[32]. Numbers of QXTs in globular clusters have been observed with X-ray telescopes like *Chandra*[33] and *XMM-Newton*[34, 35]. Since they are observed during a quiescent phase their luminosity is quite low ($\sim 10^{32-33}\text{ergs}^{-1}$). In the case of NSs belonging to a globular cluster also the crowded environment makes their observation very difficult. Thus high angular resolution X-ray telescopes are needed to measure their angular sizes[35]. Reliable radii constraints have been obtained for eight QXTs located in different globular clusters, like 47 Tuc[36, 37] and ω Cen, M13 and NGC 2808[35]. These measurements have suggested radii in the 9.9-11.2 km range for a $\sim 1.5 M_\odot$ NS[37]. BNSs are instead NSs from which recurring and strong photospheric bursts are observed. These are helium flashes generated by the material accreting the NS in a low-mass X-ray binary system. During these events the star luminosity increases so much that it can reach the Eddington limit. In these cases the radiation forces overcome the gravitational ones lift the star photosphere off of its surface. Numbers of studies make use of a combination of the Eddington flux measured during the burst and the distance computed through a high resolution X-spectra analysis to extract information about NSs radius. For instance, in [38] the distance of the low-mass X-ray binary 4U 1608-52 has been evaluated by modeling the individual absorption edges of the elements Ne and Mg in the high resolution X-ray spectrum obtained with *XMM-Newton*, then analyzing the time-resolved X-ray spectra of Type-I X-ray bursts observed from this source a mass of $1.74 \pm 0.14\ M_\odot$ and a radius of 9.3 ± 1.0 km were found. Moreover, by combining this method with the measure of R_{obs} one is able to break the relativistic mass-dependence showed in eq.1.2 and thus to estimate the radius of a NS independently by the measure of its gravitational mass. Several measurements from QXTs and BNSs seems to be consistent with a range of values for the observed NSs radii of $9.8 - 11$ km [19]. Another approach that has been used for radius measurements is to study the spectral evolution of photospheric bursts during its cooling phase[39, 40]. By the observed spectral distortion one can extract information about the effective surface gravity and the emitted flux during the burst and thus estimate the stellar mass and radius. This method has been applied to some BNSs but the results are ambiguous: some yielding too large[40] and others too small [39] radii. As mentioned before there is also an other class of methods which use timing investigations in order to constrain the NSs radii. By analyzing the periodic brightness oscillations which are originated from temperature anisotropies on the surface of a spinning pulsar, the properties of the spacetime near the star and thus of the beam of the emerging radiation can be probe. Several theoretical models has been employed to describe the features of the emitted radiation allowing observers to probe the pulsars spacetime, masses and radii. However, in order to obtain accurate measurements, the corrections due to the rotation are required. There are already several studies which use them, considering both slow and high rotation regimes. They have noted that for 3 ms spin periods, the pulse fractions can be as much as an order of magnitude larger than with simple, slowly rotating (Schwarzschild) estimates[41]. Moreover the analysis of the pulse profiles have shown that neglecting the oblateness of the neutron star surface leads to $\sim 5-30\%$ errors in the calculated profiles and neglecting the quadrupole moment leads to $\sim 1-5\%$ errors at a spin frequency of ~ 600Hz[42]. This class of methods has been applied to several types of NSs, like slow-pulsars[43] and magnetars[44]. Some constraints about NSs radii have been obtained for accretion-powered millisecond pulsars (AP-MSPs), RP-MSPs and thermonuclear X-ray BNSs. Anyway, large uncertainties in the radius measurements are generated by various geometrical factors which appear during the modeling of the pulse profiles[19].

1.2 Rotating Newtonian stars: a background

The angular momentum is one of the most important properties of astrophysical objects. We konw from the Classical Mechanics that a field of central forces conserves the angular momentum when measured in a fixed reference frame. Being the gravity the central force which governs many astrophysical events, such as the formation and the evolution of stars, planets and galaxies, the conservation of the angular momentum looks like an holy rule in the Universe: every motion involved during an event in which gravity dominates the other forces obeys it. At the beginning of the formation of most astrophysical objects a certain amount of angular momentum was contained in interstellar clouds which became gravitationally unstable and collapsed towards smaller mass clumps, sharing the angular momentum over them. Because of the conservation law a large part of this angular momentum has been conserved till today. We can observe rotation in several astrophysical objects and with different regimes. The Earth rotates like a rigid-body, i.e. with constant spin frequency within it (*uniform rotation*), at $\approx 1 \times 10^{-5}$Hz. The rotation makes it slightly flat at the poles; this flattening can be measured by the difference between the equatorial and polar radii ($R_e - R_p \sim 20$km). Stars also rotate and because of their gaseous composition the rotational effects can be more evident. They can appear more flat and farther their spin frequency can change within them unlike solid-bodies (*differential rotation*). The Sun happens to be the only star of which differential rotation is observationally well studied. It rotates rather slowly, with a equatorial spin frequency of 4.55×10^{-7}Hz changing at the pole of more than 10%.

The theory of rotating stars is a notoriously difficult subject. The rotation plays a crucial role for these systems. It does not only change their shape but also influences the processes occurring inside them, i.e. it may accelerate or decelerate thermonuclear reactions in certain conditions, it changes the gravitational field outside the objects and it is one of the main factors that defines the lifespan of all stars, from their birth until their death[45, 46, 47]. Thanks to the centrifugal force, rotating stars can sustain more mass and have larger radii respect to the non rotating ones. Since the topic of this thesis is the role of the rotation in relativistic stars, which are more complex to investigate, a brief discussion about rotating Newtonian stars can be useful to the reader. Let us consider the case of a self-gravitating and uniformly rotating fluid within the framework of Classical Mechanics. By assuming an adiabatic motion of the fluid, the equations which describe the dynamical evolution of the system in a co-rotating Eulerian reference frame are the following:

$$\frac{\partial \rho}{\partial t} + \vec{\nabla} \cdot (\rho \mathbf{v}) = 0 \tag{1.4}$$

$$\frac{\partial \mathbf{v}}{\partial t} + (\mathbf{v} \cdot \vec{\nabla})\mathbf{v} = -\frac{1}{\rho}\vec{\nabla} P - \vec{\nabla}\Phi - \boldsymbol{\Omega} \wedge (\boldsymbol{\Omega} \wedge \mathbf{r}) - 2\boldsymbol{\Omega} \wedge \mathbf{v} + \nu \nabla^2 \mathbf{v} \tag{1.5}$$

$$\nabla^2 \Phi = 4\pi G \rho \tag{1.6}$$

where ρ is the density field, $\boldsymbol{\Omega}$ is the angular velocity vector, P is the pressure, Φ is the gravitational potential and ν is the cinematic viscosity of the fluid. There are five equations and ten unknowns (ρ, P, $\mathbf{v}$, Φ, $\boldsymbol{\Omega}$, ν) in the above set of equations. In order to find a unique solution of the problem other five equations are required. We can use a relation $P = P(\rho)$, which is an equation of state independent on the fluid temperature (according to the adiabaticity condition). This is named as *barotropic* equation of state. Moreover, being Ω constant within the fluid, it's easy to show that $\boldsymbol{\Omega} \wedge (\boldsymbol{\Omega} \wedge \mathbf{r}) = -1/2\vec{\nabla}\|\boldsymbol{\Omega} \wedge \mathbf{r}\|^2$. Thus eq.1.5 can be written as:

$$\frac{\partial \mathbf{v}}{\partial t} + (\mathbf{v} \cdot \vec{\nabla})\mathbf{v} = -\frac{1}{\rho}\vec{\nabla} P - \vec{\nabla}(\Phi - \frac{1}{2}\|\boldsymbol{\Omega} \wedge \mathbf{r}\|^2) - 2\boldsymbol{\Omega} \wedge \mathbf{v} + \nu \nabla^2 \mathbf{v} \tag{1.7}$$

This equation shows that uniform rotation decreases the strength of the gravitational potential by defining a new effective potential $\Phi_{eff}(\boldsymbol{\Omega}) = \Phi - 1/2\|\boldsymbol{\Omega} \wedge \mathbf{r}\|^2$. This is the effect of the centrifugal forces, which push out the mass fluid elements against the gravitational collapse. The latest two terms in the right hand side of eq.1.7 represent the Coriolis (the former) and the viscous (the latter) forces per unit of mass. Because of the second spatial derivative $\nabla^2 \mathbf{v}$ the viscosity action is relative to the smaller length scales respect to the other terms. This allows us to neglect it in the description of big size systems, like astrophysical objects, thus considering the simple case of an ideal fluid[2]. For the hydrostationary equilibrium configuration the ultimate set of equations is[3]:

$$\Phi_{eff}(\boldsymbol{\Omega}) + \int \frac{1}{\rho}\vec{\nabla} P = \text{const.} \tag{1.8}$$

$$\nabla^2 \Phi_{eff}(\boldsymbol{\Omega}) = 4\pi G \rho - 2\Omega^2 \tag{1.9}$$

$$P = P(\rho) \tag{1.10}$$

where the integral in eq.1.8 is done along a streamline. Once $\boldsymbol{\Omega}$ is fixed the entire system of equations can be solved and we can study the dynamics of the rotating

---

[2] This is clearly true only when not much high viscosities are taken into account. We don't consider this case here.

[3] In cylindrical coordinates: $\nabla^2(\frac{1}{2}\|\boldsymbol{\Omega} \wedge \mathbf{r}\|^2) = \frac{1}{\varpi}\frac{\partial}{\partial \varpi}\left[\varpi \frac{\partial}{\partial \varpi}\left(\frac{1}{2}\Omega^2 \varpi^2\right)\right] = 2\Omega^2$.

fluid. It is important to highlight a point. With the respect of non rotating configurations, rotating models require to fix a major number of quantities in order to be computed uniquely. Hydrostationary equilibria draw sequences of models with a higher number of dimensions than sequences of hydrostatic equilibria. This comes from the own expression of the structure equations. When one wants to solve directly (i.e. without approximations) the above set of ordinary linear differential equations, he has to specify appropriate boundary conditions. We will see later that for the non rotating case, i.e. $\Omega = 0$, this correspond to fix a value of one single parameter. Generally, the central mass density or the maximum value of it are specified. This fixing corresponds to compute the constant in eq.1.8 (with $\Omega = 0$) and thus to compute one single solution, i.e. one single stellar model. Moreover, changing the parameter allows to build one-parameter sequences of hydrostatic equilibrium configurations. Nevertheless, if rotation is present, fixing one parameter in eq.1.8 corresponds to compute a sequence of solutions; this being parameterized by the angular velocity Ω changing among different models. Therefore to compute unique solutions we need to specify more parameters. In particular for the above problem, where Ω is constant, one can choose to fix the own spin frequency. Thus a single stellar model is linked by a couple of parameters within the solutions space, for instance (ρ_c, Ω) where ρ_c is the central mass density of the model. In the presence of differential rotation the situation becomes more tricky and appropriate numerical technique can be applied to solve the structure equations. We will discuss them later.

Several approaches have been used to find solutions of the Ω-constant problem over the years. One is the so-called *slow-rotation* approximation. This method was invented by James B. Hartle[48] who applied it firstly to Newtonian stars and then to relativistic stars in order to study the effects of rotation on NSs. Subsequently, Hartle and K. Thorne used it to create a code which computed equilibrium configurations of rotating NSs applying some realistic equation of state[49]. The powerful of this approach is its analyticity. When a star is rotating slowly[4] the calculation of its equilibrium bulk properties is much simpler, because then the rotation can be considered as a small perturbation on an already-known non-rotating configuration[48]. A solution for the non-rotating problem is used as the leading term in an expansion of the rotating problem solution in powers of the angular velocity Ω to the order Ω^2. Then the equations governing the second-order terms are determined and a spherical harmonics expansion of the these terms is done. Eventually the equations for each pole are studied. This approach is useful to investigate some properties of rotating stars, like their shape and their change on the mass over its non-rotating value for a fixed central mass density[5]. However it is only valid for slowly-rotating stars. Errors come out when considering rotating fluids with arbitrary angular velocity. In these cases higher orders approximations can be developed in order to compute more ac-

---

[4] This means that $\Omega \ll \Omega_k$, where Ω_k is the Keplerian angular velocity that defines the so-called *mass-shedding limit*, i.e. the rotation rate at which the centrifugal forces at the star's equator start to overcome the gravity pressure. In the Hartle formalism this implies that the relative changes in pressure, energy density and gravitational field due to the rotation are all much smaller than the unity.

[5] Since the gravity strength is reduced by the action of the centrifugal forces, the effective mass of a rotating star is smaller than its value in a non-rotating configuration for the same central mass density.

curate solutions. We will not discuss them in this thesis but we will describe after the slow-rotation method applied to rotating relativistic stars. In particular we will focus on the order $O(\Omega)$.

An other approach was to study analytically the gravitational equilibrium of rotating masses probing the geometrical deformation on their shapes induced by the rotation. Starting with the studies of Newton about the shape of the Earth, which showed that *the effect of a small rotation on the figure must be in the direction of making it slightly oblate*[50], this analysis was carried on by some of the greatest physicists and mathematicians of the nineteenth century. Let us consider the equilibrium configuration of a uniformly rotating fluid whose dynamical evolution is described by the equations 1.8-1.10. We also consider the case of an homogeneous fluid. Thus eq.1.8 becomes:

$$\frac{P}{\rho} + \Phi - \frac{1}{2}\|\mathbf{\Omega} \wedge \mathbf{r}\|^2 = \text{const.} \tag{1.11}$$

We take $\hat{z}$ as the rotation axis (i.e. $\mathbf{\Omega} = (0, 0, \Omega)$). Because we are interested on the shape of the fluid let us look at the geometry of its surface, which is defined by the condition $P = 0$. Keeping this in mind, in a Cartesian coordinate system the eq.1.11 reduces to the following:

$$\Phi - \frac{1}{2}\Omega^2(x^2 + y^2) = \text{const.} \tag{1.12}$$

We want to study an ellipsoidal figure of equilibrium. Thus the analytical expression for the boundary surface has to be:

$$\frac{x^2}{a^2} + \frac{y^2}{b^2} + \frac{z^2}{c^2} = 1 \tag{1.13}$$

It can be shown that the gravitational potential at any point inside the ellipsoid is given by[51]:

$$\Phi(x, y, z) = \pi G\rho(\alpha_0 x^2 + \beta_0 y^2 + \gamma_0 z^2 - \chi_0) \tag{1.14}$$

where

$$\alpha_0 = abc \int_0^\infty \frac{d\lambda}{(a^2 + \lambda)\Delta} \tag{1.15}$$

$$\beta_0 = abc \int_0^\infty \frac{d\lambda}{(b^2 + \lambda)\Delta} \tag{1.16}$$

$$\gamma_0 = abc \int_0^\infty \frac{d\lambda}{(c^2 + \lambda)\Delta} \tag{1.17}$$

$$\chi_0 = abc \int_0^\infty \frac{d\lambda}{\Delta} \tag{1.18}$$

$$\Delta = [(a^2 + \lambda)(b^2 + \lambda)(c^2 + \lambda)]^{1/2} \tag{1.19}$$

By inserting the expression 1.14 for the gravitational potential within the eq.1.12 for the surface, we obtain that:

$$\Big(\alpha_0 - \frac{\Omega^2}{2\pi G\rho}\Big)x^2 + \Big(\beta_0 - \frac{\Omega^2}{2\pi G\rho}\Big)y^2 + \gamma_0 z^2 = \text{const.} \tag{1.20}$$

Since eq.1.13 and eq.1.20 must hold simultaneously the coefficients of x^2, y^2 and z^2 have to be proportional. Thus we obtain an important result:

$$\left(\alpha_0 - \frac{\Omega^2}{2\pi G\rho}\right)a^2 = \left(\beta_0 - \frac{\Omega^2}{2\pi G\rho}\right)b^2 = \gamma_0 c^2 \tag{1.21}$$

By solving the above equation we can compute ellipsoidal equilibrium configurations. Classical studies showed that in the case of a non rotating self gravitating fluid in a hydrostatic equilibrium configuration the system must be spherical[52]. Traditionally, for the case of a uniformly rotating fluid in hydrostationary equilibrium it is assumed that the system is *axially-symmetric*. Then we assume the axial symmetry of the system respect to the rotation axis $\hat{z}$. This implies $a = b$, with $a, b > c$ for the case of an oblate ellipsoid. The condition $a = b$ makes more easy the integration of eq.1.15-1.18; for instance:

$$\alpha_0 = a^2 c \int_0^\infty \frac{d\lambda}{(a^2+\lambda)^2(c^2+\lambda)^{1/2}} = \cdot\cdot = -\frac{2c}{ae^3}\int_e^0 \frac{\omega^2 d\omega}{(1-\omega^2)^{1/2}} \tag{1.22}$$

which can be solved using trigonometrical functions and where $e = \left(1 - c^2/a^2\right)^{1/2}$ is the eccentricity of the ellipsoid. By taking $a = b$ inside eq.1.21 and solving all the integrals in eq.1.15-1.18 one obtains that:

$$\frac{\Omega^2}{\pi G\rho} = \frac{2(1-e^2)^{1/2}}{e^3}(3-2e^2)\sin^{-1} e - \frac{6(1-e^2)}{e^2} \tag{1.23}$$

The equation describes how the uniform rotation modifies the figure of the fluid for a given uniform density. Maclaurin in 1740[51] first demonstrated the existence of such spheroidal solutions, which were called *Maclaurin spheroids* in his honour. The graph of the normalized square angular velocity $\Omega^2/\pi G\rho$ as a function of the eccentricity e is shown in Figure1.2. We can see that when the fluid is non-rotating it has a spherical shape ($\Omega = 0$, $e = 0$). When a certain amount of angular momentum

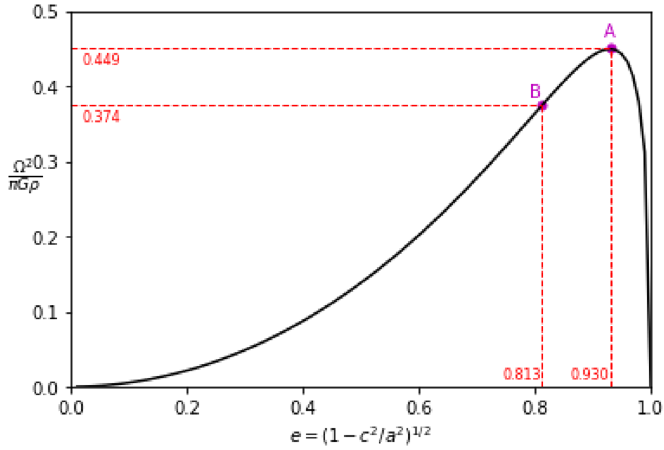

Figure 1.2: Graph of the relation between the normalized square angular velocity $\Omega^2/\pi G\rho$ and the eccentricity e. See more details in the text.

is imprinted on the fluid it starts to rotate ($\Omega > 0$) and it acquires a spheroidal shape ($e > 0$). By giving it more angular momentum, Ω increases and the spheroid becomes more and more flat until the point A. At this point, when $e = 0.930$, the angular velocity reaches a maximum value. Then an extra amount of angular momentum makes the spheroid more flat slowing it down at the same time. A simple argument explains this. Because of the assumption that the rotation axis is also the symmetry axis of the system, the module of the angular momentum is $L = I\Omega$ where I is the moment of inertia. If we increase L ($\delta L > 0$) then both Ω and I can vary. Since $I \sim Ma^2$, being M the mass of the fluid, an increase of e for a fixed minor semi-axis c corresponds to an increase of a and thus of I. In particular:

$$\delta L = I\delta\Omega + \Omega\delta I \Rightarrow \delta\Omega = \frac{\delta I}{I}\Big(\frac{\delta L}{\delta I} - \Omega\Big) \tag{1.24}$$

Since $\delta L, \delta I > 0$ the sign of $\delta\Omega$ is defined by the sign of the term inside the brackets. If the increase of I is sufficiently large we can have $\delta L/\delta I < \Omega$ and thus a decrease of the angular velocity[6]. Furthermore, the behaviour of the spheroid at the point B plotted on Figure1.2 was explained by Jacobi in 1834[51]. He showed that the eq.1.20 can admit other solutions which are associated to triaxial ellipsoids. In particular Jacobi demonstrated that:

- for $e < 0.813$ only solutions with $a = b > c$ exist (Maclaurin spheroids)
- for $e > 0.813$ also solutions with $a \neq b \neq c$ (all real numbers) can exist

The latest were called *Jacobi ellipsoids*. Thus for $e < 0.813$ there is one possible solution which is a Maclaurin spheroid. Instead for $e \geq 0.813$ there are two possible solutions: one of these is again a Maclaurin spheroid and the other is a Jacobi ellipsoid, with three unequal axes. From the point B the Jacobi sequence of ellipsoidal equilibrium configurations "bifurcates" from the Maclaurin sequence. Jacobi discovered the important fact that *uniformly rotating homogeneous fluids can be not axially symmetric.* The axial symmetry that is traditionally assumed to describe rotating configurations is *only* a mere assumption. "A priori" the general rotational problem has not specific symmetries. By imprinting a sufficient amount of angular momentum to a Maclaurin spheroid a Jacobi ellipsoid can be obtained breaking the axial symmetry. The meaning of this spontaneous symmetry breaking is more clear when one considers the energy of the system. It can be shown that the Jacobi ellipsoid has less rotational kinetic energy compared to the Maclaurin spheroid[51] for the same mass and angular momentum. Beyond the bifurcation point B the Maclaurin spheroid becomes *secularly unstable.* "Secular instability" means that if one considers the general problem in which also dissipative mechanisms are included (such as viscosity, heat flows or also gravitational radiation) and studies the time evolution of the system by starting with a initial equilibrium configuration and applying a small perturbation to it, then a slowly[7] evolution of the system towards an unstable configuration is noted. During this process the system dissipates energy and lies into

---

[6] It can be shown that $\delta L/\delta I < \Omega$ exactly correspond to the condition $e > 0.930$.

[7] This means that the instability evolves in timescales longer than the *dynamical* timescale τ_{dyn}, which corresponds to a prompt collapse/explosion of the fluid caused by the gravitational/pressure forces. For rotating NSs this timescale is $\tau_{dyn} \sim$ms [4].

quasi-equilibrium configurations. In the case of a Maclaurin spheroid the secular instability starts when $e = 0.813$, then if some angular momentum is added and if some dissipative mechanisms are present the spheroid relaxes to a triaxial ellipsoid. This is a *non-axisymmetric* instability and it can be studied in the perturbative analysis considering bar-modes[8]. Newtonian stars develop bars in secular timescales when this instability occurs[50]. Instead of the oblateness, one often uses the ratio $\beta = T/|W|$ between the rotational kinetic energy T and the gravitational energy W, which reaches the value 0.1376 at the bifurcation point. Therefore, we can state that:

- if $\beta \lesssim 0.14$ the rotating fluid is secularly stable
- if $\beta \gtrsim 0.14$ the rotating fluid is secularly unstable and develop bars

All these results are valid for homogeneous and uniformly rotating fluids but they can also be used to describe the stability of realistic rotating Newtonian stars. It can be shown that Newtonian stars develop bars on a *dynamical* timescale when $\beta \gtrsim 0.27$, while they develop bars on a *secular* timescale for $\beta \gtrsim 0.14$ via gravitational radiation or viscosity[53]. Moreover the β parameter has been also used by several authors (e.g. [54]) in order to define the "slow-rotation" regime without regard to the equatorial spin frequency. According these authors, a star is considered to be "slowly-rotating" when $\beta \ll 1$ and "rapidly-rotating" when the kinetic energy of rotation is comparable to the gravitational energy (i.e. $\beta \approx 1$). After the studies of Maclaurin and Jacobi lots of work has been done. For instance the Roche model in which the self-gravitating fluid shows a not constant density profile within it (i.e. without the assumption of homogeneous fluid) and practically all the mass is in the center[55]. In this model one can estimate the value of the Keplerian frequency for uniform rotation Newtonian stars. It turns out to be[56]:

$$\Omega_k = \left(\frac{GM}{R_e^3}\right)^{1/2} \tag{1.25}$$

where M and R_e are the mass and the equatorial radius of the system respectively. We will not go more into detail about this approach in this thesis. However the results concerning the bar-mode instability and the lack of an already-known symmetry of rotating fluids will be very important during the analysis of relativistic stellar models. Generally, when one wants to study rotating stars he starts computing an axially symmetric model and after the stability against axisymmetric and non-axisymmetric modes is tested through the perturbative analysis. The axial-symmetry is just an initial assumption in order to simplify the treatment and to obtain an initial model whose stability is studied afterwards.

All the models described until now have concern only the case of the uniform rotation. More elaborate models consider also the differential rotation. In the astrophysical universe we find many objects rotating not like a rigid body. We know from classical physics that in the case of a fluid rotating with differential rotation the viscosity tends to stop the relative motions amongst different fluid elements. However

---

[8] These are modes associated with different values of the number m in the spherical harmonics expansion of the physical quantities of the problem. We will not discuss them here.

because of its action is relative to the small length scales, the viscous damping require time and in the case of astrophysical scales this time can be very long. Moreover astrophysical objects often present some physical mechanisms which can maintain the differential rotation[51] or are related to it, like the magnetic field in the case of the Sun which is involved in the dynamo process. The differential rotation can affect the stability of rotating bodies. In particular, not all types of differential rotation are stable. An important result obtained by Rayleigh[57] is that a differentially rotating uniform density fluid is stable against local and axisymmetric disturbances if:

$$\frac{d}{d\varpi}[(\varpi^2\Omega)^2] \geq 0 \tag{1.26}$$

where ϖ is the distance from the rotation axis. This is known as *Rayleigh's criterion*. The equation 1.26 can be also written as:

$$\frac{d\ln\Omega}{d\ln\varpi} \geq -2 \tag{1.27}$$

Thus the variation of the angular velocity along ϖ inside the fluid cannot be much sharp in order to obtain stable equilibria. In particular Ω can't decrease more rapidly than ϖ^{-2}. It should be noted that we considered $\Omega = \Omega(\varpi)$. This is correct when one studies differentially rotating, axisymmetric and barotropic fluids in hydrostationary equilibrium. In fact with these conditions by writing eq.1.5 in cylindrical coordinates (ϖ,ϕ,z) in the case of axial-symmetry respect to the $\hat{z}$ axis (i.e. all the terms in the equations are independent on ϕ) we obtain:

$$\begin{cases} \frac{1}{\rho}\frac{\partial P}{\partial \varpi} + \frac{\partial \Phi}{\partial \varpi} - \Omega^2\varpi = 0 \\ \frac{1}{\rho}\frac{\partial P}{\partial z} + \frac{\partial \Phi}{\partial z} = 0 \end{cases} \tag{1.28}$$

Taking the $\partial/\partial z$ of the first equation and the $\partial/\partial\varpi$ of the second equation we have:

$$\begin{cases} -\frac{1}{\rho^2}\frac{\partial \rho}{\partial z}\frac{\partial P}{\partial \varpi} + \frac{1}{\rho}\frac{\partial^2 P}{\partial z\partial \varpi} + \frac{\partial^2 \Phi}{\partial z\partial \varpi} - 2\Omega\frac{\partial \Omega}{\partial z}\varpi = 0 \\ -\frac{1}{\rho^2}\frac{\partial \rho}{\partial \varpi}\frac{\partial P}{\partial z} + \frac{1}{\rho}\frac{\partial^2 P}{\partial \varpi\partial z} + \frac{\partial^2 \Phi}{\partial \varpi\partial z} = 0 \end{cases} \tag{1.29}$$

By considering that $P = P(\rho)$ and applying the well known Schwarz theorem, the difference between the two above equations gives $\partial\Omega/\partial z = 0$ (the so-called *Poincaré-Wavre theorem*). Also these results about differentially rotating objects are useful in the treatment of rotating relativistic stars and we will apply them later.

The last approach that we want to discuss here is the numerical one, which is based on the application of numerical techniques in order to solve the more general set of equations of rotating fluids and thus computing more realistic stellar models. In particular we focus on one numerical method developed to study rapidly rotating Newtonian stars. In all the models discussed before (the Maclaurin spheroids and the Jacobi ellipsoids) besides the restrictions to very special cases for the density profile and the spin frequency there is not even the possibility to investigate rapidly rotating objects (β approaches the value of 0.5 for the most flattened Maclaurin spheroids[54]). Rapid rotation can severely warp stars. It can bring to the formation of ring structures, self-gravitating accretion disks or even dumbbell structures. This plays an important role during the contact-phase of binary systems. NSs can be fast rotators and non-approximate solutions of the relativistic equations of motion (i.e. which are obtained without the Hartle formalism) can be computed only through appropriate numerical codes. In particular one of the relativistic codes used in this thesis to compute rapidly-rotating NSs is based on the formalism developed in the Newtonian code that we are going to discuss here: the so-called "Hachisu Self-Consistent Field Method" (HSCF method). This has been advanced by Hachisu in 1986[58] and it represents a development of the numerical approach used by Ostriker&Mark in 1968[54]. The HSCF method is able to converge in the case of very rapidly-rotating and distorted configurations with high accuracy and numerical stability. It seems also that it has no limitations for its applicability to various configurations of gaseous bodies and to various equations of state[59]. The HSCF method is based on a integral representation of the basic equations of motion. This allows to handle the boundary conditions in a much easier manner and with more high numerical stability than the differential representation. Let us consider the undefined integral of the two equations in 1.28. The equation for the hydrostationary equilibrium of an axisymmetric fluid rotating around the rotation axis $\hat{z}$ can be written as:

$$H + \Phi - \int [\Omega(\varpi)]^2 \varpi d\varpi = \text{const.} \tag{1.30}$$

where $H := \int (1/\rho) dP$ is the so-called *enthalpy* of the fluid. We consider also a barotropic fluid whose equation of state has a polytropic form: $P = K\rho^{1+1/N}$; where K is a constant and N is the polytropic index. The expression for the gravitational potential can be obtained by using the Green's function of the three-dimensional Laplace operator in the Poisson equation[9] $\nabla\Phi = 4\pi G\rho$ and it is the following:

$$\Phi = -G \int \frac{\rho(\mathbf{r}')d\mathbf{r}'}{\|\mathbf{r} - \mathbf{r}'\|} = -G \int_0^\infty dr' \int_0^\pi d\theta' \int_0^{2\pi} d\phi' (r')^2 \sin\theta' \frac{\rho(r', \theta')}{\|\mathbf{r} - \mathbf{r}'\|} \tag{1.31}$$

where the spherical coordinates (r', θ', ϕ') and the axial-symmetry respect to the $\hat{z}$ axis have been used in the last integral. This can be computed numerically by using the expansion series for the Green's function:

$$\frac{1}{\|\mathbf{r} - \mathbf{r}'\|} = \sum_{n=0}^{\infty} f_n(r, r') \Big\{ P_n(\cos\theta) P_n(\cos\theta') + 2 \sum_{m=1}^{n} \mathcal{P}_{nm}(\theta, \theta', \phi, \phi') \Big\} \tag{1.32}$$

$$\mathcal{P}_{nm}(\theta, \theta', \phi, \phi') = \frac{(n-m)!}{(n+m)!} P_n^m(\cos\theta) P_n^m(\cos\theta') \cos[m(\phi - \phi')]$$

where $P_n(\cos\theta)$ are the Legendre polynomials, $P_n^m(\cos\theta')$ are the associated Legendre functions, $n, m \in \mathbb{N}$ and

$$f_n(r, r') = \frac{1}{r}\left(\frac{r'}{r}\right)^n \Theta(r' - r) + \frac{1}{r'}\left(\frac{r}{r'}\right)^n \Theta(r - r') \tag{1.33}$$

---

[9] The Green's function of $\nabla := \frac{\partial^2}{\partial x^2} + \frac{\partial^2}{\partial y^2} + \frac{\partial^2}{\partial z^2}$ is $G(\mathbf{x}, \mathbf{x}') = -\frac{1}{4\pi} \frac{1}{\|\mathbf{x} - \mathbf{x}'\|}$.

Thus by using the following results:

$$\int_0^{2\pi} \cos\left[m(\phi-\phi')\right]d\phi' = \frac{1}{m}\cos m\phi \int_0^{2m\pi} \cos\zeta d\zeta + \tag{1.34}$$

$$+\frac{1}{m}\sin m\phi \int_0^{2m\pi} \sin\zeta d\zeta = 0 \tag{1.35}$$

and[10]

$$\int_0^{\pi} d\theta' \sin\theta' \rho(r',\theta') P_n(\cos\theta') = \int_{-1}^{1} d\mu' \rho(r',\mu') P_n(\mu') = 2\int_0^1 d\mu' \rho(r',\mu') P_{2n}(\mu') \tag{1.36}$$

we obtain for the gravitational potential:

$$\Phi = -4\pi G \sum_{n=0}^{\infty} \int_0^{\infty} dr' f_{2n}(r,r') \int_0^1 d\mu' \rho(r',\mu') P_{2n}(\mu) P_{2n}(\mu') \equiv \Phi[\rho(r,\mu)] \tag{1.37}$$

For a polytropic equation of state we have also:

$$H = NK(1+1/N)\rho^{1/N} + \text{const.} \tag{1.38}$$

By inserting all these results into eq.1.30, the equation for the equilibrium becomes:

$$\rho(r,\mu) = \left[\frac{1}{K(1+N)}\Big(\text{const.} - \Phi[\rho(r,\mu)] + \int [\Omega(\varpi)]^2 \varpi d\varpi\Big)\right]^N \equiv F[\rho(r,\mu)] \tag{1.39}$$

This is a self-consistence problem for the density profile $\rho(r,\mu)$, which can be solved numerically by iterations[11]. The constant in the equation 1.39 is determined by specifying one boundary condition, for instance a value of the mass density or of the enthalpy at a certain point within the model. One has also to establish the polytropic constants, that means to specify the equation of state. Moreover, as we discussed before, fixing an other parameter is needed in order to compute uniquely rotating configurations. In the case of rigid rotation the equation 1.39 becomes the following:

$$\rho(r,\mu) = \left[\frac{1}{K(1+N)}\Big(const. - \Phi[\rho(r,\mu)] + \Omega^2\frac{\varpi^2}{2}\Big)\right]^N \tag{1.40}$$

and one can fixed the value of Ω as the second parameter of the problem. Instead, if one wants to compute differentially rotating models some constrains on the law $\Omega(\varpi)$ are also required. In the HSCF method[58] two types of differential rotation are considered:

- the so-called *v-constant* law, which is obtained by the condition on the velocity $v = \Omega\varpi \equiv v_0$. In this case the integral in eq.1.39 becomes the following:

$$\int [\Omega(\varpi)]^2 \varpi d\varpi = v_0^2 \int \frac{d\varpi}{\varpi} = v_0^2 \ln\varpi + \text{const.}$$

---

[10] Here $\mu' = \cos\theta'$. We're also considering the symmetry respect to the equatorial plane, which is an other symmetry observed on Newtonian rotating fluids, and the relation $P_n(\mu') \sim (\mu')^n$.

[11] The convergence of the iterations to the solution of the problem is ensured by the Banach-Caccioppoli fixed-point theorem. The iteration process is stopped when errors are below a fixed threshold.

- the so-called *j-constant* law, which is obtained by the condition on the specific angular momentum $j = \Omega\varpi^2 \equiv j_0$. In this case the integral in eq.1.39 becomes the following:

$$\int [\Omega(\varpi)]^2 \varpi d\varpi = j_0^2 \int \frac{d\varpi}{\varpi^3} = -j_0^2 \frac{1}{2\varpi^2} + \text{const.}$$

Once the rotation law is established, the rotational parameter has to be fixed. For instance one can fix v_0 (j_0) in the case of the v-constant (j-constant) law. However, the numerical procedure developed by Hachisu works in the following way. A simple density profile is chosen as initial guess and $\Phi[\rho(r,\mu)]$ is computed. Then with eq.1.39 a new density profile is calculated for a specific rotation law and fixed polytropic constants and it is used as the initial guess for the next iteration. In the HSCF method the numerical procedure to compute uniquely equilibrium models is done by using adimensional quantities which are obtained by fixing two parameters: the maximum value for the density profile ρ_{max} and the axis ratio r_p/r_e. The last corresponds to the rotational parameter and in particular it allows to determine solutions in a numerically more stable manner compared to the code of Ostriker&Mark[58]. Hachisu applied this method to study rapidly rotating polytropes and withe dwarfs by using polytropic and fully degenerate equations of state respectively. Both uniformly and differentially rotating models have been computed. The HSCF method is a very powerful, brand-new, self-consistent field method for the Newtonian gravity[59]. This approach has been extended to study rapidly rotating relativistic stars within the framework of general relativity as we will see later.

1.3 Rotating NSs

Ordinary Newtonian stars are not strongly rotating objects. The centrifugal effects on these stars are largely less evident respect to the gravitational ones. Because of this we can study ordinary stars applying non-rotating and spherically symmetric models and obtaining reasonably good results. However the situation is more complicated in the case of compact stars. During the gravitational collapse leading to the formation of these objects, the conservation of the angular momentum enhances the rotation. For instance, being $\Omega \sim 1/r^2$ (because of the conservation of the angular momentum), we can roughly estimate the ratio between the strength of gravity and centrifugal forces in the following way:

$$\sim \frac{1/r^2}{\Omega^2 r} \sim \frac{r^3}{r^2} = r \tag{1.41}$$

Since the great decrease of the stellar radius during the collapse, one could expect a remarkable enhancement of the rotation and thus of the centrifugal effects in compact stars. However one has also to take in account general relativistic effects. Indeed the collapse makes the gravity so strong inside the star that these ones cannot be neglected. Centrifugal forces in general relativity show a different behaviour compared to the non-relativistic case. When a compact star rotates, the spacetime close to it is involved in the rotation. A rotating spacetime generates some very peculiar effects which cannot be describe within the framework of classical mechanics. One of these effects is the "dragging" of the local inertial frames, which is named as *Lense-Thirring effect.* This means that an inertial frame near a rotating star is found to rotate around its center relative to the distant stars. In particular, the closer it approaches the star, the more rapidly it rotates. This should be impossible within the Newtonian physics because of the angular momentum conservation law. However, in the relativistic case, one has to keep in mind that all the energy sources located at a certain point of the spacetime are also gravitational sources and then they influence the fabric of spacetime itself. Because of this, the rotational kinetic energy of the star is employed on modeling the gravity field and thus the spacetime, affecting the inertial frames which fill it. The rotation of local inertial frames influences the structure of rotating stars and also the efficiency of centrifugal forces. In particular, for an observer located in a given point on the star the relativistic centrifugal effect as well as the Keplerian angular velocity are not determined by the spin frequency Ω of the star but rather by the ratio Ω/ω, where ω is the own dragging frequency of a local inertial frame. The dependence between them can be analitically found by using the slow-rotation approximation. In this way one discovers that the dragging of the local inertial frames reduces the effects of the centrifugal force at the observed frequency Ω because ω is in the same sense as Ω[60].

The conservation of the angular momentum can yield very rapidly rotating neutron stars at birth. Simulations of the rotational core collapse of evolved rotating progenitors have demonstrated that rotational core collapse could result in the creation of neutron stars with rotational periods of the order of 1ms[61]. This evolution can be complicated by the presence of magnetic fields. These can be very strong at the birth of a compact star because the conservation of the magnetic flux during the collapse. According some studies, more slowly rotating neutron stars could be expected at birth as the result of the coupling between the magnetic field and the angular velocity between the core and the surface of the star[62]. Rotational periods of NSs have been well explored over the years. Pulsars exhibit a remarkable stable rotational period with a very slowly increase in time. The observed spin frequencies are higher than those of Newtonian stars. Observations have revealed pulsars time period approximately from 1 ms to 10 seconds[63] (i.e. from 10^{-1} to 10^{3} Hz). One can distinguish two populations of pulsars: the so-called 'normal pulsars' with a period of few seconds which increase secularly at rates $\sim 10^{-15} s/s$ and the MSPs with rotational period 1.4ms$\lesssim P \lesssim$ 30ms and increasing rate $\lesssim 10^{-19} s/s$[64]. MSPs are believed to be old NSs spun-up to millisecond periods by the accretion of matter from a binary companion[8]. Most of the observed MSPs are seen in the radio and γ-rays. For some MSPs we can also detect X-ray signals generated by the accretion mechanism, which allow us to measure their spin frequency. The measurements concern mainly the case of X-ray APMSPs and thermonuclear X-ray BNSs. For the first ones, X-ray pulsations due to the presence of hot spots on the stellar surface are observed. The spin frequencies of 15 X-ray APMSPs have been measured with a great accuracy[8]. In the case of X-ray BNSs, oscillations during thermonuclear X-ray bursts are used to constrain the angular velocity. One can estimate the pulsar spin frequency indirectly by measuring the frequency of these oscillations. Through this method it has been possible to determine the spin frequency of 10 X-ray BNSs[8].

Several observed pulsars have frequency bigger than 100 Hz. In particular, 10 X-ray APMSPs and 14 radio/gamma-ray pulsars rotate at $\geq$500 Hz. So far, the fastest X-ray APMSP is 4U1608-522 with a frequency of 620 Hz[65](1.613 ms). Among all the NSs the radio MSPs PSR J1748-244 is the fastest rotating observed up to now, with a spin frequency of 716 Hz (1.396 ms). It is located in the globular cluster Terzan 5 and it was detected using the Green Bank Telescope (GBT). Terzan 5 appears to be a particularly good place to search for fast pulsars, and is now known to contain 5 of the 10 fastest-spinning pulsars observed anywhere in the Galaxy[66]. The frequencies of currently observed radio and γ-ray pulsars and X-ray MSPs rotating at a frequency larger than 100 Hz are shown in Figure1.3.

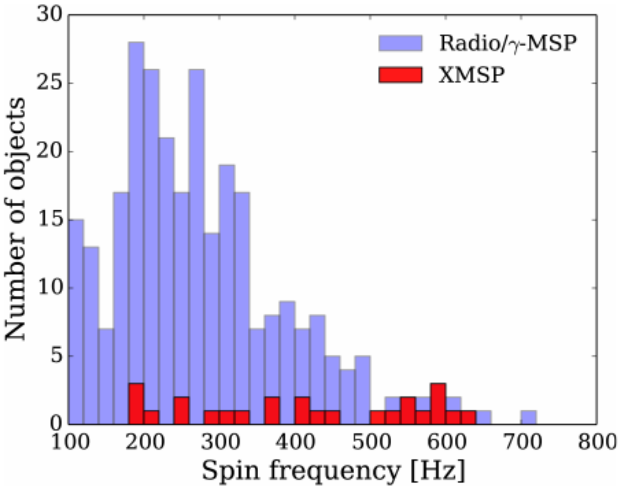

Figure 1.3: Currently observed spin frequencies of radio/gamma-ray MSPs and X-ray MSPs. Reference: *Haensel et al. 2016, European Physical Journal A.*

NSs are faster rotators compared Newtonian stars, however it's easy to show that even the most rapidly spinning pulsar is distorted by rotation only slightly. In fact if we consider again the ratio between centrifugal forces and gravity we obtain for PSR J1748-244 that $\Omega^2 R^3/GM \approx 0.11 \ll 1$, where we put the observed value of Ω and we assumed $M = 1.4M_{\odot}$, $R = 10$ km. Therefore, the deviations from the spherical symmetry induced on the stellar structure by the rotation are generally quite small, at least for ordinary NSs. Because of these we can be computed models applying for instance the Hartle formalism. Within this approach it is possible to find quite simple relations between masses, radii and rotational periods. Therefore a measure of the spin frequency of NSs provides further constraints on the equation of state of ultra dense matter when combined with masses and radii measurements. By modeling rotating NSs we can see that rotation increase the limiting mass and the equatorial radius of the stars. This effect doesn't appear at the first order of the slow-rotation approximation but we have to probe higher order terms in which, for instance, multipole corrections on the gravitational mass are included. Clearly if one wants to investigate rapidly rotating configurations the approximate approach is not more valid and numerical codes are required to solve the fully general relativistic equations. Considering high spin frequency regimes, i.e. near the Keplerian-limit, could be useful to probe binary systems in which a NS is strongly accreted by a companion. In principle, accretion could drive a compact star to its mass-shedding limit. During the recycling, the NS could attain few millisecond periods after accreting only $\sim 0.1 M_\odot$ and $\sim 0.25 M_\odot$ to attain submillisecond periods[67]. For a wide range of candidates for NS equation of state, it has been show that the Keplerian limit sets a minimum period of about $0.5 - 0.9$ ms[43]. It can be shown that the Keplerian frequency can be estimated with the following empirical formulae[8]:

- $f_K(M_s) \approx 1.08\mathrm{kHz}\big(M_s/M_\odot\big)^{1/2}\big(R_s/10\mathrm{km}\big)^{-3/2}$
- $f_K(EOS) \approx 1.22\mathrm{kHz}\big(M_{s,max}/M_\odot\big)^{1/2}\big(R_{s,max}/10\mathrm{km}\big)^{-3/2}$

The first estimate is valid for NSs with or without exotic core; here M_s, R_s are the mass and the radius of a static configuration with the same baryon mass of the Keplerian configuration. Moreover. this estimate is valid within the gravitational mass range $[0.5M_\odot, 0.9M_{s,max}]$, where $M_{s,max}$ is the mass of the non-rotating equilibrium configuration with maximum mass. The second equation instead is valid both for NSs and for strange-quark stars; it gives the value of the maximum frequency along the sequence of Keplerian models. Here $R_{s,max}$ is the radius of the star with mass $M_{s,max}$. The dependence of this equation on $M_{s,max}$ implies a tight dependence also on the equation of state of NS, as we will see later. In particular, we could apply it together with the condition for the stability of stars $\Omega < \Omega_K$ in order to constrain the equation of state. However, it is clear by the equation that rotation rates faster than a millisecond are required to rule out equations of state[68]. Nevertheless, these rapidly rotating NSs have not been observed so far.

At birth a NS is expected to be rotating differentially. However after few time, several dissipative processes act to damp the differential rotation, sharing the angular momentum among different layers and enforcing the uniform rotation. The shear viscosity represents the slowest mechanism; it acts against the differential rotation on a timescale of dozens of years[69]. Other mechanisms like convective and turbulent motions can enforce the uniform rotation within less time ($\sim$ 1 day[70]). More recent studies used MHD simulations to probe the stability of differentially rotating isolated NSs. Some suggest that magnetic braking and viscosity combine together to drive the star towards the uniform rotation, even if the seed magnetic field and the viscosity are small[71]. A timescale $\sim$ 1 min for the setting of the uniform rotation is provided by these investigations. All of these results allow us to model accurately isolated rotating relativistic stars with an equilibrium configuration of a uniformly rotating relativistic fluid. We will discuss later the bulk properties of uniformly rotating NSs which are modeled numerically with high accuracy codes. We will focus on both slowly-rotating and rapidly-rotating objects showing how the fully relativistic treatment is necessary near the Keplerian-limit. In particular we will probe the effects of the rotation and of the equation of state on the maximum mass attainable by rotating stars. Moreover, even if differential rotation seems to be an energetically unfavorable regime when a NS is already formed, the stellar evolution can restore it at a certain moment of the star's life. Numerical simulations in fully general relativity[72] have shown that differentially rotating NSs can be formed after the merging of two compact stars. It is very important to know if the outcome of such event is a Black Hole (BH) or a compact star, since this affects greatly the astrophysical phenomena happening during the post-merger phase. In particular, the signals detected from the merging (GWs, GRBs, Kilonovae, etc.) are very different among the two cases. It has been shown that rotation allows very high masses for neutron stars. A uniform rotation can increase the maximum NS mass up to 20% more than the upper limit on the mass of non rotating NSs. In particular, NSs with rest masses higher than the maximum rest mass of static models with the same equation of state are referred to as *supramassive* stars[73]. In the case of differentially rotating NSs the increase is even more high and rest masses bigger than the maximum of uniformly rotating NSs are allowed. These objects are referred to as *hypermassive* stars[53]. Their masses depend on the rotational profile within them. In the case of a slowly rotating envelope, the inner part of these stars can rotate very fast without bringing the star towards the Keplerian limit. Therefore, the differential rotation allows to reach equilibria with rapid central rotations and high masses and which don't loose matter from the equator. It has been shown[74] for several equations of state that the increment on the mass becomes bigger with the increase of the ratio between the central and the equatorial frequencies (Ω_c/Ω_e) up to a moderate value of it, then a decrease is seen for higher values of the ratio. More stiff equations of state also allow bigger mass increment for the same Ω_c/Ω_e. Some configurations exceed the maximum allowed mass of the corresponding non rotating star by more than a factor of 2. However, even if the differential rotation allows to reach these high masses equilibria, most of them are unstable. The simulations have shown that hypermassive NSs are often unstable for non-axisymmetric modes[53]. Nevertheless, configurations which are only secular unstable for these modes can show an increment on the mass with respect to the maximum of a static configuration of $\sim 50-60\%$ (about $30-40\%$ more than the uniformly rotating case)[74]. With a more high mass attainable, even if secularly unstable, a differentially rotating NS could survive for a sufficiently long time. In particular, as we will discuss late, in the case of a NS-NS merger this could allow delayed collapses to BHs. Instabilities driven by viscous processes, magnetic field and also GWs, could also bring the hypermassive NS towards a uniformly rotating configuration, which could remain stable for several years as supramassive star. There are lots of research which have studied the importance of the differential rotation during the merging of two compact stars and during the post-merger phase. We will focus on them in the last chapter of this thesis. In particular, we will try to model the post-merger phase of GW170817 by applying several studies concerning uniformly and differentially rotating NSs. In order to do this a theoretical overview about relativistic stars is needed. We discuss this in the next two chapters.

Chapter 2

General Relativity

Most of the stars in the Universe can be described with very high accuracy by the Newton's theory of gravity. We often refer to us as "Newtonian stars". Above all, each moment of the life of low-mass stars ($M \lesssim 8M_{\odot}$) until their death can be investigated within the classical physics. This approach doesn't fail to explain gravity also when handling degenerate objects like withe dwarfs, for which quantum mechanics is necessary to describe the behaviour of particles inside the star. However, compact objects generated by dying massive stars cannot be probed in this way. In these configurations several solar masses are confined within radii less than ~ 15 km and thus the inner density can reach values few times bigger than the nuclear density at the saturation. Neutron stars seem like giant atomic nuclei but with masses comparable to the mass of the Sun. The gravitational potential of these stars can be described only within the framework of the General Relativity. In the following paragraphs we are going to discuss the relativistic[1] theory of neutron stars. We will focus particularly on the relativistic description of rotating compact stars examining numerical approaches applied to solve the Einstein equations.

2.1 Preliminaries

Einstein's theory of general relativity describes the nature through laws of physics which have the same form among different arbitrary (i.e. not only inertial) reference frames. This is the so-called *General Covariance Principle.* In particular, he formulated the so-called *Equivalence Principle* which is based on the equality of the inertial and the gravitational mass. At every space-time point in an arbitrary gravitational field it is possible to choose a "locally inertial coordinate system" such that, within a sufficiently small region of the point in question, the laws of nature take the same form as in unaccelerated Cartesian coordinate systems in the absence of gravitation[75]. The laws of physics within inertial reference frames are known from the Special Theory of Relativity. Because of the above principle, to extend them to the case of accelerated observers one has to think about a gravitational field filling the spacetime. The key to achieve this aim represents probably the "heart" of the

---

[1] As we will see in the Chapter3 also the Quantum Physics is indispensable to deal with neutron stars because the strong dependence of their bulk properties on the equation of state of nuclear matter.

General Relativity: gravity *curves* spacetime. The laws of nature within accelerated observers are obtained by considering curved spacetimes. Inertial reference frames lie on a flat, homogeneous and isotropic spacetime while accelerated reference frames lie on a curved, inhomogeneous and anisotropic spacetime.

Let us consider the line element within the framework of special relativity for an inertial observer:

$$ds^2 = \eta_{\mu\nu} dx^\mu dx^\nu \tag{2.1}$$

where $\eta_{\mu\nu}$ are the covariant components of the Minkowsky metric. We can perform a coordinate transformation $x^\mu \to x^{\mu\prime}$ from the inertial frame to an accelerated frame, whose spacetime coordinates are labeled by $x^{\mu\prime}$. During the transformation the line element ds^2 doesn't change because it is a relativistic invariant. If we denote with $g_{\mu\nu}$ the covariant components of the new metric of the accelerated observer, because of the transformation we have that:

$$ds^{2\prime} = g_{\mu\nu} dx^{\mu\prime} dx^{\nu\prime} = g_{\mu\nu} \frac{\partial x^{\mu\prime}}{\partial x^\rho} \frac{\partial x^{\nu\prime}}{\partial x^\sigma} dx^\rho dx^\sigma = ds^2 = \eta_{\rho\sigma} dx^\rho dx^\sigma \tag{2.2}$$

Thus we can write the coefficients of the new metric as:

$$g_{\mu\nu} = \eta_{\rho\sigma} \Big(\frac{\partial x^{\rho\prime}}{\partial x^\mu}\Big)^{-1} \Big(\frac{\partial x^{\sigma\prime}}{\partial x^\nu}\Big)^{-1} \tag{2.3}$$

where $\partial x^{\rho\prime}/\partial x^\mu = (\partial x^{\rho\prime}/\partial x^\mu)(x)$ represents the coefficients of the matrix of the transformation between the two reference frames, which change among different points of the spacetime because of its inhomogeneity. Given the transformation law between the two systems, one can compute the new metric $g_{\mu\nu}$. This metric is associated with a curved spacetime. By definition we have also that $g_{\mu\nu} = g_{\nu\mu}$. Moreover, the general covariance principle ensures that always $g_{\mu\nu} = \eta_{\mu\nu}$ locally on the spacetime. Concerning the case of a particle freely moving within a curved spacetime, one finds the so called "geodesic equation":

$$\frac{d^2 x^{\mu\prime}}{d\lambda^2} + \Gamma^\mu_{\nu\rho} \frac{dx^{\nu\prime}}{d\lambda} \frac{dx^{\rho\prime}}{d\lambda} = 0 \tag{2.4}$$

where $\Gamma^\mu_{\nu\rho} := \frac{\partial x^{\mu\prime}}{\partial x^\alpha} \frac{\partial^2 x^\alpha}{\partial x^{\nu\prime} \partial x^{\rho\prime}}$ are the coefficients of the so-called *Affine Connection.* In particular, the affine connection for the curved spacetime of general relativity, which is characterized by a local flatness, is called *Levi-Civita Connection.* This is symmetric in its lower indices: $\Gamma^\mu_{\nu\rho} = \Gamma^\mu_{\rho\nu}$ (because of the Schwarz theorem). This quantity can be defined within a covariant form in terms of the first derivatives of the metric tensor as follows:

$$\Gamma^\mu_{\nu\rho} = \frac{1}{2} g^{\mu\lambda} \Big(\frac{\partial g_{\lambda\rho}}{\partial x^\nu} + \frac{\partial g_{\lambda\nu}}{\partial x^\rho} - \frac{\partial g_{\rho\nu}}{\partial x^\lambda}\Big) \tag{2.5}$$

An other relevant question concerns the definition of the differential operator within the framework of general relativity. This is a matter of great interest because we often want to study differential equations associated with relativistic systems, like neutron stars. Therefore, for a generic tensor field, one defines the covariant derivative ∇_ξ as follows:

$$\nabla_\xi T^{\mu\ldots\nu}_{\rho\ldots\sigma} = \frac{\partial}{\partial x^\xi} T^{\mu\ldots\nu}_{\rho\ldots\sigma} + \Gamma^\mu_{\xi\lambda} T^{\lambda\ldots\nu}_{\rho\ldots\sigma} + \ldots + \Gamma^\nu_{\xi\lambda} T^{\mu\ldots\lambda}_{\rho\ldots\sigma} - \Gamma^\lambda_{\xi\rho} T^{\mu\ldots\nu}_{\lambda\ldots\sigma} - \ldots - \Gamma^\lambda_{\xi\sigma} T^{\mu\ldots\nu}_{\rho\ldots\lambda} \tag{2.6}$$

In particular one finds that $\nabla_\xi g_{\mu\nu} = 0$. This is an other important feature of the Levi-Civita connection. Moreover, by taking the double covariant derivative of a vector A_μ:

$$\nabla_\rho \nabla_\sigma A_\mu - \nabla_\sigma \nabla_\rho A_\mu = A_\lambda R^\lambda_{\mu\sigma\rho} \tag{2.7}$$

where the quantity $R^\lambda_{\mu\sigma\rho}$ is the so-called *Riemann curvature tensor* which is defined as:

$$R^\lambda_{\mu\sigma\rho} := \frac{\partial}{\partial x^\sigma}\Gamma^\lambda_{\mu\rho} - \frac{\partial}{\partial x^\rho}\Gamma^\lambda_{\mu\sigma} + \Gamma^\alpha_{\mu\rho}\Gamma^\lambda_{\alpha\sigma} - \Gamma^\alpha_{\mu\sigma}\Gamma^\lambda_{\alpha\rho} \tag{2.8}$$

We can see that because of the expression of the connection in terms of the derivatives of the metric, the Riemann tensor contains second order derivatives of the metric. These describe the curvature of spacetime. By lowering the index on the Riemann tensor $R_{\lambda\mu\sigma\rho} = g_{\lambda\alpha} R^\alpha_{\mu\sigma\rho}$ it can be shown that it satisfies the following identities:

$$R_{\lambda\mu\sigma\rho} = -R_{\mu\lambda\sigma\rho} = -R_{\lambda\mu\rho\sigma} \tag{2.9}$$

$$R_{\lambda\mu\sigma\rho} = R_{\sigma\mu\lambda\rho} = R_{\mu\sigma\rho\lambda} \tag{2.10}$$

$$R_{\lambda\mu\sigma\rho} + R_{\lambda\sigma\rho\mu} + R_{\lambda\rho\mu\sigma} = 0 \tag{2.11}$$

$$\nabla_\xi R_{\lambda\mu\sigma\rho} + \nabla_\sigma R_{\lambda\mu\rho\xi} + \nabla_\rho R_{\lambda\mu\xi\sigma} = 0 \tag{2.12}$$

The trace component of the Riemann tensor is the so-called *Ricci tensor*, that is defined as $R_{\mu\nu} := R^\alpha_{\mu\alpha\nu}$. It describes the deformation in the volume of bodies produced by a local source of gravitational field and it vanishes in the case of an empty spacetime. From the Ricci tensor we can also define the *scalar curvature*: $R = g^{\mu\nu} R_{\mu\nu}$.

From the identities 2.9-2.12 we can obtain the following result:

$$\nabla_\xi (R^{\mu\nu} - \frac{1}{2} R g^{\mu\nu}) = 0 \tag{2.13}$$

The object inside the brackets is the so-called *Einstein curvature tensor*:

$$G^{\mu\nu} := R^{\mu\nu} - \frac{1}{2} R g^{\mu\nu} \tag{2.14}$$

that is a covariant divergenceless tensor. It is constructed from the Riemann curvature tensor and it is symmetric. In particular since only the Ricci tensor and the scalar curvature appear inside the definition of $G^{\mu\nu}$, solutions of the equation $\nabla_\xi G^{\mu\nu} = 0$ give us information about the non-tidal curvature of the spacetime produced by gravity. There are three possible minimal[2] solutions, which are known as *Einstein's filed equations*:

$$G^{\mu\nu} = 0 \tag{2.15}$$

$$G^{\mu\nu} = k T^{\mu\nu} \tag{2.16}$$

$$G^{\mu\nu} = k T^{\mu\nu} + \Lambda g^{\mu\nu} \tag{2.17}$$

where k and Λ are constants. Eq.2.15 is the set of differential equations describing the case of an empty spacetime. This can be used for instance to describe the spacetime outside a relativistic star. Equations 2.16, 2.17 instead concern the case

---

[2] This means with the least number of terms inside equations.

of a not empty spacetime where there are gravitational sources which warp it. The last is a mathematical extension of eq.2.16 and it contains the so-called *cosmological constant* Λ. Cosmological theories deal with this constant and associate it with the vacuum energy. This is currently related to the so-called *dark energy* that has been hypothesized to explain the observed accelerated expansion of the Universe. According to recent estimates[76] the value of the cosmological constant is very small ($\Lambda = (4.24 \pm 0.11)10^{-66} eV^2$). Its effect is indeed cosmological, stellar structures are unaffected by it. Because we want to study compact stars we focus on eq.2.16. In this equation the right hand side term represents the reason of the spacetime curvature. Clearly, this contains also the case of an empty space (i.e. $T^{\mu\nu} = 0$). According the Einstein's Theory of General Relativity, the tensor $T^{\mu\nu}$ describes all the mass-energy contributions to the curvature of the spacetime. It also has to be covariant divergenceless in order to satisfy the equality with the Einstein tensor. This particular quantity is the so-called *stress-energy tensor*. Its expression depends on the properties of the mass-energy distribution associated with a system, including viscosities, charge and magnetic fields. We need the proper form of $T^{\mu\nu}$ according to the kind of physical system that we want to consider. Eventually, into the eq.2.16 we have $k = 8\pi G/c^4$ because the Poisson equation is the Newtonian limit of the Einstein's field equation. Once we know the metric of the spacetime that wraps bodies and assuming a suitable form for the stress-energy tensor, we can make use of eq.2.16 in order to investigate the mass-energy distribution within these objects, their mass-energy density and the particles motion. Otherwise, if we know all the contributions of mass and energy, the Einstein's field equations allow us to compute the structure of the spacetime close and inside bodies.

Besides the gravitational field equations one needs other dynamical equations to study the structure and the evolution of self-gravitating systems. Indeed we saw that the dynamics of Newtonian barotropic self-gravitating fluids is described also by a continuity equation (eq.1.4) and by the Navier-Stokes equation (eq.1.5). Also for relativistic bodies we require other equations besides the Einstein's field equations. Within general relativity, the dynamical evolution of a relativistic fluid is governed by the following differential equations:

$$\nabla_\nu T^{\mu\nu} = 0 \tag{2.18}$$

$$\nabla_\xi (\rho u^\xi) = 0 \tag{2.19}$$

where ρ is the baryon density scalar field and $u^\xi = dx^\xi/d\lambda$ is the 4-velocity vector field. The first equation is the vanishing divergence of the stress-energy tensor, the second describes the conservation of baryons. We can define the projection operator orthogonal to the 4-velocity as: $q^{\alpha\beta} = g^{\alpha\beta} + u^\alpha u^\beta$. Given a vector V^μ, the projection along u^ν is the scalar product $g_{\mu\nu} V^\mu u^\nu$ and the projection orthogonal to u^ν is given by the vector[3] $q^{\nu\lambda} g_{\lambda\mu} V^\mu$. As we will see soon, the projection orthogonal to the 4-velocity of the eq.2.18 gives the relativistic Euler equation; this can be used together with the Einstein equations to solve the structure problem of a barotropic ideal relativistic fluid in equilibrium.

---

[3] In fact we have that: $u^\alpha g_{\alpha\nu} q^{\nu\lambda} g_{\lambda\mu} V^\mu = u^\lambda V_\lambda + (g_{\alpha\nu} u^\alpha u^\nu) u^\lambda g_{\lambda\mu} V^\mu = u^\lambda V_\lambda - g_{\lambda\mu} u^\lambda V^\mu = 0$, where we used the normalization of the 4-velocity $g_{\alpha\nu} u^\alpha u^\nu = -1$.

During our previous discussion about Newtonian fluids we have showed that the study of equilibrium configurations is often done making some assumptions about the symmetry degree of the problem. Symmetries yield more handy problems because they reduce the number of degrees of freedom. In particular if one choose a suitable coordinate system, these symmetries make more simple the dynamical equations. Symmetries are not only a mathematical guile but they are related to actual "good" properties of natural systems. Clearly, we cannot find in nature systems which are perfectly symmetric. A symmetric problem is an approximation of the real one. However, there are some situations in which the symmetric approach works well and it allows us to find solutions that are very close to the reality. For instance, this is the case of non-rotating and rotating self-gravitating systems that we described before within the Newtonian fluid dynamics. Now we want to study symmetries within the framework of general relativity. The first consideration is the following: if there are some symmetries associated with a relativistic system, these imply a symmetric configuration of matter, mass and energy and thus of the spacetime itself. Because of this, the symmetries of relativistic bodies are revealed by the own metric of their spacetime. A symmetry of the spacetime is a coordinate transformation which preserves the metric tensor $g_{\mu\nu}$ and that is called *isometry.* Isometries of the spacetime are studied through the formalism of the Lie-derivatives and the Killing fields. Briefly, the Lie-derivative is a differential operator which measures the change of a tensor field along the flow associated with a vector field. It arises naturally in the context of the Newtonian fluid dynamics when one wants to consider quantities which are preserved along streamlines. Within the classical mechanics, a scalar field ϕ is preserved or *dragged along* by the flow of a fluid if its value is constant on fluid elements, that is:

$$\frac{d}{dt}\phi = \frac{\partial}{\partial t}\phi + \mathbf{v} \cdot \vec{\nabla}\phi = 0 \tag{2.20}$$

where $\mathbf{v}$ is the velocity vector field of the fluid. In this case it's said that ϕ is *Lie-derived* by the vector field $\mathbf{v}$ that generates the flow and the Lie-derivative operator is defined as: $\mathcal{L}_{\mathbf{v}} := \partial_t + \mathbf{v} \cdot \vec{\nabla}$. This notion can be generalized to the case of vector and tensor fields and within curved spacetimes. We will not go into details about this. The general expression for the Lie-derivative of a tensor field $T^{a_1...a_m}_{b_1...b_n}$ in a curved spacetime is the following:

$$\mathcal{L}_{\mathbf{v}} T^{a_1...a_m}_{b_1...b_n} = v^c \nabla_c T^{a_1...a_m}_{b_1...b_n} - T^{c...a_m}_{b_1...b_n} \nabla_c v^{a_1} - ... - T^{a_1...c}_{b_1...b_n} \nabla_c v^{a_m} + T^{a_1...a_m}_{c...b_n} \nabla_{b_1} v^c + ... T^{a_1...a_m}_{b_1...c} \nabla_{b_n} v^c \tag{2.21}$$

where v^c are controvariant components of the vector field $\mathbf{v}$ and all the indices are spatiotemporal. By using the definition of the covariant derivative one obtains that:

$$\begin{aligned}\mathcal{L}_{\mathbf{v}} T^{a_1...a_m}_{b_1...b_n} = {} & (..) + [v^c(\Gamma^{a_1}_{cs} T^{s...a_m}_{b_1...b_n} + ... + \Gamma^{a_m}_{cs} T^{a_1...s}_{b_1...b_n} - \Gamma^{s}_{cb_1} T^{a_1...a_m}_{s...b_n} - ... - \Gamma^{s}_{cb_n} T^{a_1...a_m}_{b_1...s})] + \\ & + [-T^{c...a_m}_{b_1...b_n} \Gamma^{a_1}_{cs} v^s - ... - T^{a_1...c}_{b_1...b_n} \Gamma^{a_m}_{cs} v^s + T^{a_1...a_m}_{c...b_n} \Gamma^{c}_{b_1 s} v^s + ... + T^{a_1...a_m}_{b_1...c} \Gamma^{c}_{b_n s} v^s]\end{aligned}$$

where the first right hand side term inside the brackets contains all the terms associated with partial derivatives. It's easy to note that for the spacetime of the General relativity the two last terms inside the square brackets delete one each other. This is because of the property of the Levi-Civita connection: $\Gamma^{\mu}_{\nu\rho} = \Gamma^{\mu}_{\rho\nu}$. Thus the

Lie-derivative on the spacetime of general relativity can be written as follows:

$$\mathcal{L}_{\mathbf{v}}T^{a_1...a_m}_{b_1...b_n} = v^c\partial_c T^{a_1...a_m}_{b_1...b_n} - T^{c...a_m}_{b_1...b_n}\partial_c v^{a_1} - ... - T^{a_1...c}_{b_1...b_n}\partial_c v^{a_m} + T^{a_1...a_m}_{c...b_n}\partial_{b_1}v^c + ... T^{a_1...a_m}_{b_1...c}\partial_{b_n}v^c \tag{2.22}$$

A vector field ξ^α is called *Killing field* if the metric tensor is Lie-derived by it: $\mathcal{L}_\xi g_{\mu\nu} = 0$. We note that:

$$\mathcal{L}_\xi g_{\mu\nu} = \xi^\lambda \nabla_\lambda g_{\mu\nu} + g_{\lambda\nu}\nabla_\mu \xi^\lambda + g_{\mu\lambda}\nabla_\nu \xi^\lambda = \nabla_\mu g_{\nu\lambda}\xi^\lambda + \nabla_\nu g_{\mu\lambda}\xi^\lambda = \nabla_\mu \xi_\nu + \nabla_\nu \xi_\mu$$

where we used the fact that the metric tensor is covariant divergenceless. Thus a Killing field is a vector field ξ^α that satisfy the so-called *Killing equation*:

$$\nabla_\mu \xi_\nu + \nabla_\nu \xi_\mu = 0 \tag{2.23}$$

This equation is very important. If one solves it determining all the vectors ξ^α thus *all* the isometries of the spacetime are revealed. In fact if we have that $\mathcal{L}_\xi g_{\mu\nu} = 0$ for a given Killing field ξ^α, then the coordinate transformation $x^{\alpha\prime} = x^\alpha + \xi^\alpha$ among the two different reference frames (x^μ) and $(x^{\mu\prime})$ preserves the metric. Vice-versa if we know that the transformation $x^{\alpha\prime} = x^\alpha + \xi^\alpha$ preserves the metric, then ξ^α is a Killing field satisfying the Killing equation. It is important to note that generally an expression for the metric tensor $g_{\mu\nu}$ doesn't show all the spacetime symmetries. In these situations one has to probe the Killing equation. Using Killing fields is the only way to handle spacetime symmetries. Like the Newtonian case, usually one studies relativistic physical systems assuming some reasonable symmetries and to do this he applies the Killing fields formalism. However, there are special cases in which the metric tensor shows some symmetries. These correspond to the situations where the metric is independent on some coordinates $x^{\mu*}$, i.e. $\partial g_{\mu\nu}/\partial x^{\mu*} = 0$. In these cases we can state that the transformation $x^{\mu*\prime} = x^{\mu*} + \alpha^{\mu*}$ for a constant vector $\alpha^{\mu*}$ is an isometry of the spacetime. In these cases $\xi := \partial/\partial x^{\mu*}$ is a Killing field, whose controvariant components are $\xi^\alpha = \partial x^\alpha/\partial x^{\mu*} = \delta^\alpha_{\mu*} = g^{\alpha\rho}\delta_{\rho\mu*}$. Eventually, from the geodesic equation 2.4 one can obtain the following expression:

$$\frac{d}{d\lambda}u_\nu = \frac{1}{2}\Big(\frac{\partial}{\partial x^\nu}g_{\alpha\beta}\Big)u^\alpha u^\beta \tag{2.24}$$

This equation shows that if there is a symmetry into the expression of the metric tensor, for instance $\partial g_{\mu\nu}/\partial x^{\mu*} = 0$, then the quantity $u_{\mu*}$ is a constant of motion.

Before starting with the study of relativistic stars some few considerations are useful. Generally, NSs have a very complicated structure (such as solid crust, outer and inner magnetic fields, quark core, differentially rotating layers, etc.) and several extreme events can mark their evolution (such as mergers, strong accretion phases, bursts, etc.). Their description represents a challenge also for the most advanced physical theories. However there is the possibility to make some theoretical assumptions in order to simplify the treatment. Depending on which phase of the lifetime of these stars one wants to investigate, several physical effects can be neglected. At birth, a NS is expected to be hot and differentially rotating. However, if isolated, a short time after its formation ($\lesssim$ 1 year[61]) the NS cools down below roughly 10^9K and because of several mechanisms (that we discussed before) it starts to rotate rigidly. The temperature corresponds to a thermal energy of particles that is much smaller than their Fermi energy[4], which is very high ($\sim$ 60MeV) because of

---

[4] Because the high densities, fermionic matter which reside inside NSs is completely degenerate.

the enormous densities inside the star. Moreover the magnetic fields, although really important for the phenomena observed in the magnetosphere and for the damping of the differential rotation, do not alter the structure of NSs, unless in the case of configurations with magnetic field strengths significantly higher than the typical observed values[61]. Because of all these reasons we can assume a barotropic, uniformly rotating and perfect fluid to model isolated NSs. We will study differentially rotating objects only during the analysis of post-merger neutron star configurations that we will probe in the last part of this thesis. Within the assumption of barotropic fluid[5] we need to solve only the Einstein equations and the Euler equations in order to compute equilibrium configurations. Moreover a perfect fluid is a medium in which the pressure is isotropic in the rest frame of each fluid element and shear stresses and heat transport are absent. The Special Theory of Relativity shows that the stress-energy tensor describing a perfect fluid takes the following form within an arbitrary (inertial) frame:

$$T_{\mu\nu} = P\eta_{\mu\nu} + (P+\epsilon)u_\mu u_\nu \tag{2.25}$$

where P and ϵ are the local values of the fluid pressure and total mass-energy density respectively. It should be noted that ϵ and P haven't the same unit of measure; actually, P and ϵc^2 have the same unit of measure. In the eq.2.25 we assumed $c = 1$. Hereafter we will ever use the so called *gravitational units*, for which: $G = c = k_B = 1$ (k_B is the Boltzmann constant). The generalization of the stress-energy tensor within the framework of the General Relativity can be obtained directly by applying the covariance principle. Therefore, eq.2.25 is true locally on the spacetime and for its generalization we need only to change the metric:

$$T_{\mu\nu} = Pg_{\mu\nu} + (P+\epsilon)u_\mu u_\nu \tag{2.26}$$

With this expression we can formulate the structure equations in their final form. The Einstein equations become:

$$R^{\mu\nu} - \frac{1}{2}Rg^{\mu\nu} = 8\pi[Pg^{\mu\nu} + (\epsilon+P)u^\mu u^\nu] \tag{2.27}$$

Concerning the Euler equations we note that the projection orthogonal to u^ξ of the eq.2.18 is $q^{\xi\lambda}g_{\lambda\mu}\nabla_\nu T^{\mu\nu} = 0$. Moreover[6]:

$$\begin{aligned}
0 = q^{\xi\lambda}g_{\lambda\mu}\nabla_\nu T^{\mu\nu} &= (g^{\xi\lambda} + u^\xi u^\lambda)g_{\lambda\mu}\nabla_\nu(Pg^{\mu\nu} + (P+\epsilon)u^\mu u^\nu) = \\
&= (g^{\xi\nu} + u^\xi u^\nu)\nabla_\nu P + \nabla_\nu((P+\epsilon)u^\xi u^\nu) + u^\xi u_\mu \nabla_\nu((P+\epsilon)u^\mu u^\nu) = \\
&= q^{\xi\nu}\nabla_\nu P + \nabla_\nu((P+\epsilon)u^\xi u^\nu) + u^\xi(P+\epsilon)u^\nu u_\mu \nabla_\nu u^\mu - u^\xi\nabla_\nu((P+\epsilon)u^\nu) = \\
&= q^{\xi\nu}\nabla_\nu P + (P+\epsilon)u^\nu\nabla_\nu u^\xi
\end{aligned}$$

---

[5] As we discussed before, this condition implies that we can neglect thermal effects on the equation of state; thus $P = P(\rho)$, where ρ is the mass density field (Newtonian case). Within the relativistic case, the equation of state of a barotropic fluid is $P = P(\epsilon)$, where ϵ represent the total mass-energy density. This contains both the contributions of the mass and the internal energy (e) densities: $\epsilon = \rho + e$. The presence of e is needed because of the mass-energy equality.

[6] Here we use the fact that $g_{\mu\nu}u^\mu u^\nu = -1 \implies \nabla_\rho(u^\nu u_\nu) = 0 \implies u_\nu\nabla_\rho u^\nu = 0$.

Thus the differential equations become:

$$(g^{\xi\nu} + u^{\xi}u^{\nu})\frac{\nabla_{\nu}P}{P+\epsilon} = -u^{\beta}\nabla_{\beta}u^{\xi} \tag{2.28}$$

It can be shown that in the Newtonian limit eq.2.28 reduce exactly to the classical Euler equations (the Navier-Stokes equations for a perfect fluid).

We start now with modeling relativistic objects. Firstly, we discuss briefly the case of non rotating fluids. Here we describe the metric of the spacetime and its symmetries, then we focus on the equations of motions and on the method applied to solve them. We discuss the main properties of models computed by solving these equations. Eventually, in the following paragraphs, we will focus on rotating configurations.

2.2 Static, spherically symmetric spacetimes

We have seen before that non-rotating self gravitating Newtonian fluids in a hydrostatic equilibrium configuration are spherically symmetric. The same result for the relativistic case is not so obvious and only recently it has been proved for a generic equation of state: static general relativistic and perfect fluid stars in asymptotically-flat[7] spacetimes are spherically symmetric for physically reasonable equations of state[77]. Therefore in order to describe non rotating relativistic stars we consider a static and spherically symmetric spacetime. Static means that we can choose a coordinate reference frame in which the metric is time-independent, that is $\partial g_{\mu\nu}/\partial t = 0$. Moreover, the spherical symmetry implies that the spacetime is isotropic, i.e. its metric tensor is invariant under spatial rotations. Within the Special Theory of Relativity we know that the metric for the homogeneous and isotropic spacetime is the Minkowsky metric $\eta_{\mu\nu}$. By assuming a signature $(-,+,+,+)$ and using a Cartesian coordinate frame, the line element defined by this metric is:

$$ds^2 = \eta_{\mu\nu}dx^{\mu}dx^{\nu} = -dt^2 + dx^2 + dy^2 + dz^2 \tag{2.29}$$

This expression of the metric shows four Killing fields $(-1,0,0,0)$, $(0,1,0,0)$, $(0,0,1,0)$ and $(0,0,0,1)$, which represent the symmetry of the metric tensor for translations along the coordinate axes, that is the homogeneity of the spacetime. By writing this metric in spherical coordinates we have that:

$$ds^2 = \eta_{\mu\nu}dx^{\mu}dx^{\nu} = -dt^2 + dr^2 + r^2d\theta^2 + r^2\sin^2\theta d\phi^2 \tag{2.30}$$

Now the metric shows not constant coefficients and thus the homogeneity of the spacetime is not more evident from its expression. Nevertheless, this is only because we changed the coordinate frame. The spacetime doesn't change when others coordinates are chosen. By computing all the Killing fields one can finds again the previous isometries. However, the change of coordinates that we done is useful to show the isotropy of the spacetime. Indeed this new expression for the metric shows the presence of an other Killing field in spherical coordinate $(0,0,0,1)$, which comes from

---

[7] The curved spacetime of general relativity must become flat far away from all the gravitational sources. "Asymptotically-flat" means flat at infinite distance from gravitational sources.

the symmetry under ϕ-rotations: $\partial\eta_{\mu\nu}/\partial\phi = 0$. The same vector in Cartesian coordinates is $(0, -y, x, 0)$ that correspond correctly to a ϕ-rotation (a rotation around the $\hat{z}$-axis). The other two Killing fields that represent the other two rotations under which the spacetime is invariant are $(0, z, 0, x)$ (a rotation around the $\hat{y}$-axis) and $(0, 0, -z, y)$ (a rotation around the $\hat{x}$-axis). Thus by finding all the Killing fields we can demonstrate the homogeneity and the isotropy of the spacetime described with the metric 2.30. However, the static and spherically symmetric spacetime of the General Relativity must have a quite different metric tensor. Indeed, although it still preserves the condition of time-independence and isotropy, it is not more homogeneous. Thus we expect that the new metric tensor $g_{\mu\nu}$ in spherical coordinates has a form similar to 2.30 but with coefficients which can vary. However, this variation must respect the isotropy of the spacetime and its time-independence; thus the coefficients can be only functions of the radial coordinate r. It can be shown that in this case the most general form of the line element is:

$$ds^2 = -e^{2\nu(r)}dt^2 + e^{2\lambda(r)}dr^2 + r^2 d\theta^2 + r^2 \sin^2\theta d\phi^2 \tag{2.31}$$

Within this spacetime we want investigate the dynamics of a barotropic and perfect fluid. The components of the 4-velocity field are the following[8]:

$$\begin{aligned} u^\mu &= \frac{dx^\mu}{d\tau} = (e^{-\nu(r)}, 0, 0, 0) \\ u_\mu &= g_{\mu\sigma}u^\sigma = (-e^{\nu(r)}, 0, 0, 0) \end{aligned}$$

Therefore from the definition of the stress-energy tensor for perfect fluids (2.26) we obtain that:

$$\begin{aligned} T^{00} &= \epsilon(r)e^{-2\nu(r)} \\ T^{11} &= P(r)e^{-2\lambda(r)} \\ T^{22} &= \frac{P(r)}{r^2} \\ T^{33} &= \frac{P(r)}{r^2\sin^2\theta} \\ T^{i0} &= 0 \ \ \forall i = 1, 2, 3 \end{aligned}$$

Moreover, in the Euler equations (2.28) we have $\nu \equiv 1$ because the pressure depends only on the radial coordinate. Thus by using the above results concerning the 4-velocity we can obtain that:

$$\frac{1}{P(r) + \epsilon(r)}\frac{dP}{dr} = -e^{-2\nu(r)}\Gamma^1_{00} \tag{2.32}$$

By considering the covariant expression for the Christoffel symbols (2.5) one can obtain $\Gamma^1_{00} = e^{-2\lambda(r)}e^{2\nu(r)}d\nu(r)/dr$ and thus the Euler equations become the following:

$$\frac{1}{P(r) + \epsilon(r)}\frac{dP}{dr} = -e^{-2\lambda(r)}\frac{d\nu}{dr} \tag{2.33}$$

---

[8] Here we choose the proper time τ as the parameter of the fluid elements worldlines.

We need also to solve the Einstein equations (2.27) in order to compute stellar models. The solutions of them can be found by the calculation of the Ricci curvature tensor and the scalar curvature with the metric 2.31. In order to do this one has to compute all the coefficients of the Christoffel symbols. We will not discuss the details of this calculus here. However from the analysis of the Einstein equations, by defining the mass[9]:

$$m(r) = \int_0^r 4\pi r^2 \epsilon(r) dr \tag{2.34}$$

one finds that:

$$e^{-2\lambda(r)} = 1 - 2\frac{m(r)}{r} \tag{2.35}$$

$$\frac{d\nu}{dr} = \frac{m(r) + 4\pi r^3 P(r)}{r(r - 2m(r))} \tag{2.36}$$

Eventually to close the problem we need also an equation of state for the barotropic fluid, i.e. $P = P(\epsilon)$. The final set of structure equations whose solutions are relativistic spherical stellar models in hydrostatic equilibrium is obtained by combining equations 2.33-2.34-2.35-2.36 and it is the following:

$$\begin{aligned}
\frac{dm}{dr} &= 4\pi r^2 \epsilon(r) \\
\frac{dP}{dr} &= -[P(r) + \epsilon(r)]\frac{m(r) + 4\pi r^3 P(r)}{r^2} \\
\frac{d\nu}{dr} &= \frac{m(r) + 4\pi r^3 P(r)}{r(r - 2m(r))} \\
e^{-2\lambda(r)} &= 1 - 2\frac{m(r)}{r} \\
P &= P(\epsilon)
\end{aligned}$$

This is a problem of five equations in five unknowns P, ϵ, ν, m, λ; thus if one solves it a unique model is obtained. However in the above set we have three ODEs and so we need three boundary conditions in order to compute a unique solution. Concerning the third ODE we can use the fact that the analytical expression of $\nu(r)$ is known outside the star. This is the Schwarzschild solution, which is obtained for a spherically symmetric, static and empty spacetime by solving the equation 2.15 with the metric 2.31. This is the following:

$$ds^2 = -\left(1 - \frac{2M}{r}\right)dt^2 + \left(1 - \frac{2M}{r}\right)^{-1} dr^2 + r^2 d\theta^2 + r^2 \sin^2\theta d\phi^2 \quad (r \geq R) \tag{2.37}$$

Here $M = m(R)$ is the "gravitational mass" of the star[10], and R is the stellar radius that is defined by the condition $P(R) = 0$ (the pressure vanishes at the edge of the

---

[9] The name "mass" derives from the similar expression for the mass of a Newtonian fluid within a sphere of radius r. However this is not the same mass: ϵ contains also the contribution of the internal energy density together with the mass density ρ. Thus $m(r)$ corresponds to the total mass-energy contained within the radius r. We will discuss several "masses" of NSs in the next paragraph.

[10] We will explain its meaning in the next paragraph.

star[11]). From the Schwarzschild solution we know that $\nu(r) = 1/2 \ln{(1 - 2M/r)}$ for $r \geq R$ and thus the boundary condition for the third ODE is $\nu(R) = 1/2 \ln{(1 - 2M/R)}$. To fix the values of R and M we need to solve the first two ODEs. The boundary condition for the first one is $m(0) = 0$ (a null mass is contained within a radius $r = 0$). Concerning the second one (which is the so-called *TOV-equation*) we take the boundary condition $P(0) = P_0$, which correspond to fix the value of the central mass-energy density $\epsilon(0) = \epsilon_c$ in the case of a barotropic equation of state. Actually, the solution of the structure problem is a sequence of equilibrium stellar configurations parameterized by the central mass-energy density. This is a so-called *one-parameter sequence*. For each value of ϵ_c we can compute a unique model of static relativistic star. In the following we report some results concerning non-rotating models of NSs and we discuss their properties. We have computed models of static NSs by using the `RNS` code. This code is mainly employed to study models of rapidly rotating compact stars with polytropic or realistic equations of state. However it contains also a task which allows to compute static configurations. Since we will use it to investigate rotating NSs we will discuss after in details how it works. The following models lie on three different one-parameter sequences because they are computed applying three different realistic equations of state (EoS). The mean range of values of ϵ_c that we have considered for these sequences is $\sim [4 \cdot 10^{14}, 5 \cdot 10^{15}]\mathrm{gcm}^{-3}$. The EoSs are taken from[78] and their profiles are plotted on Figure 2.1 and 2.2. We choose these EoSs because they are already included into the code. Moreover this selection is done only to probe very general features of NS models; indeed, they are quite old EoSs (see [79] and [80] for references). This means that actually we will probe after recent models of nuclear equations of state, in which we will base the main results of this work. Anyway, although a deep investigation about the equation of state of nuclear matter will be done in the Chapter3, some considerations are needed to understand the differences between the three sequences of models reported here.

A barotropic EoS for the nuclear matter inside NSs can be determined through two different approaches. The first corresponds to choose an approximate and analytical form of EoS, which is the so-called *polytropic* EoS. We discussed it before for the case of Newtonian fluids. This has a very simple form: $P = K\rho^{\Gamma}$, where K and Γ are constants. Lots of studies about NSs are currently done using this type of EoS. However it is only useful to probe some general features of relativistic stars. If one wants to investigate in details the bulk properties of NSs and how it is affected by the matter inside them, he has to use the other approach. This corresponds to establish what kind of particles constitute the NS matter and modeling properly the interactions between them. There is a big number of theories which describe differently both the particles and the interactions which are thought to be found inside these objects. In particular the problem concerns the inner core of these stars. Nowadays we know what kind of equations of state are suitable for the description of the envelope of neutron stars (for instance the HW or the BPS[60]). This is possible

---

[11] Sometime instead of the condition $P = 0$ one uses $P = P_{sur} \neq 0$, where P_{sur} is the pressure computed from the equation of state at the equilibrium density of ^{56}Fe ($\sim 7.86 gcm^{-3}$). This is a more realistic condition for the surface of NSs, because from the knowledge about stellar evolution we know that the crust of a NS is mainly composed by iron nuclei in chemical equilibrium.

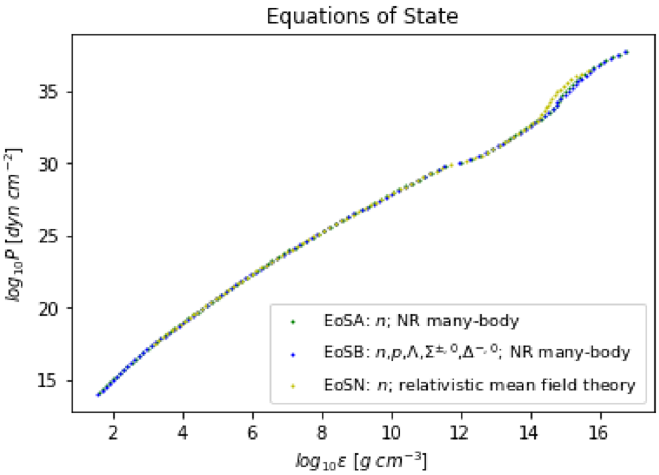

Figure 2.1: Graph of the function $P = P(\epsilon)$ on a logarithmic scale for three different equations of state: EoSA, EoSB, EoSN (see the text for details).

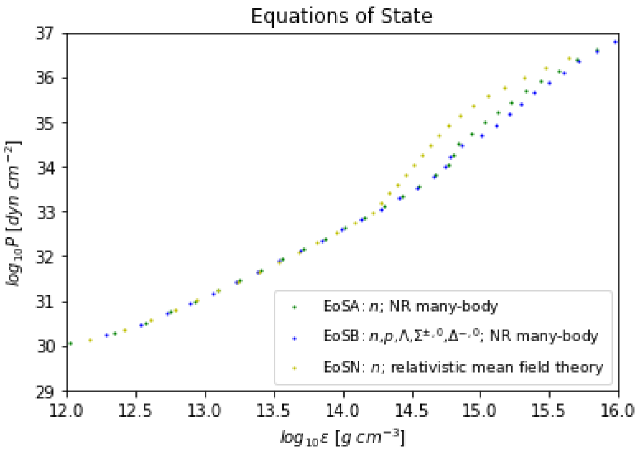

Figure 2.2: Zoom of the Figure2.1. The different behaviour of the three EoSs at the highest densities range is considered. We can see that EoSB is a softer equation of state with the respect to EoSA and EoSN. The latter is the most stiff among them.

because inside these regions the NS matter has densities below the nuclear saturation density, thus it can be investigated in the laboratories. However, generally, lots of several EoSs which match the low density EoS before the saturation point show a completely different behavior above $\rho_0 = 2.7 \cdot 10^{14} gcm^{-3}$. The reason of this is that *we actually don't know what is inside the core of NSs.* This happens because, as discussed during the introduction, current terrestrial experiments are not able to probe the ultra-densities expected here. In this thesis we will consider several types of realistic EoSs. In particular, the main results of this thesis will be obtained with EoSs for strange quark matter that we will discuss in the Chapter3. For the current analysis concerning the general features of static NS models we apply three EoSs well known in the literature. The first equation of state EoSA describes the nuclear matter inside NSs as an ensemble of neutrons, whose interactions are modeled with a non-relativistic many-body approach. The second one EoSB is characterized by a major number of particles. It adds protons p and the so-called *exotica* and describes the particle interactions in the same way as EoSA. Here with "exotica" we mean hadrons heavier than baryons (i.e. with a higher rest-mass); in particular they can be *hyperons* (hadrons containing strange quarks) or Δ-*resonances* (baryons with spin number 3/2). EoSB contains n,p, the hyperons Λ, $\Sigma^{\pm,0}$ and the resonances $\Delta^{-,0}$. These particles are assembled within a neutrally charged system[12]. Eventually EoSN considers only neutrons as EoSA but it models the particle interactions using a relativistic mean field theory. The behaviour of $P(\epsilon)$ for these three EoSs is plotted in Figure2.1. We can note from the plot that all of them show the same behaviour below the nuclear saturation density. Instead, they have completely different profiles above that density. In particular they show a different stiffness, i.e. different values of local pressure for a fixed mass-energy density. Figure2.2 shows the same plot of Figure2.1 but with a zoom on the highest densities range. Here we can see that when approaching the highest densities, EoSB is the most soft among the three EoSs, and EoSN is the most stiff. EoSB becomes softer than EoSA because it introduces exotica at high densities. Indeed, because of the complete degeneracy of the hadronic matter inside NSs, particles are all distributed among different Fermi energy levels according to the Fermi-Dirac statistics and the Pauli Principle. Then adding hyperons, for instance, means that the hyperonization of the neutrons and protons at the top of their Fermi seas (i.e. the most high energy particles) happens inside the system. Only these high energy particles can be converted into hyperons because they can reach the rest-mass values of hyperons with their chemical potential. Hyperons can exist only within a very energetic environments. The conversion into hyperons[13], which are more massive and thus occupying lower Fermi energy levels, reduces the number of neutrons and protons at the top of their Fermi seas thus lowering the total degeneracy pressure of the system. The argument is similar for the Δ-resonances. Eventually, the great stiffness of EoSN is due to the different modeling of the particles interaction. It can be shown that with relativistic mean field theories very stiff EoSs can be obtained. However one has always to consider the causality limit, i.e. $dP/d\epsilon < 1$ (the speed of sound must be lower than c). We focus now on the bulk properties of NSs models, observing how a different stiffness in the EoS can affect them.

In Figure2.3 we report the diagram gravitational mass versus central mass-energy density for the three sequences of models. Here we can see that for all the EoSs, by increasing the value of the parameter ϵ_c, the sequences are characterized by an initial rapid increase of the gravitational mass until a maximum value followed by a slow decrease of the mass. Hereafter we will call this maximum value for the gravitational mass of the non-rotating NSs as M_{TOV}. The existence of a maximum value of the gravitational mass of NSs for a fixed EoS is predicted by the General Relativity.

---

[12] In all the NS models the fluid is assumed to be neutrally charged.

[13] The hyperonization is driven by the weak interactions, which can change the strangeness of the system.

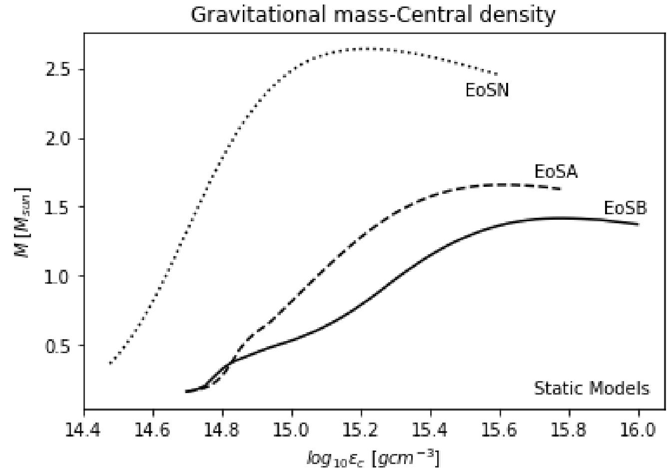

Figure 2.3: Plot of the relation between the gravitational mass and the central mass-energy density for NS hydrostatic equilibrium sequences, which are computed applying different EoSs. Each sequence is labeled with the name of the EoS used to compute the models.

Indeed by writing the TOV-equation in the following way[14]:

$$\frac{dP}{dr} = -\frac{\epsilon(r)m(r)}{r^2}\Big(1+\frac{P(r)}{\epsilon(r)}\Big)\Big(1+\frac{4\pi r^3 P(r)}{m(r)}\Big)\Big(1-\frac{2m(r)}{r^2}\Big)^{-1} \tag{2.38}$$

we can see that compared to its Newtonian limit it contains the pressure in the right hand side terms. This terms represent the gravitational acceleration which acts towards the collapse of the star and that is balanced by the pressure gradient on the left hand side term, in analogy with Newtonian self-gravitating fluids. However, for relativistic stars also the own pressure brings to the collapse. If we increase the mass, the pressure gradient must become more large in order to hold an equilibrium configuration but, at the same time, this increases also the contribution of the pressure to the gravitational collapse. At a certain point, when the mass is sufficiently high, the gravitational collapse of the star is unavoidable. This is briefly the reason of the existence of a maximum gravitational mass for relativistic stars. From the plot we can clearly note also that *more stiff is the EoS more high is the value of the maximum NS gravitational mass.* The reason of this is the different internal pressure values which are reached near the core of NSs by the three different EoSs. EoSs more stiff are characterized by more high internal pressures at a fixed central mass-energy density. This allows NS models to hold more high masses against the gravitational collapse. Thus only with very stiff EoSs (like EoSN) we are able to compute NS models with masses $\sim 2-2.5M_{\odot}$. EoSA, EoSB allow to build models with $M_{TOV} \approx 1.4-1.6M_{\odot}$. Moreover we can see that the maximum value of the NS mass is reached at different values of ϵ_c for the three EoSs. In particular EoSB can reach more high values of the central mass-energy density. This happens because it describes nuclear matter with more heavy hadronic particles, which required

---

[14] The TOV-equation reduces to the Newtonian hydrostatic equilibrium equation within the weak field limit. This is obtained by considering the conditions: $P/\epsilon \ll 1$ (that implies also $(4\pi r^3 P)/m \ll 1$) and $2m \ll r^2$.

a more energetic environment to exist, as we briefly discussed before. Eventually, from the perturbative analysis of the structure equations, the stability of static models can be investigated. In particular, because of the spherical symmetry, one can study the evolution of radial pulsations inside this objects. It can be shown[81] that the fundamental radial oscillation mode (i.e. the mode associated with the value $n = 0$ in the perturbative analysis) becomes unstable from the point with maximum mass towards higher central mass-energy densities. Thus *configurations lying on the decreasing gravitational mass branch along an equilibrium barotropic sequence represent dynamical unstable equilibria.* The unstable NS models are configurations which collapse to a BH within a dynamical timescale.

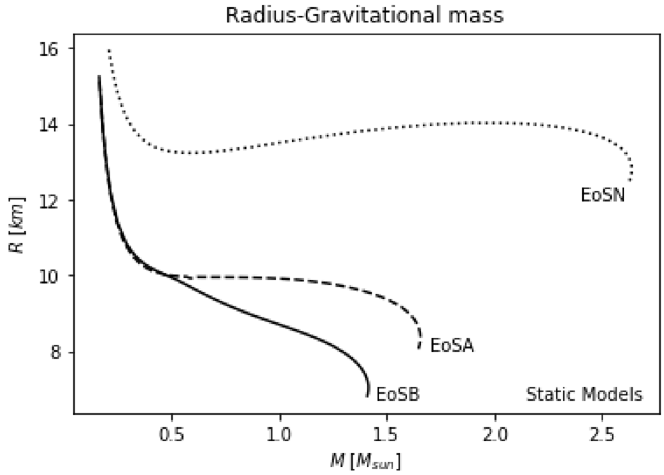

Figure 2.4: Plot of the relation between the radius and the gravitational mass for NS hydrostatic equilibrium sequences, which are computed applying different EoSs. Each sequence is labeled with the name of the EoS used to compute the models.

In Figure2.4 we report the diagram radius versus gravitational mass. Here we can show again the existence of an upper limit for the gravitational mass of NSs, which depends on the applied EoS. In particular, the stellar radius shows a clear decrease with an increase of the mass. This is natural for gravitationally bound stars: more high is the mass, more high is the strength of the gravitational pressure and thus more compact are the stars. Moreover, the three different EoSs show an other remarkable general property. *Stiffer EoSs yield models more massive and with bigger radii, softer EoSs yield models less massive and more compact.* This is clear that because in the case of a fixed mass, more high values of the internal pressure reduce the strength of gravity and thus implying more big stellar radii.

2.3 Stationary, axially symmetric spacetimes

In the following we describe the theoretical overview about rotating relativistic stars. We introduce the equations which are applied to compute rotating NS models. Then in the next paragraphs we will describe in details how these equations are handled by numerical codes particularly focusing on their approach and we will discuss the main features of equilibrium models of rotating NSs.

As a first step we need to define what kind of metric of the spacetime can be related to rotating relativistic stars. It's known that within the Newtonian limit we are able to probe the classical approximation of the general relativistic quantities. This can be useful for a better understanding about their physical meaning. For instance, the weak field limit of the Schwarzschild solution 2.37 is:

$$ds^2 = -(1 - 2\Phi)dt^2 + (1 + 2\Phi)dr^2 + r^2 d\theta^2 + r^2 \sin^2\theta d\phi^2 \tag{2.39}$$

where Φ represents the Newtonian gravitational potential. This implies that the coefficients of the metric tensor of the general relativistic spacetime are related to the Newtonian gravitational potential. Because of this, since we have seen that in the case of rotating Newtonian fluids the rotation affects the strength of the gravitational potential by defining a new effective potential, we can expect that the rotation of relativistic stars modifies their spacetime metric. Moreover we have seen during the introduction that it is usual to assume an axial-symmetry of the system when treating rotating fluids. However this symmetry is only a mere assumption because rotating fluids can be non-axially symmetric systems. Thus, at the beginning one assumes the axial-symmetry and after he has to study the stability of the models against axisymmetric and non axisymmetric modes. The geometry of the spacetime associated with rotating relativistic objects in equilibrium is obtained through the following assumptions:

- the spacetime is *stationary* and *axisymmetric*. Thus there exist two Killing fields: one is an asymptotically time-like symmetry vector t^μ and the other is a rotational symmetry vector ϕ^μ
- the spacetime is asymptotically flat. This implies $t^\mu t_\mu = -1$, $\phi^\mu \phi_\mu = +\infty$ and $t^\mu \phi_\mu = 0$ at spatial infinity
- the spacetime is circular, i.e. there are no meridional currents
- the Killing vectors commute, i.e. $[t, \phi] = 0$
- there is an isometry of the spacetime that simultaneously reverses the direction of ϕ^μ and t^μ, i.e.: $t^\mu \to -t^\mu \ \wedge \ \phi^\mu \to -\phi^\mu$

The Differential Geometry allows us to infer that[61] in this case there exists a family of 2-surfaces orthogonal to t^μ and ϕ^μ, i.e. surfaces of constant t and ϕ. It is natural to choose as coordinates $x^0 = t$ and $x^3 = \phi$; thus, in this way ϕ describes rotations around the $\hat{z}$ axis. In the absence of meridional currents, the 2-surfaces orthogonal to t^μ and ϕ^μ can be parameterized by the remaining coordinates x^1, x^2. Within this coordinates frame we can write an expression for the metric tensor whose coefficients are independent on t and ϕ. Thus by using the Killing fields formalism we can write:

$$t^\mu = (\partial_t)^\mu = \delta^\mu_t \tag{2.40}$$
$$\phi^\mu = (\partial_\phi)^\mu = \delta^\mu_\phi \tag{2.41}$$

and also:

$$t_\mu t^\mu = g_{\mu\alpha}\delta_t^\alpha \delta_t^\mu = g_{tt} \tag{2.42}$$

$$\phi_\mu \phi^\mu = g_{\phi\phi} \tag{2.43}$$

$$t_\mu \phi^\mu = g_{t\phi} = g_{\phi t} \tag{2.44}$$

In the case of a static spacetime, defining as T the time-reversal operator, we have that:

$$g_{t\phi}(t, x^1, x^2, \phi) = (T \circ g)_{t\phi}(t, x^1, x^2, \phi) = -g_{t\phi}(-t, x^1, x^2, \phi) = -g_{t\phi}(t, x^1, x^2, \phi) \tag{2.45}$$

where we applied the isometry of the static spacetime $\partial g_{\mu\nu}/\partial t = 0$. Thus $g_{t\phi} = t_\mu \phi^\mu = 0$, i.e. within a static spacetime the two Killing fields t and ϕ are orthogonal. Nevertheless, a rotating spacetime is not more invariant with the respect of the only time-reversal operation: $t \to -t$. Thus the two Killing fields t and ϕ are no more orthogonal. This implies $g_{t\phi} \neq 0$. The lack of the orthogonality between the two Killing fields is the reason of the dragging of inertial frames that we discussed during the introduction and that we now relate to the metric coefficient $g_{t\phi}$. In particular, we describe this effect with a metric potential ω. Because of this the new metric is no more diagonal, but it presents some mixing terms related to space-time intervals dtdϕ. *Rotations around the $\hat{z}$-axis affect the flow of time and the time flow is associated with ϕ-rotations of reference frames*: this is the Lense-Thirring effect. There are several choice for the coordinates x^1, x^2. We use the so-called "quasi-isotropic coordinates", for which $g_{r\theta} = 0$ and $g_{\theta\theta} = r^2 g_{rr}$ (in spherical coordinates). Therefore the general form of the new metric describing the stationary axisymmetric spacetime is the following:

$$ds^2 = -e^{2\nu(r,\theta)}dt^2 + e^{2\alpha(r,\theta)}(dr^2 + r^2 d\theta^2) + e^{2\psi(r,\theta)} r^2 \sin^2\theta (d\phi - \omega dt)^2 \tag{2.46}$$

It's important to note that now there is also an angular dependence of the metric coefficients. Clearly, they can depend only on the angle θ and not on ϕ because of the axial-symmetry. From the new metric we can compute the 4-velocity field associated with the fluid elements, which rotate at a frequency Ω around the $\hat{z}$-axis. We have that:

$$u^r = u^\theta = 0$$

$$u^\phi = \frac{d\phi}{d\tau} = \frac{dt}{d\tau}\frac{d\phi}{dt} = u^t \Omega$$

From the above equations and the normalization $g_{\mu\nu}u^\mu u^\nu = -1$, one can find that:

$$u^t = \frac{e^{-\nu(r,\theta)}}{\sqrt{1 - v^2}} \tag{2.47}$$

where we defined the quantity: $v = (\Omega - \omega)e^{\{\psi(r,\theta) - \nu(r,\theta)\}} r \sin\theta$. Thus we can write the general expression of the 4-velocity field as follows:

$$u^\mu = u^t(t^\mu + \Omega \phi^\mu) \tag{2.48}$$

In describing the rotating fluid is useful to introduce a family of zero-angular-momentum local observers, the so-called ZAMOs[82, 83]. These are reference frames whose worldlines are normal to the spacelike hypersurfaces Σ defined by the condition t =const. They are stationary observers, because dragged at the same frequency of the rotating fluid: $\omega = \Omega$. Thus they are locally non-rotating frames[84]. Because of this, the ZAMOs 4-velocity field is defined as follows:

$$u^{\mu}_{ZAMO} = u^{t}_{ZAMO}(t^{\mu} + \omega\phi^{\mu}) = e^{-\nu(r,\theta)}(t^{\mu} + \omega\phi^{\mu}) \tag{2.49}$$

where the last identity derives from $v_{ZAMO} = 0$. The advantage of the introduction of these reference frames concerns the better interpretation of the physical quantities. Firstly, we note that v is a non covariant quantity, because it changes among different local reference frames. Thus we have to specify the physical frame with respect to which it is measured. With the introduction of the ZAMOs it becomes clear that v represents the 3-velocity of the fluid elements with respect to these observers. Moreover from the last identity on the eq.2.49, we note that $e^{-\nu(r,\theta)}$ corresponds to the time dilation factor relating the proper time of the local ZAMO to the coordinate time t.

From the metric tensor 2.46 we can note also that there are four metric potentials which we have to compute in order to determine the structure of the spacetime. When an equation of state has been specified and if equilibrium solutions exist, the structure of a relativistic rotating star and the spacetime close and inside it are determined by solving four components of the Einstein's field equations 2.27 together with the equations of the hydrostationary equilibrium. The former are obtained by computing all the components of the stress-energy tensor and of the Ricci tensor. Indeed the Einstein equations can be written also in the following form:

$$R_{\mu\nu} = 8\pi\Big(T_{\mu\nu} - \frac{1}{2}g_{\mu\nu}T^{\alpha}_{\alpha}\Big) \tag{2.50}$$

It can be shown[59] that three of these equations can be obtained from three coefficients of the Ricci tensor ($t - t$, $\phi - \phi$ and $t - \phi$) combined with the respective expressions of the coefficients of the stress-energy tensor (in the case of a perfect fluid). They look like:

$$\nabla[\rho e^{\gamma/2}] = S_{\rho}(r,\mu) \tag{2.51}$$

$$\Big(\nabla + \frac{1}{r}\frac{\partial}{\partial r} - \frac{1}{r^2}\mu\frac{\partial}{\partial\mu}\Big)\gamma e^{\gamma/2} = S_{\gamma}(r,\mu) \tag{2.52}$$

$$\Big(\nabla + \frac{2}{r}\frac{\partial}{\partial r} - \frac{2}{r^2}\mu\frac{\partial}{\partial\mu}\Big)\omega e^{(\gamma-2\rho)/2} = S_{\omega}(r,\mu) \tag{2.53}$$

where:

$$\nabla = \frac{1}{r^2}\frac{\partial}{\partial r}\Big(r^2\frac{\partial}{\partial r}\Big) + \frac{1}{r^2}\Big[\frac{1}{\sin\theta}\frac{\partial}{\partial\theta}\Big(\sin\theta\frac{\partial}{\partial\theta}\Big) + \frac{1}{\sin^2\theta}\frac{\partial^2}{\partial\phi^2}\Big] \tag{2.54}$$

$$\gamma = \psi + \nu \tag{2.55}$$

$$\rho = \nu - \psi \tag{2.56}$$

$$\mu = \cos\theta \tag{2.57}$$

and the expressions of the terms (very long) $S_\rho(r,\mu)$, $S_\gamma(r,\mu)$ and $S_\omega(r,\mu)$ are reported in [59] (here β corresponds to our ψ). These terms are very complicated functions of r, μ and also of γ, ρ, α, ω and P, ϵ and Ω (the last comes from the coefficients of u^μ in the stress-energy tensor). The three equations 2.51, 2.52 and 2.53 are three second order PDEs in an elliptical form. These are Poisson-like equations, where the Newtonian gravitational potential is replaced by the metric potentials and on the right hand side there are the source terms. These are the analogous of the scalar density field in the Poisson equation 1.6. Eventually, the last forth equation for the metric potentials is obtained by using identities concerning some coefficients of the Ricci tensor, which are valid *only* in the case of a perfect-fluid stress-energy tensor. This is a long first order PDE (8 lines) on the metric potential α and it is listed in [59]. Together with the Einstein equations we need also the hydrostationary equilibrium equations. In particular we need other three equations to solve the problem; so far, we have four equations in seven unknowns γ, ρ, α, ω, P, ϵ and Ω. The condition of hydrostationary equilibrium is derived from the generalized Euler equation 2.28. Here $\nu = r, \theta$. Thus, by knowing that $u^r = u^\theta = 0$ and $g_{\xi\nu}g^{\xi\nu} = 1$, the Euler equation becomes:

$$\frac{\nabla_\nu P}{P+\epsilon} = -u^\beta \nabla_\beta u_\nu = -u^\beta\Big(\frac{\partial u_\nu}{\partial x^\beta} - \Gamma^\lambda_{\beta\nu} u_\lambda\Big)$$

Now, because $\beta = t, \phi$ and the spacetime is symmetric under t-translations and ϕ-rotations, by using the definition of the Christoffel symbols the last equation reduces to:

$$\frac{\nabla_\nu P}{P+\epsilon} = \frac{1}{2} g^{\lambda k}\Big(\frac{\partial g_{k\nu}}{\partial x^\beta} + \frac{\partial g_{k\beta}}{\partial x^\nu} - \frac{\partial g_{\beta\nu}}{\partial x^k}\Big) u^\beta u_\lambda$$

Thus by defining $\partial_\alpha \equiv \partial/\partial x^\alpha$ we have:

$$\begin{aligned}\frac{\nabla_\nu P}{P+\epsilon} = \frac{1}{2}[&u^t(g^{t\phi}\partial_\nu g_{\phi t} + g^{tt}\partial_\nu g_{tt})u_t + u^t(g^{\phi\phi}\partial_\nu g_{\phi t} + g^{\phi t}\partial_\nu g_{tt})u_\phi \\ &+ u^\phi(g^{tt}\partial_\nu g_{\phi t} + g^{t\phi}\partial_\nu g_{\phi\phi})u_t + u^\phi(g^{t\phi}\partial_\nu g_{\phi t} + g^{\phi\phi}\partial_\nu g_{\phi\phi})u_\phi]\end{aligned}$$

Then by considering that $u^\phi = \Omega u^t$ and arranging the metric coefficients we obtain that:

$$\begin{aligned}\frac{\nabla_\nu P}{P+\epsilon} &= \frac{1}{2}(u^t)^2\Big[-\partial_\nu\Big(\frac{1}{(u^t)^2}\Big) - \Big(2g_{\phi t} + 2\frac{u^\phi}{u^t} g_{\phi\phi}\Big)\partial_\nu \Omega\Big] = \\ &= \frac{1}{2}(u^t)^2 \frac{2u^t\partial_\nu u^t}{(u^t)^4} - u^t(g_{\phi t}u^t + g_{\phi\phi}u^\phi)\partial_\nu\Omega = \partial_\nu(\ln u^t) - u^t u_\phi \partial_\nu \Omega\end{aligned}$$

Because $\nabla_\nu P = \partial_\nu P$, we can define the vector $\vec{\nabla} = (\partial/\partial r, (1/r)\partial/\partial\theta)$ on the subspace $r - \theta$ and we can write:

$$\frac{\vec{\nabla} P}{P+\epsilon} = \vec{\nabla}(\ln u^t) - u^t u_\phi \vec{\nabla}\Omega \tag{2.58}$$

Moreover we note that:

$$\begin{aligned}
& u^t u_\phi = u^t u_t \frac{u_\phi}{u_t} = (-1 - u^\phi u_\phi)\frac{u_\phi}{u_t} = \Big(-1 - \Omega u^t u_t \frac{u_\phi}{u_t}\Big)\frac{u_\phi}{u_t} \\
\Longrightarrow \; & u^t u_t = \frac{-1}{1 + \Omega \frac{u_\phi}{u_t}} \\
\Longrightarrow \; & u^t u_\phi = \frac{l}{1 - \Omega l} = \frac{(\Omega - \omega) e^{2(\psi - \nu)} r^2 \sin^2\theta}{1 - (\Omega - \omega)^2 e^{2(\psi-\nu)} r^2 \sin^2\theta} \qquad (2.59)
\end{aligned}$$

where we defined[15] $l := -u_\phi / u_t$. Thus the final form of the hydrostationary equilibrium equations is the following:

$$\frac{\vec{\nabla} P}{P + \epsilon} = \vec{\nabla}(\ln u^t) - \frac{l}{1 - \Omega l}\vec{\nabla}\Omega \qquad (2.60)$$

We can define the enthalpy of the relativistic fluid similarly as we did in eq.1.30. For the relativistic barotropic fluid we must take in account the contribution of the mass-energy density to the enthalpy. We define:

$$H(P) := \int_0^P \frac{dP'}{\epsilon(P') + P'} \qquad (2.61)$$

and we can note that:

$$\begin{aligned}
& \vec{\nabla} H(P) = \vec{\nabla}\Big[\int_0^P \frac{dP'}{\epsilon(P') + P'}\Big] = \frac{\vec{\nabla} P}{P + \epsilon(P)} - 0 \frac{1}{P + \epsilon(P)} + \int_0^P dP' \vec{\nabla}\Big(\frac{1}{P' + \epsilon(P')}\Big) \\
\Longrightarrow \; & \vec{\nabla} H(P) = \frac{\vec{\nabla} P}{P + \epsilon(P)}
\end{aligned}$$

By defining the function:

$$F := \frac{l}{1 - \Omega l} = \frac{(\Omega - \omega) e^{2(\psi - \nu)} r^2 \sin^2\theta}{1 - (\Omega - \omega)^2 e^{2(\psi-\nu)} r^2 \sin^2\theta} \qquad (2.62)$$

we can write the eq.2.60 in the following form:

$$\frac{\partial}{\partial x^i}(H - \ln u^t) = -F \frac{\partial \Omega}{\partial x^i} \qquad (2.63)$$

where $i = 1, 2$. If we take the derivative $\partial / \partial x^j$ of the above equation and we use the spherical coordinates frame, the Schwarz theorem implies that:

$$\frac{\partial F}{\partial r}\frac{\partial \Omega}{\partial \theta} = \frac{\partial F}{\partial \theta}\frac{\partial \Omega}{\partial r} \qquad (2.64)$$

This equation means that the jacobian of the coordinate change $(r, \theta) \to (\Omega, F)$ is identically zero. Hence the variables Ω, F are not independent. Thus it must exist a function $\Phi : \mathbb{R}^2 \to \mathbb{R}$ such that $\Phi(\Omega, F) = 0$. There are two possibilities:

---

[15] It can be shown that this quantity is the relativistic specific angular momentum j.

- $\partial\Phi/\partial F = 0$, then the equation $\Phi(\Omega, F) = 0$ implies $\Omega = const.$ that is the case of a uniformly rotating fluid
- $\partial\Phi/\partial F \neq 0$, then the implicit function theorem ensures that $F = F(\Omega)$. Thus F is *only* a function of Ω and this represents the case of a differentially rotating fluid

Because of this we can derive some interesting results. Firstly, the equation 2.60 can be written in the following form:

$$\frac{\vec{\nabla} P}{P + \epsilon} = \vec{\nabla}\Phi_{eff} \tag{2.65}$$

where

$$\Phi_{eff} = \left(\ln u^t - \int_{\Omega_0}^{\Omega} F(\Omega')d\Omega'\right) \tag{2.66}$$

that is the analogous of the differential form of the equation 1.8 for the relativistic case. We can see again the lowering of the gravity strength as an effect of the rotation[16]. Moreover, the global first integral of the hydrostationary equilibrium equations is the following:

$$H - \ln u^t + \int_{\Omega_0}^{\Omega} F(\Omega')d\Omega' = \text{const.} \tag{2.67}$$

where the constant is established by fixing two boundary conditions: one related to the enthalpy/mass-energy density profile, for instance ϵ_c like for non rotating objects; the other labeling the rotation inside the objects, for instance the constant value of the spin frequency in the case of rigidly rotating models[17] or its value at a certain point within the model in the case of differential rotation (in eq.2.67 this is labeled as Ω_0). Moreover, like in the HSCF method, in the case of differential rotation, one has to establish the rotation law. This means to define an expression for $F(\Omega)$, from which together with eq.2.62 one can obtain the profile of Ω inside the star. There are different choices for $F(\Omega)$ in the literature[59, 73, 53, 85, 86]. In this thesis we will consider only the one more used by the authors. This has the following parametric form:

$$F(\Omega) = A^2(\Omega_c - \Omega) \tag{2.68}$$

and it is termed[85] as "j-const. law". Indeed, by considering eq.2.62 and the definition of the function F we have the following Newtonian limit:

$$A^2(\Omega_c - \Omega) = \frac{l}{1 - \Omega l} = \frac{(\Omega - \omega)e^{2(\psi-\nu)}r^2\sin^2\theta}{1 - (\Omega - \omega)^2 e^{2(\psi-\nu)}r^2\sin^2\theta} \approx \Omega r^2 \sin^2\theta$$
$$\implies \Omega = \frac{A^2\Omega_c}{A^2 + r^2\sin^2\theta}$$

---

[16] Here we noted that the term $\ln u^t$ contains the metric potential ν which is the analogous of the gravitational potential in the weak field limit.

[17] In this case eq.2.65 does not contain the spin frequency anymore but Ω is still present in the Einstein's field equations, thus we need to specify it.

and within the limit $A \ll 1$ one can write that:

$$\Omega = \frac{A^2 \Omega_c}{r^2 \sin^2 \theta} \tag{2.69}$$

This corresponds to the case of a Newtonian fluid which rotates with constant specific angular momentum $j_0 = A^2\Omega_c$ within it. This is exactly the same law that we have seen during the discussion of the HSCF method. Clearly, the law 2.68 satisfies the Rayleigh criterion for the local dynamical stability against axisymmetric disturbances 1.26. In fact in the Newtonian limit $\Omega\varpi^2 = j$, hence the Rayleigh criterion implies that j should not decrease outward. This is clearly satisfied for a j-constant rotation law. Eventually the parameter A is related to the degree of differential rotation. In particular, it's easy to note that when $A \to \infty$ thus $\Omega \to \Omega_c$ and the fluid becomes rigidly rotating; instead, smaller values of A imply an high differential rotation degree. As an example, we report in Figure2.5 and Figure2.6 some profiles of the j-constant law in the Newtonian approximation and computed at the equator of the rotating fluid, i.e. $\theta = \pi/2$. In particular, in Figure2.5 several profiles obtained for different values of A^{-1} and for a fixed $\Omega_c/2\pi = 1000$Hz are shown. Here we can note that the more big is A the more rigid is the rotation. In particular, for a fixed equatorial radius, bigger values of A imply more high equatorial speed frequencies. In Figure2.6 several rotational profiles computed for different values of A and for a fixed equatorial frequency $\Omega_e/2\pi = 150$Hz at an equatorial radius of 13km are shown. Here we can note that the bigger is A, the lower is the central angular velocity of the fluid.

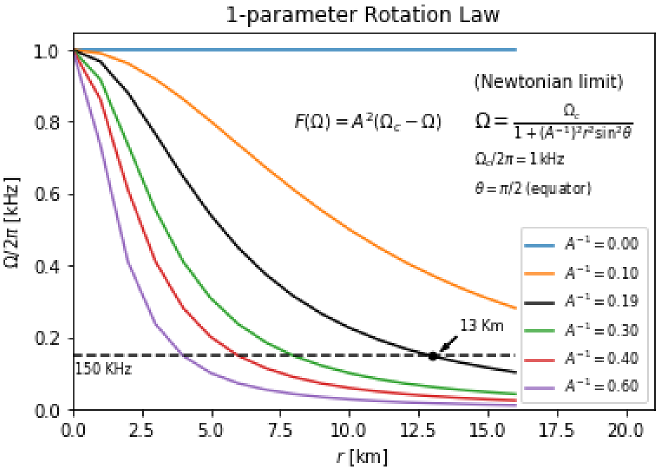

Figure 2.5: Different profiles of the j-constant law obtained in the Newtonian approximation for a fixed central frequency $\Omega_c/2\pi = 1000$Hz and several values of A^{-1}. On the legend the values of A^{-1} are reported. Moreover, the rotational profile of the model with equatorial speed frequency of 150Hz and equatorial radius of 13km is marked.

Although the hard resolution, the problem of computing rotating star models in general relativity has a quite simple structure. As we seen before, there are seven unknowns overall: the four metric potentials (γ, ρ, α and ω) and the quantities associated with the system fluid dynamics P, ϵ and Ω. Therefore, we have four

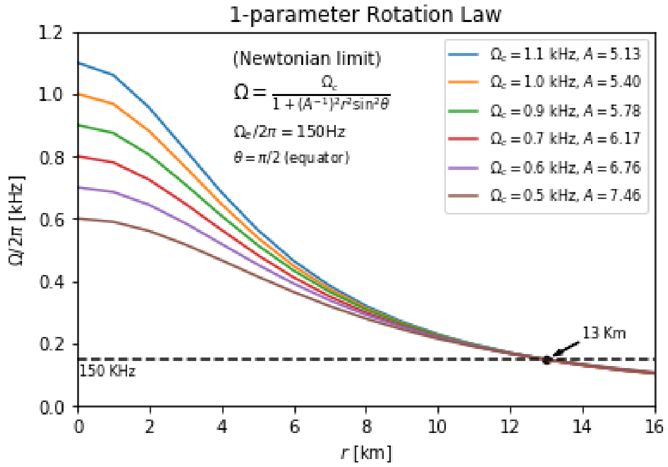

Figure 2.6: Different profiles of the j-constant law obtained in the Newtonian approximation for a fixed equatorial frequency $\Omega_e/2\pi = 1000$Hz at an equatorial radius of 13km and several values of A. On the legend the values of A are reported. The more big is A, the more low is the central frequency.

PDEs coming from the Einstein equations, which will need appropriate boundary conditions in order to be solved (these will be fixed by considering the asymptotic flatness of the spacetime). The fifth equation is the global first integral of the hydrostationary equilibrium equations, which is solved by fixing two parameters. Then, in the case of differential rotation with the parametric form of $F(\Omega)$ indicated in eq.2.68, one will must fix also the parameter A. In this way, if we choose the two parameters of the hydrostationary equilibrium equation as ϵ_c and Ω_0, a unique differentially rotating model will be linked by the triad $(\epsilon_c,\ \Omega_0,\ A)$; thus we will deal with a 3-dimensional solutions space. Eventually the last two equations required to close the problem are the barotropic equation of state $P = P(\epsilon)$ and the equation 2.62; the latter allowing to specify the rotational profile inside the models.

Several bulk quantities can be define in order to describe relativistic rotating fluids. Thanks to the formalism of the Killing fields we are able to define some of them through really general expressions. First of all, the mass. Its definition is quite tricky and, above all, it is not unique. However, because of the mass-energy equality, we expect that the definition of the "total" mass of a relativistic system is a sort of definition of its "total" energy. In particular, this definition should be in agreement with the mass M of the static and spherically symmetric configuration that we have seen before (the Schwarzschild solution). Since it's known that the conservation of the energy of systems is related to their invariance under time translations, we search for a definition of the mass in terms of the Killing vector t. This is possible thanks to the so-called *Komar integrals*[87, 88]. Let us consider a Killing field ξ that is related to a certain symmetry of the spacetime. We can define the current:

$$J^{\mu}_{(\xi)} = 8\pi q R^{\mu\nu}\xi_{\nu} = 8\pi q\Big(T^{\mu\nu}\xi_{\nu} - \frac{1}{2}T^{\alpha}_{\alpha}g^{\mu\nu}\xi_{\nu}\Big) \tag{2.70}$$

where q is a constant and the last identity is obtained by using 2.50. It can be shown[88] that this is a conserved 4-current, i.e. $\nabla_{\mu}J^{\mu}_{(\xi)} = 0$. We can define a conserved charge associated with the conserved current. The charge passing through a spacelike hypersurface Σ is given by an integral over the coordinate x^i within a positively oriented chart $\{x^0, x^1, x^2, x^3\}$. In particular, Σ is the hypersurface defined by the condition $x^0 = const.$ and by the induced metric ${}^3g_{\mu\nu} = g_{\mu\nu} + n_\mu n_\nu$, where

$$n_\mu = -\frac{\delta^0_\mu}{\sqrt{-g^{00}}} \tag{2.71}$$

is the future pointing unit vector orthogonal to Σ. Here we applied again a metric signature $(-,+,+,+)$. Therefore, being ${}^3g$ the determinant of the induced metric, we write the integral as:

$$Q_\xi = \int_\Sigma n_\mu J^\mu_{(\xi)} \sqrt{{}^3g}\, d^3x = 8\pi q \int_\Sigma n_\mu \Big(T^{\mu\nu}\xi_\nu - \frac{1}{2} T^\alpha_\alpha g^{\mu\nu}\xi_\nu \Big) \sqrt{{}^3g}\, d^3x \tag{2.72}$$

By using the generalized divergence theorem we can write this integral as a surface integral over a 2-sphere at spatial infinity. Indeed, it can be shown that Killing fields satisfy the following identity:

$$\nabla_\nu \nabla_\mu \xi^\nu = R_{\mu\nu}\xi^\nu \tag{2.73}$$

Therefore we have that:

$$J^\mu_{(\xi)} = 8\pi q R^{\mu\nu}\xi_\nu = 8\pi q \nabla_\nu \nabla^\mu \xi^\nu$$

By inserting the last result into the integral 2.72 and applying the generalized divergence theorem we have:

$$Q_\xi = 8\pi q \int_\Sigma n_\mu \nabla_\nu \nabla^\mu \xi^\nu \sqrt{{}^3g}\, d^3x = 8\pi q \int_{S_\infty} n_\mu \sigma_\nu \nabla^\mu \xi^\nu \sqrt{{}^2g}\, d^2x \tag{2.74}$$

where $S_\infty := \lim_{r\to\infty} \int_{S_r}$ (S_r is a 2-sphere of constant radial coordinate r appropriate to an asymptotically flat spacetime), ${}^2g_{\mu\nu} ={}^3 g_{\mu\nu} - \sigma_\mu\sigma_\nu$ is the induced metric on S and $\sigma_\mu = \delta^1_\mu ({}^3g^{11})^{-1/2}$. The last integral is called *Komar integral* associated with the Killing field ξ. Therefore we can define the so-called *Komar mass* as the Komar integral associated with the Killing field t of a static or even stationary spacetime for a constant $q = 1/32$. This is the following:

$$M_t = \frac{1}{4\pi} \int_{S_\infty} n_\mu \sigma_\nu \nabla^\mu t^\nu \sqrt{{}^2g}\, d^2x \tag{2.75}$$

This mass corresponds exactly with the mass M found in the Schwarzschild solution when considering the case of the static and spherically symmetric empty spacetime. Indeed:

$$n_\mu \sigma_\nu \nabla^\mu t^\nu \sqrt{{}^2g} = n_0 \sigma_1 \Gamma^1_{00} t^0 \sqrt{{}^2g} = \Big(1 - \frac{2M}{r^2}\Big)^{1/2} \Big(1 - \frac{2M}{r^2}\Big)^{-1/2} \frac{M}{r^2} r^2 \sin\theta = M \sin\theta$$

and thus:

$$M_t = \frac{1}{4\pi} \int_{S_\infty} M \sin\theta\, d\theta\, d\phi = M$$

Hereafter we will call the Komar mass as the *Gravitational mass* M_G. This mass represents the entire amount of mass-energy contained within the relativistic system, i.e. the contributions of the baryonic density ρ, the internal energy e, the gravitational binding energy[18] W and all the other possible forms of energy held by the fluid (for instance the rotational kinetic energy in the case of rotating stars). The contribute of the baryonic density can be estimated by using the conservation law 2.108 and the generalized divergence theorem. It follows that:

$$M_B = \int_\Sigma \rho u^t \sqrt{^3g} d^3x \tag{2.76}$$

that is the so-called *Baryonic mass* (or even "rest mass") of the relativistic fluid. Similarly, we define the contribution of the internal energy as:

$$U = \int_\Sigma e u^t \sqrt{^3g} d^3x \tag{2.77}$$

Therefore, in the case of a rotating NS with a rotational kinetic energy T, the gravitational binding energy will be $W = M_G - M_B - U - T$. Moreover, because of the existence of an other Killing field ϕ which is related to the spacetime symmetry for rotations around the $\hat{z}$-axis, we can define an other Komar integral (now $q = -1/64$):

$$J = -\frac{1}{8\pi} \int_{S_\infty} n_\mu \sigma_\nu \nabla^\mu \phi^\nu \sqrt{^2g} d^2x \tag{2.78}$$

that corresponds to the total *Angular momentum* of the axially symmetric[19] rotating relativistic fluid. In particular, given the frequency Ω of the fluid we can define also the moment of inertia and the rotational kinetic energy of the fluid as follows:

$$I = \frac{J}{\Omega} \tag{2.79}$$

$$T = \frac{1}{2} \int \Omega dJ \tag{2.80}$$

Eventually by expanding all the terms contained on the two Komar integrals, from the definition 2.72 one finds that:

$$M_G = \int_\Sigma (2T^t_t + T^\alpha_\alpha) \sqrt{-g} d^3x \tag{2.81}$$

$$J = \int_\Sigma T^t_\phi \sqrt{-g} d^3x \tag{2.82}$$

these expressions allow to compute the gravitational mass and the total angular momentum of NSs from the metric and the stress-energy tensor components.

---

[18] This is contained also in the Schwarzschild mass. In fact, by using the covariant volume element $M = 4\pi \int_0^R \epsilon r^2 \sqrt{g_{rr}} dr$, in the Newtonian limit we obtain: $M \approx 4\pi \int_0^R \epsilon r^2 dr + \int_0^M -(m/r) dm$. The last term is the classical gravitational binding energy.

[19] Since the rotation axis is also the symmetry axis as we assumed at the beginning, the total angular momentum is the angular momentum respect to the rotational axis.

The last quantity that we need to know when studying rotating fluids is the so-called *mass-shedding limit.* We defined it during the introduction about rotating Newtonian stars. This quantity is very important because it introduces a limit on the sequences of equilibrium rotating fluids. Rotating configurations which exceed this limit with their spin frequency are dynamical unstable. When $\Omega > \Omega_K$, they start to loose mass from the surface, firstly from the equator, because the fluid elements at the surface are no more gravitationally bound: the centrifugal forces acting to them are overcoming the gravitational ones. In order to compute this frequency, one consider the rotational motion of particles at the star equator. Thus in the metric 2.46 we consider that: $dr = 0$, $d\theta = 0$, $r = R$ and $\theta = \pi/2$. Therefore the proper time of the particles can be written as follows:

$$\begin{aligned} d\tau = \sqrt{-ds^2} &= [e^{2\nu(R,\pi/2)}dt^2 - e^{2\psi(R,\pi/2)}R^2(d\phi - \omega dt)^2]^{1/2} \\ &= [e^{2\nu(R,\pi/2)} - e^{2\psi(R,\pi/2)}R^2(\Omega - \omega)^2]^{1/2}dt \end{aligned}$$

where we used the fact that $\Omega = d\phi/dt$ is the particles angular velocity. When $\Omega = \Omega_K$ the particles move along a geodesic path. This path can be obtained as the extremum of the proper time. Therefore we apply the variational principle along the radial coordinate to the above equation:

$$\begin{aligned} 0 = \delta\tau = \delta\Big\{\int_{t_1}^{t_2} [e^{2\nu(R,\pi/2)} - e^{2\psi(R,\pi/2)}R^2(\Omega - \omega)^2]^{1/2}dt\Big\} &= \\ = \int_{t_1}^{t_2} \delta\{[e^{2\nu(R,\pi/2)} - e^{2\psi(R,\pi/2)}R^2(\Omega - \omega)^2]^{1/2}\}dt \end{aligned}$$

where we used the fact that the variation vanishes at the end points $\delta R(t_1) = \delta R(t_2) = 0$. This implies that:

$$\begin{aligned} 0 &= \delta[e^{2\nu(R,\pi/2)} - e^{2\psi(R,\pi/2)}R^2(\Omega - \omega)^2] = \\ &= e^{2\nu}2\delta\nu - e^{2\psi}2\delta\psi(\Omega - \omega)^2R^2 + e^{2\psi}2(\Omega - \omega)R^2\delta\omega - e^{2\psi}(\Omega - \omega)^2 2R\delta R \\ &= [2\nu' e^{2\nu} - 2\psi' e^{2\psi}(\Omega - \omega)^2R^2 + 2R^2\omega' e^{2\psi}(\Omega - \omega) - e^{2\psi}2R(\Omega - \omega)^2]\delta R \\ &= 2\nu' e^{2\nu} - 2\psi' e^{2\psi}(\Omega - \omega)^2R^2 + 2R^2\omega' e^{2\psi}(\Omega - \omega) - e^{2\psi}2R(\Omega - \omega)^2 \end{aligned}$$

where we define $(..)' = \delta(..)/\delta R$. Now by using the velocity v defined in 2.47 computed at the equator, $v = (\Omega - \omega)e^{\psi-\nu}R$, we obtain after some algebra that:

$$\Big(\psi' + \frac{1}{R}\Big)v^2 - \omega' R e^{\psi-\nu}v - \nu' = 0 \tag{2.83}$$

which is a second order equation on the variable v whose solutions are:

$$v_{\pm} = \frac{R\omega'}{2\zeta'}e^{\psi-\nu} \pm \Big[\Big(\frac{\omega' R e^{\psi-\nu}}{2\zeta'}\Big)^2 + \frac{\nu'}{\zeta'}\Big]^{1/2} \tag{2.84}$$

where we defined $\zeta' = \psi' + 1/R$. We are interested only on the positive solution because it is related to the co-rotational motion of the fluid elements. Then by inserting this value of v into its definition we find the Keplerian frequency:

$$\Omega_K = \omega + \frac{\omega'}{2\zeta'} + \Big[\Big(\frac{\omega'}{2\zeta'}\Big)^2 + \frac{e^{2(\nu-\psi)}}{R^2}\frac{\nu'}{\zeta'}\Big]^{1/2} \tag{2.85}$$

This is the general expression of the relativistic Keplerian frequency. If we consider the Newtonian weak field limit of the above equation we obtain:

$$\begin{aligned} \omega \approx 0 &\implies \omega' \approx 0 \\ e^{2\psi} \approx 1 &\implies \psi \approx 0, \psi' \approx 0 \\ \zeta' &\approx \frac{1}{R} \\ e^{2\nu(R)} \approx 1 - \frac{2M}{R} &\implies \nu(R) \approx \ln\sqrt{1 - \frac{2M}{R}}, \nu'(R) \approx \frac{M}{R}\Big(1 - \frac{2M}{R}\Big)^{-1} \end{aligned}$$

therefore:

$$\Omega_K \approx \Big(\frac{M}{R^3}\Big)^{1/2} \tag{2.86}$$

which is the same expression of the Newtonian Keplerian frequency (eq.1.25) in gravitational units.

2.4 Numerical approaches

The problem of obtaining axisymmetric rotating stationary star models has been solved by a number of authors over the years. Two major general relativistic approaches have been adopted:

- an ”approximate” one concerning slowly rotating fluids, devised by Hartle as a perturbation of a spherically symmetric configuration
- the ”exact” one concerning arbitrarily rotating configurations. This was based on two different formulations: the Bonazzola&Maschio one[89], improved after by Bonazzola&Schneider[90], and the Bardeen&Wagoner one[84]. Thereafter, both these approaches have been developed and revisited more times together with lots applications on computing relativistic stellar models. Several numerical codes based on them are currently used by physicists to investigate rapidly rotating NSs

We are going to discuss some of these numerical approaches, starting with a brief analysis of the Hartle method applied to relativistic rotating objects. Afterwards, we will describe in detail one exact code based on the formalism developed in [90]. We will also provide equilibrium models obtained with this numerical code. Eventually we will discuss something about an other code, this based on the formalism developed in [84]. We will focus mainly on the comparison between the two exact codes.

2.4.1 Approximate solutions: the Hartle-Thorne method

The method developed by Hartle[48] allows to compute slowly rotating relativistic star models. We discussed during the introduction the main features of this approach. Here we want to provide some technical details about its procedure, and probe models obtained with it. Following [48], one has to compute firstly a static and spherically symmetric model of a barotropic perfect fluid, for a given equation of state $P = P(\epsilon)$. This means that he has to solve numerically the set of static equations described before. Once this model is computed, all the quantities $\nu(r), \lambda(r), m(r), P(r), \epsilon(r)$, the gravitational mass M and the radius R of the star are known.

Let us consider now the rigidly rotating barotropic perfect fluid, with the same equation of state of the static one, whose spin frequency is very smaller than the Keplerian frequency, i.e. $\Omega \ll \Omega_K$. The last condition implies that the relative changes in pressure, energy density and gravitational field of the static model due to the rotation are all much smaller than the unity. We also assume the axial-symmetry of the system with respect to the rotational axis. The metric tensor is similar to 2.46 but with a different choice for the metric coefficients; in particular, the Hartle's formalism adopts the spherical coordinates frame with the condition $g_{\phi\phi} = g_{\theta\theta}\sin^2\theta$ and maintains the signature $(-,+,+,+)$. Thus, the metric of the spacetime has the following general expression:

$$ds^2 = -H^2(r,\theta)dt^2 + Q^2(r,\theta)dr^2 + r^2K^2(r,\theta)[d\theta^2 + \sin^2\theta(d\phi - L(r,\theta)dt)^2] \quad (2.87)$$

Because of the stationary and axially symmetric spacetime, the metric must to behave in the same way under time reversal $t \to -t$ as under a reversal in the direction of the rotation of the system $\Omega \to -\Omega$. Therefore the dependence of the metric coefficients H, Q, K, L on the frequency Ω cannot be arbitrary. An expansion in powers of the angular velocity of the coefficients H, Q, K can contain only even powers of Ω, instead only odd powers can be contained by an expansion of L. In the Hartle analysis[48] the effects of the perturbation on the spherical solution due to the rotation are calculated to the order Ω^2. Here we discuss the approach only to the order Ω. A first-order slow-rotation approximation provides the dragging effect and allows to define the star's angular momentum and inertia momentum. We will provide after some numerical results obtained with the Hartle method by using a code based on the Ω-order. Higher order effects are interesting and concern mainly the rotational corrections on the energy-pressure distribution, on the gravitational mass and on the shape of the star. A second-order slow-rotation approximation allows to define the star's quadrupole moment. Clearly, the more high orders one considers, the more accurate are the results. There are some works[91, 92] where expansions to the order Ω^3 or even Ω^4 are treated. A considerable feature of the slow-rotation approximation approach is the analyticity on defining the properties of rotating relativistic stars. However, in general, these definitions are not accurate enough to robustly indicate instabilities of models and thus, to obtain accurate results for any rotation rate, one needs to change the way the problem is posed[8]. In these cases exact numerical approaches are considered.

To the first order in Ω only the metric coefficient L is perturbed, while $H^2 = e^{2\nu(r)}$, $Q^2 = e^{2\lambda(r)}$ and $K^2 = 1$ as in the non rotating case. This implies that one has to use again the structure equations of the non rotating fluid. Because of this the gravitational mass and the radius of the perturbed configuration have the same values of the static one. Also the pressure and the mass-energy density profiles don't change. However now there is an extra unknown: $L = \omega(r,\theta) + O(\Omega^3)$. Thus we need an other structure equation containing ω in order to compute the slowly rotating model. Since ω is related to the metric coefficient $g_{t\phi}$, one looks for this equation by probing $\phi - t$ components of the Einstein's field equations. In particular one considers the following equation:

$$R^t_\phi - \frac{1}{2} R g^t_\phi = 8\pi T^t_\phi \tag{2.88}$$

We immediately note that:

$$g^t_\phi = g^{t\alpha} g_{\alpha\phi} = g^{tt} g_{t\phi} + g^{t\phi} g_{\phi\phi} = -\frac{g_{\phi\phi} g_{t\phi}}{(g_{t\phi})^2 - g_{tt} g_{\phi\phi}} + \frac{g_{\phi\phi} g_{t\phi}}{(g_{t\phi})^2 - g_{tt} g_{\phi\phi}} = 0$$

and also that:

$$T^t_\phi = P g^t_\phi + (P+\epsilon) u^t u_\phi = (P+\epsilon) e^{-2\nu(r)} r^2 \sin^2\theta (\Omega - \omega(r,\theta)) + O(\Omega^3)$$

Therefore, by neglecting orders higher than Ω within T^t_ϕ and R^t_ϕ (see [93] for the full expression of R^t_ϕ), we obtain for $\bar{\omega}(r,\theta) := \Omega - \omega(r,\theta)$ the following equation:

$$\frac{1}{r^4}\frac{\partial}{\partial r}\Big[r^4 e^{-(\lambda+\nu)}\frac{\partial}{\partial r}\bar{\omega}(r,\theta)\Big] + \frac{e^{\lambda-\nu}}{r^2\sin^3\theta}\frac{\partial}{\partial\theta}\Big(\sin^3\theta\frac{\partial}{\partial\theta}\bar{\omega}(r,\theta)\Big) - 16\pi(P+\epsilon)e^{\lambda-\nu}\bar{\omega}(r,\theta) = 0 \tag{2.89}$$

where $\nu = \nu(r)$, $\lambda = \lambda(r)$, $P = P(r)$ and $\epsilon = \epsilon(r)$. Now, by defining the quantity:

$$j(r) := e^{\lambda(r)-\nu(r)} = \begin{cases} e^{-\nu(r)}\sqrt{1 - \frac{2m(r)}{r}}, & r < R \\ 1, & r \geq R \end{cases}$$

such that:

$$\frac{d}{dr} j(r) = -e^{-\nu}\frac{1}{\sqrt{1-\frac{2m}{r}}}\Big(\frac{4\pi r^3\epsilon - m}{r^2}\Big)e^{-(\lambda+\nu)}\Big[\frac{m + 4\pi r^3 P}{r(r-2m)}\Big] = -4\pi(\epsilon+P)e^{\lambda-\nu} r \tag{2.90}$$

we obtain from eq.2.89 the following identity:

$$\frac{1}{r^4}\frac{}{\partial r}\Big[r^4 j(r)\frac{\partial}{\partial\theta}\bar{\omega}(r,\theta)\Big] + \frac{4}{r}\bar{\omega}(r,\theta)\frac{d}{dr}j(r) + \frac{e^{\lambda-\nu}}{r^2\sin^3\theta}\frac{\partial}{\partial\theta}\Big(\sin^3\theta\frac{\partial}{\partial\theta}\bar{\omega}(r,\theta)\Big) = 0 \tag{2.91}$$

The above equation can be solved by separation of variables. However an expansion of $\bar{\omega}(r,\theta)$ in Legendre polynomials will not separate the equation because ω transforms under rotations not like a scalar but like a component of a vector. This is related to the presence of $\sin^3\theta$ in the equation instead of $\sin\theta$, that is typical of the angular part of the Laplace operator in spherical coordinates. $\omega(r,\theta)$ is the angular velocity acquired by an observer who falls freely from infinity to the point (r,θ), thus it is associated to a vector in the space. Because of this, to solve the above equation by separation of variables, an expansion in vector spherical harmonics must be used. From these one can show that the appropriate expansion of $\bar{\omega}(r,\theta)$ is the following:

$$\bar{\omega}(r,\theta) = \sum_{l=1}^{\infty}\bar{\omega}_l(r)\Big(-\frac{1}{\sin\theta}\frac{dP_l}{d\theta}\Big) \tag{2.92}$$

where $P_l = P_l(\cos\theta)$ are the Legendre polynomials. By inserting this expansion inside the eq.2.91 we have that:

$$\sum_{l=1}^{\infty}\Big\{f_l(r)\Big(-\frac{1}{\sin\theta}\frac{dP_l}{d\theta}\Big)+g_l(r)\Big[\frac{1}{\sin^3\theta}\frac{d}{d\theta}\Big(\sin^3\theta\frac{d}{d\theta}\Big(-\frac{1}{\sin\theta}\frac{dP_l}{d\theta}\Big)\Big)\Big]\Big\}=0 \tag{2.93}$$

where:

$$f_l(r)=\frac{1}{r^4}\frac{d}{dr}\Big(r^4 j(r)\frac{d}{dr}\bar{\omega}_l(r)\Big)+\frac{4}{r}\Big(\frac{d}{dr}j(r)\Big)\bar{\omega}_l(r) \tag{2.94}$$

$$g_l(r)=\frac{e^{\lambda-\nu}}{r^2}\bar{\omega}_l(r) \tag{2.95}$$

The separation of variables allows us to solve eq.2.98 by defining a new quantity ξ_l such that the equation can be split into the two following equations:

$$\sum_{l=1}^{\infty}[f_l(r)-\xi_l g_l(r)]=0 \tag{2.96}$$

$$\sum_{l=1}^{\infty}\Big[\frac{1}{\sin^3\theta}\frac{d}{d\theta}\Big(\sin^3\theta\frac{d}{d\theta}\Big(-\frac{1}{\sin\theta}\frac{dP_l}{d\theta}\Big)\Big)+\xi_l\Big(-\frac{1}{\sin\theta}\frac{dP_l}{d\theta}\Big)\Big]=0 \tag{2.97}$$

By solving the eq.2.97 we find that $\xi_l = l(l+1)-2$. Therefore from the equation 2.96 we obtain for the radial functions the following result:

$$\frac{1}{r^4}\frac{d}{dr}\Big(r^4 j(r)\frac{d}{dr}\bar{\omega}_l(r)\Big)+\frac{4}{r}\Big(\frac{d}{dr}j(r)\Big)\bar{\omega}_l(r)-e^{\lambda-\nu}\frac{l(l+1)-2}{r^2}\bar{\omega}_l(r)=0 \tag{2.98}$$

Now we study the asymptotically behaviour of the above expression. Firstly, we consider the limit $r \to 0$. It is useful to note that from the derivative of $j(r)$ we have:

$$\frac{d}{dr}j(r)\to 0,\ r\to 0 \implies \lim_{r\to 0} j(r)=j_0<\infty$$

Moreover, from the static solution we can know the values of λ and ν at the origin; we call them λ_0, ν_0. Therefore within the limit $r \to 0$ the equation 2.98 becomes:

$$\frac{j_0}{r^4}\frac{d}{dr}\Big(r^4\frac{d}{dr}\bar{\omega}_l(r)\Big)-e^{\lambda_0-\nu_0}\frac{l(l+1)-2}{r^2}\bar{\omega}_l(r)=0 \tag{2.99}$$

Here by assuming a power expansion $\bar{\omega}_l(r)=\sum_{s=0}^{\infty}C_l r^s$, we solve the equation obtaining that:

$$s_{1,2}=-\frac{3}{2}\pm\sqrt{\frac{9}{4}+[l(l+1)-2]\frac{e^{\lambda_0-\nu_0}}{j_0}}$$

$$\bar{\omega}_l(r)=A_{l,1}r^{s_1}+B_{l,2}r^{s_2},\ r\to 0$$

Moreover, we require the regular behaviour of the solution; thus $\bar{\omega}_l(r)\to 0$ when $r \to 0$. Because of this we have the following result:

$$\bar{\omega}_l(r)\propto r^s,\ r\to 0$$

$$s=-\frac{3}{2}+\sqrt{\frac{9}{4}+[l(l+1)-2]\frac{e^{\lambda_0-\nu_0}}{j_0}}$$

Now we study the behaviour of the solution $\bar{\omega}_l(r)$ when $r \to \infty$. We require the asymptotic flatness of the spacetime. We know that $e^{\lambda(r)}, e^{\nu(r)} \to 1$ when $r \to +\infty$. Therefore within this limit, eq.2.98 reduces to:

$$\frac{1}{r^4}\frac{d}{dr}\Big(r^4\frac{d}{dr}\bar{\omega}_l(r)\Big) - \frac{l(l+1)-2}{r^2}\bar{\omega}_l(r) = 0 \tag{2.100}$$

Here by assuming a power expansion $\bar{\omega}_l(r) = \sum_{s=0}^{\infty} C_l r^s$, we solve the equation obtaining that:

$$\begin{aligned} s_1 &= l-1 \\ s_2 &= -l-2 \\ \bar{\omega}_l(r) &= A'_{l,1}r^{s_1} + B'_{l,2}r^{s_2},\ r \to \infty \end{aligned}$$

However, we remember the definition: $\bar{\omega}(r,\theta) = \Omega - \omega(r,\theta)$ where we assumed $\Omega = const.$ (rigid rotation). Thus, since $\omega(r,\theta) \to 0$ when $r \to \infty$ because of the asymptotic flatness of the spacetime, it is required that $\bar{\omega}(r,\theta) \to \Omega$ when $r \to \infty$. Since $-l-2 < 0\ \forall l$, the term $B'_{l,2}r^{s_2}$ must be associated to $\omega(r,\theta)$ when $r \to \infty$; instead, the *only* possibility that the other term is associated to Ω when $r \to \infty$ is that $l \equiv 1$. This is the solution of the problem such that $\bar{\omega}(r,\theta) \to \Omega$ when $r \to \infty$. In particular since $l = 1$ we have also that $\xi_l = l(l+1) - 2 = 0$; thus, *the actual solution of the problem hasn't an angular dependence, but it is only a radial function*: $\bar{\omega}(r,\theta) \equiv \bar{\omega}(r)$. In order to compute a slowly rotating equilibrium model to the first order in Ω, the equation that we need to solve together with the structure equations of non rotating relativistic fluids is the following:

$$\frac{1}{r^4}\frac{d}{dr}\Big[r^4 j(r)\frac{d}{dr}\bar{\omega}(r)\Big] + \frac{4}{r}\Big[\frac{d}{dr}j(r)\Big]\bar{\omega}(r) = 0 \tag{2.101}$$

where:

$$\begin{aligned} \bar{\omega}(r) &= \Omega - \omega(r) \\ j(r) &= \begin{cases} e^{-\nu(r)}\sqrt{1-\frac{2m(r)}{r}},\ r < R \\ 1,\ r \geq R \end{cases} \end{aligned}$$

It is also important to note that because $l = 1$ we have:

$$\begin{aligned} &\bar{\omega}_l(r) \propto r^s,\ r \to 0 \\ &s = -\frac{3}{2} + \sqrt{\frac{9}{4} + [l(l+1)-2]\frac{e^{\lambda_0-\nu_0}}{j_0}} = 0 \end{aligned}$$

thus $\bar{\omega}(r) \to const.$ when $r \to 0$. This is important because it implies that $(d\bar{\omega}/dr)(0) = 0$. Therefore, one of the boundary conditions required to solve the 2-order ODE associated with $\bar{\omega}(r)$ corresponds to the condition of regular solution at the origin, i.e. $(d\bar{\omega}/dr)(0) = 0$. In order to compute models within this approximation one has to fix two parameters. One is ϵ_c that is needed to solve the structure equations of the non rotating model, and the other is for instance the central value of $\omega(r)$, i.e. $\omega(0) = \omega_c$ ($\implies \bar{\omega}(0) = \Omega - \omega_c$). We can also note that from eq.2.101 and eq.2.90 it follows that:

$$\begin{aligned} \int_0^R \frac{d}{dr}\Big[r^4 j(r)\frac{d}{dr}\bar{\omega}(r)\Big]dr &= \int_0^R \Big[16\pi(\epsilon+P)e^{\lambda-\nu}r^4\bar{\omega}(r)\Big]dr \\ \implies R^4\frac{d\bar{\omega}}{dr}(R) &= \int_0^R \Big[16\pi(\epsilon+P)e^{\lambda-\nu}r^4\bar{\omega}(r)\Big]dr \end{aligned}$$

The left hand side term of the last equation has the dimension of an angular momentum in the gravitational units. Therefore we can define form it the *total angular momentum* of a slowly rotating relativistic system as follows:

$$J \coloneqq \frac{1}{6}\Big[R^4\frac{d\bar{\omega}}{dr}(R)\Big] = \frac{8\pi}{3}\int_0^R r^4\frac{P(r)+\epsilon(r)}{\sqrt{1-\frac{2m(r)}{r}}}[\Omega-\omega(r)]e^{-\nu(r)}dr \tag{2.102}$$

It can be shown[60] that this result corresponds exactly to the slow-rotation approximation of the angular momentum of arbitrary rotating fluid defined with the Komar integral 2.82. Moreover, its Newtonian weak field limit ($P(r) \ll \epsilon(r)$, $\epsilon(r) \approx \rho(r)$, $2m/r \ll 1$, $\omega(r) \approx 0$ and $e^{-\nu} \approx 1$) is the angular momentum of a non relativistic spherical massive body:

$$J = \frac{8\pi}{3}\Omega\int_0^R r^4\rho(r)dr \tag{2.103}$$

We can define also the *Moment of inertia* as $I \coloneqq J/\Omega$. It is important to note that since we're considering the order Ω within the slow-rotation approximation, then $\omega = O(\Omega)$ and so $J = O(\Omega)$. Because of this, within this order *the moment of inertia is independent on the star spin frequency.* Eventually, since $j(r) = 1$ outside the star we have also that:

$$\begin{aligned} \frac{1}{r^4}\frac{d}{dr}\Big[r^4\frac{d}{dr}\bar{\omega}(r)\Big] &= 0 \ (r > R) \\ \implies r^4\frac{d}{dr}\bar{\omega}(r) &= R^4\frac{d\bar{\omega}}{dr}(R) \equiv 6J \ (r > R) \\ \implies \bar{\omega}(r) &= -\frac{2J}{r^3} + \Omega \ (r > R) \\ \implies \omega(r) &= -\frac{2J}{r^3} \ (r > R) \end{aligned}$$

Therefore, outside the rotating star, the metric of the spacetime to the order Ω within the slow-rotation approximation has the following analytical expression:

$$ds^2 = -e^{2\nu(r)}dt^2 + e^{2\lambda(r)}dr^2 + r^2\Big[d\theta^2 + \sin^2\theta\Big(d\phi - -\frac{2J}{r^3}dt\Big)^2\Big] \tag{2.104}$$

Eventually we estimate the Keplerian frequency of rotating relativistic stars within the limit of slow rotation. This can be done making use of eq.2.85 and by considering that for slowly rotating NSs to the order Ω:

$$
\begin{aligned}
e^{2\nu}(R) &\approx 1-\frac{2M}{R}\\
\nu'(R) &\approx \frac{M}{R}\Big(1-\frac{2M}{R}\Big)^{-1}\\
\psi &\approx 0, \psi' \approx 0\\
\zeta' &\approx \frac{1}{R}\\
\omega'(R) &\approx -\frac{3\omega(R)}{R}
\end{aligned}
$$

Therefore it can be shown that the following expression for the mass-shedding limit turns out:

$$\Omega_K \approx \Big[1+\frac{\omega(R)}{\Omega_K}-2\Big(\frac{\omega(R)}{\Omega_K}\Big)^2\Big]^{-1/2}\sqrt{\frac{M}{R^3}} \tag{2.105}$$

where we can clearly note the dependence on the ratio ω/Ω that we discussed during the introduction. This underlines how the frame dragging affects the efficiency of the centrifugal forces, especially these are determined not by Ω but rather from Ω/ω.

We report in the following some numerical results about uniformly rotating NSs computed with a code based on the Hartle's formalism, which works to the first order approximation in Ω. The code solves numerically the set of differential equations earlier discussed (the set of equations of the static model and the equation for $\omega(r)$), particularly by splitting the 2-order ODE 2.101 in two 1-order ODEs and applying a fourth order Runge-Kutta method. The code computes models once two parameters are specified. These are chosen as the central mass-energy density ϵ_c and the constant spin frequency Ω (instead of ω_c). In Figure2.7 we report the diagram moment of inertia versus gravitational mass for equilibrium sequences of uniformly rotating

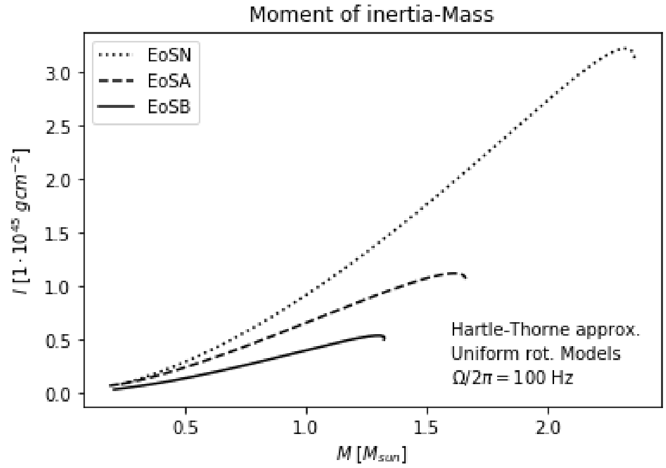

Figure 2.7: Graph of the function $I = I(M)$ for three different equilibrium sequences of NSs uniformly rotating at 100 Hz. All the models are computed within the slow-rotation approximation. The three different sequences are obtained with the three different EoSs: EoSA, EoSB and EoSN. See the text for the details.

NSs with a 100Hz frequency of rotation. The plot shows three different sequences of models computed by using the same three different EoSs described in the paragraph concerning non rotating configurations. We can see from the figure that the trend of the relation $I = I(M)$ is mostly monotonic increasing. There is an initial increase of the moment of inertia with the mass until an absolute maximum for each sequence, follows by a small decrease until the maximum value of the gravitational mass. In particular, the more stiff is the EoS the more rapidly is the increase of I. The absolute maximum of the moment of inertia is reached at a value of gravitational mass that is typically a few percent lower than the maximum value of M[4]. The latest behaviour can be explain with a simple consideration. By remembering that for these models the diagrams radius versus gravitational mass are the same plotted in Figure2.4, because we are using the slow-rotation approximation to the first order in Ω, then considering that dimensionally we have $I \sim MR^2$ therefore for a fixed mass the more stiff is the EoS the bigger is the radius and so the more high is the value of the inertia moment. Generally, the $I(M)$ dependence is much more sensitive to the stiffness of the EoS, than the $R(M)$ dependence[4]. Moreover in the figure, the considered range of masses is about $0.4 - 2.3\ M_{\odot}$. If one looks at the plot radius versus gravitational mass for these sequences within this range of masses, thus a monotonic increasing of the mass together with an almost constancy of the radius until the maximum mass can be noted. Moreover, near the maximum mass a rapid decrease of the radius for an almost constant gravitational mass is the general behaviour among all the EoSs. All of these considerations can explain the universal[20] trend of the relation $I = I(M)$: since $I \sim MR^2$, before the maximum mass $\delta M \gg 0\ \wedge\ \delta R \approx 0$, thus there will be an increase of I; near the maximum mass $\delta M \approx 0\ \wedge\ \delta R \ll 0$, thus there will be a decrease of the moment of inertia. In Figure2.8 we report the logarithmic diagram angular momentum versus moment

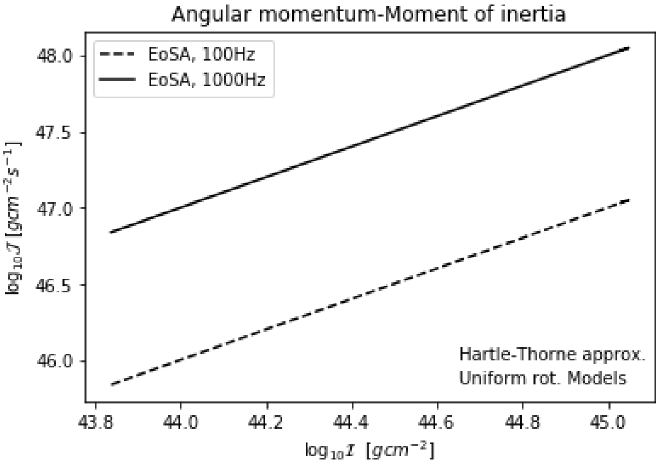

Figure 2.8: Graph of the function $J = J(I)$ on a logarithmic scale for a fixed Ω and a single EoS, EoSA. Two sequences of equilibrium models a shown, these corresponding to two different values of the angular velocity, $\Omega = 100$ Hz and $\Omega = 1000$ Hz. See the text for the details.

---

[20] This means that it is the same for different EoSs.

of inertia for a single EoS, in particular the equation of state EoSA, and for two different equilibrium sequences of uniformly rotating models computed with two different values of the spin frequency, $\Omega = 100$ Hz and $\Omega = 1000$ Hz. The plot reveals the linearity between the two quantities. This reflects the proportionality between J and I for a fixed Ω that we expect from the definition $J = I\Omega$. Moreover, within the logarithmic scale, we can clearly see that the behaviour of the relation $J = J(I)$ changes only on the intercept but not on the slope. This verifies the independence of the moment of inertia one the spin frequency for a fixed EoS, as predicted from the slow-rotation approximation to the first order in Ω. Actually, when $\Omega = 1000$ Hz the slow-rotation approximation doesn't represent more a good numerical scheme to probe rotating NSs. This is clear when looking at the Figures2.9(a)-(b) where the relations $I = I(M)$ and $I = I(R)$ are plotted for 1000 Hz uniformly rotating models computed with two different numerical codes: the approximate one, based on the Hartle's formalism, and an exact one (RNS), that we will describe in the next paragraph. We can see that the slow-rotation approximation involves wrong estimates of the quantities, underling its failing for high rotation rates.

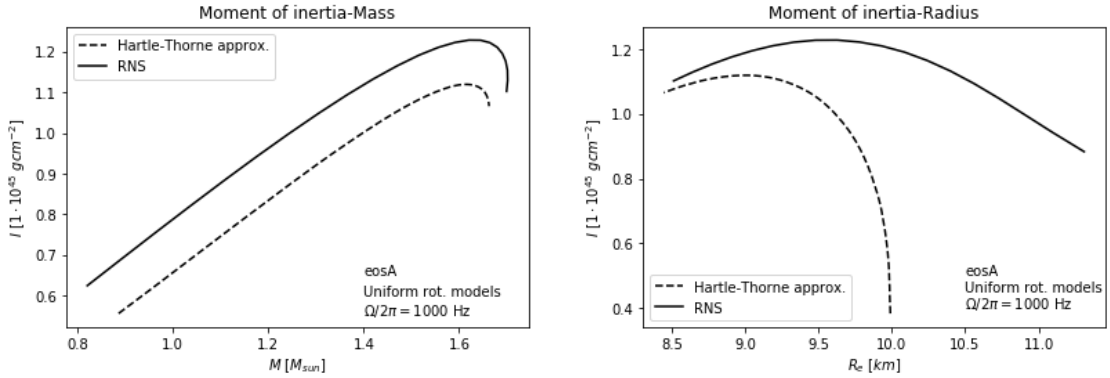

(a) Graph of the function $I = I(M)$. The two sequences correspond to 1000 Hz uniformly rotating models computed with two different codes with the equation of state EoSA.

(b) Graph of the function $I = I(R)$. The two sequences correspond to 1000 Hz uniformly rotating models computed with two different codes with the equation of state EoSA.

Figure 2.9

2.4.2 "Exact" solutions (1): the RNS code

The following method used to compute models of rotating NSs consists on an "exact" approach, in the sense that it aims to solve directly the set of structure equations without make approximations, unlike the Hartle's method. It is based on the formulation developed by Bardeen&Wagoner[84] and on the HSCF method described during the introduction. In particular, we discuss here the numerical scheme developed by Komatsu-Erigichi-Hachisu [59] (hereafter KEH) which applies an integral representation of the differential relativistic structure equations by using appropriate Green's function. The set of equations includes the three elliptical PDEs 2.51-2.52-2.53, the first-order PDE for the metric potential α, the global first integral of the hydrostationary equilibrium equations (eq.2.67), the equation for the profile of Ω (eq.2.62) associated with the parametric expression of $F(\Omega)$ (eq.2.68), and the equation of state $P = P(\epsilon)$. There are seven equations on seven unknowns, and three boundary conditions are required in order to compute unique solutions. We can obtain 1-dimensional equilibrium sequences by maintaining fixed two parameters and changing the third one, or even 2-dimensional surfaces of equilibrium models by specifying only one parameter and changing the others. Especially, like the HSCF method, the KEH scheme computes solutions through a numerical iterative procedure, during which the maximum value of the mass-energy density ϵ_{max} and the axis ratio r_p/r_e are fixed. The parameter A is also fixed in order to obtain unique differentially rotating models. The KEH scheme represents a powerful method to probe strong gravity objects with very high rotation rates in a really stable numerical manner. The integral form of the Einstein equations is useful to satisfy automatically the spacetime asymptotic flatness during the iterations. More recently, the KEH scheme has been improved in the accuracy by Cook-Shapiro-Teukolsky [73] (CST), which introduced a compactification on the radial variable. Indeed, within the KEH scheme the integrals of equations extend to radial infinity. The numerical integration requires integrals to be cut off at a certain large distance. Clearly, the accuracy of the method is aggravated by this fact. The CST compactification provides a new radial variable $s := r/(r + r_e)$, where r_e is the coordinate equatorial radius, thus mapping the integration range $[0, +\infty)$ to the finite segment $[0, 1]$. This substitution significantly increased the overall accuracy of the numerical solution, allowing boundary conditions to be exactly enforced[94]. Eventually, Stergioulas&Friedman [95, ?] implemented their own KEH code following the CST compactification; this is available as a public domain code, named `RNS`. In the following we will discuss the original KEH scheme and also we will report some numerical results concerning equilibrium models of uniformly rotating NSs computed with the `RNS` code.

The transformation of the differential form of the structure equations into an integral representation is obtained through the Green's function formalism, like HSCF method. In particular for the first equation 2.51 the Green's function of the linear operator ∇ is considered. This is the following:

$$G(\mathbf{r}, \mathbf{r}') = -\frac{1}{4\pi} \frac{1}{\|\mathbf{r} - \mathbf{r}'\|} \tag{2.106}$$

By remembering the expansion series of the function $1/\|\mathbf{r} - \mathbf{r}'\|$ reported in eq.1.32, one obtains the following integral form of the differential equation2.51:

$$\rho = -\frac{e^{-\gamma/2}}{4\pi} \int_0^\infty dr' \int_{-1}^{1} d\mu' \int_0^{2\pi} d\phi' (r')^2 S_\rho(r', \mu') \Big\{ \sum_{n=0}^{\infty} f_n(r, r') \mathcal{G}_n(\mu, \mu', \phi, \phi') \Big\} \tag{2.107}$$

where $n, m \in \mathbb{N}$ and:

$$\begin{aligned}
\mu, \mu' &= \cos\theta, \cos\theta' \\
f_n(r, r') &= \frac{1}{r}\Big(\frac{r'}{r}\Big)^n \Theta(r'-r) + \frac{1}{r'}\Big(\frac{r}{r'}\Big)^n \Theta(r-r') \\
\mathcal{G}_n(\mu, \mu', \phi, \phi') &= P_n(\mu)P_n(\mu') + 2\sum_{m=1}^{n} \frac{(n-m)!}{(n+m)!} P_n^m(\mu) P_n^m(\mu') \cos\left[m(\phi-\phi')\right]
\end{aligned}$$

where $P_n(\mu)$, $P_n(\mu')$ are the Legendre polynomials. Since the system is equatorially symmetric (see note 10 in Chapter1) $S_\rho(r', \mu') = S_\rho(r', -\mu')$, therefore $n \to 2n$ because of the typical behaviour of the Legendre polynomials $P_n(\mu) \sim \mu^n$. Moreover as we showed in eq.1.34 the term summed over m can be deleted. Thus the integral equation reduces to the following simpler form:

$$\rho = -e^{-\gamma/2} \int_0^\infty dr' \int_0^1 d\mu' (r')^2 S_\rho(r', \mu') \sum_{n=0}^{\infty} f_{2n}(r, r') P_{2n}(\mu) P_{2n}(\mu') \tag{2.108}$$

Concerning eq.2.52 one can note that:

$$\nabla + \frac{1}{r}\frac{\partial}{\partial r} - \frac{1}{r^2}\mu\frac{\partial}{\partial \mu} = \nabla + \frac{1}{r}\frac{\partial}{\partial r} + \frac{1}{r^2 \tan\theta}\frac{\partial}{\partial \theta}$$

then, by using cylindrical coordinates:

$$\begin{cases} \varpi &= r\sin\theta \\ z &= r\cos\theta \\ \phi &= \phi \end{cases}$$

one can find the following result:

$$\begin{aligned}
\nabla + \frac{1}{r}\frac{\partial}{\partial r} + \frac{1}{r^2 \tan\theta}\frac{\partial}{\partial \theta} &= \frac{1}{\varpi}\frac{\partial}{\partial \varpi} + \frac{\partial^2}{\partial \varpi^2} + \frac{1}{\varpi^2}\frac{\partial^2}{\partial \phi^2} + \frac{\partial^2}{\partial z^2} + \\
&+ \frac{1}{\sqrt{\varpi^2 + z^2}}\Big[\frac{\varpi}{\sqrt{\varpi^2+z^2}}\frac{\partial}{\partial \varpi} + \frac{z}{\sqrt{\varpi^2+z^2}}\frac{\partial}{\partial z}\Big] + \\
&+ \frac{1}{z^2+\varpi^2}\frac{z}{\varpi}\Big[z\frac{\partial}{\partial \varpi} - \varpi\frac{\partial}{\partial z}\Big] = \\
&= \frac{1}{\varpi^2}\frac{\partial}{\partial \varpi}\Big(\varpi^2 \frac{\partial}{\partial \varpi}\Big) + \frac{\partial^2}{\partial z^2} + \frac{1}{\varpi^2}\frac{\partial^2}{\partial \phi^2}
\end{aligned}$$

where the last term on ϕ can be deleted: it doesn't affect eq.2.52 since the spacetime is axially symmetric. Therefore by inserting this result in eq.2.52 we obtain the following new differential equation for the γ potential:

$$\Big(\frac{\partial^2}{\partial \varpi^2} + \frac{\partial^2}{\partial z^2}\Big)[\varpi \gamma e^{\gamma/2}] = \varpi S_\gamma(r, \mu) \tag{2.109}$$

Its integral representation can be obtained by using the Green's function of the 2-dimensional Laplace operator, which is:

$$G(\mathbf{r}, \mathbf{r}') = \frac{1}{2\pi} \ln \|\mathbf{r} - \mathbf{r}'\| \tag{2.110}$$

We use again the series expansion of the Green's functions. In particular, for the above function we have that:

$$\ln\|\mathbf{r}-\mathbf{r}'\| = -\sum_{n=1}^{\infty}\frac{1}{n} f_n^1(r,r')(\cos n\theta\cos n\theta' + \sin n\theta\sin n\theta') + g(r,r') \equiv \mathcal{F}(r,r',\theta,\theta') \tag{2.111}$$

where:

$$f_n^1(r,r') = \left(\frac{r}{r'}\right)^n \Theta(r'-r) + \left(\frac{r'}{r}\right)^n \Theta(r-r') \tag{2.112}$$

$$g(r,r') = \Theta(r-r')\ln r + \Theta(r'-r)\ln r' \tag{2.113}$$

Then, the integral form of eq.2.109 is the following:

$$r\sin\theta\gamma = \frac{1}{2\pi}e^{-\gamma/2}\int_0^{\infty} dr' \int_0^{2\pi} d\theta' \sin\theta'(r')^2 S_\gamma(r',\theta')\mathcal{F}(r,r',\theta,\theta') \tag{2.114}$$

However, $g(r,r')$ can be deleted from the equation because:

$$\begin{aligned}
\int_0^{2\pi} d\theta'\sin\theta' S_\gamma(r',\theta') &= \int_0^{\pi} d\theta'\sin\theta' S_\gamma(r',\theta') + \int_\pi^{2\pi} d\theta'\sin\theta' S_\gamma(r',\theta') = \\
&= \int_0^{\pi} d(\theta-\pi)\sin(\theta-\pi) S_\gamma(r',\theta-\pi) + \\
&+ \int_\pi^{2\pi} d\theta'\sin\theta' S_\gamma(r',\theta') = \\
&= -\int_\pi^{2\pi} d\theta\sin\theta S_\gamma(r',\theta) + \int_\pi^{2\pi} d\theta'\sin\theta' S_\gamma(r',\theta') = 0
\end{aligned}$$

For the other terms one has to use the series expansion:

$$\sin n\theta = \sum_{\substack{r=0\\ 2r+1\le n}}^{\infty} (-1)^r \binom{n}{2r+1} (\cos\theta)^{n-2r-1}(\sin\theta)^{2r+1}$$

$$\cos n\theta = \sum_{\substack{r=0\\ 2r\le n}}^{\infty} (-1)^r \binom{n}{2r} (\cos\theta)^{n-2r}(\sin\theta)^{2r}$$

and thus by solving integrals together with the condition of equatorial symmetry, the following integral representation of eq.2.109 is found:

$$\begin{aligned}
r\sin\theta\gamma = &-\frac{2}{\pi}e^{-\gamma/2}\int_0^{\infty} dr' \int_0^{1} d\mu'(r')^2 S_\gamma(r',\mu') \sum_{n=1}^{\infty}\frac{f_{2n-1}^1(r,r')}{2n-1}\cdot \\
&\cdot \sin\left[(2n-1)\theta\right]\sin\left[(2n-1)\theta'\right]
\end{aligned} \tag{2.115}$$

where $\mu' = \cos\theta'$. Eventually, concerning the third elliptical PDE (eq.2.53), by using the same analysis done before for the linear operator in eq.2.52 (now there is only a factor 2 more) and multiplying eq.2.53 by $r\sin\theta\cos\phi$, one finds that:

$$\nabla[\omega e^{(\gamma-2\rho)/2} r\sin\theta\cos\phi] = r\sin\theta\cos\phi S_\omega(r,\theta) \tag{2.116}$$

Here by using again the Green's function of the 3-dimensional Laplace operator and its series expansion, it follows that:

$$\begin{aligned}\omega r\sin\theta\cos\phi = &-\frac{1}{4\pi}e^{(2\rho-\gamma)/2}\int_0^\infty dr'\int_0^\pi d\theta'\int_0^{2\pi} d\phi'(r')^3\sin^2\theta'\cos\phi' S_\omega(r',\theta')\cdot\\ &\cdot\Big\{\sum_{n=0}^{\infty} f_n(r,r')\mathcal{G}_n(\theta,\theta',\phi,\phi')\Big\}\end{aligned} \tag{2.117}$$

Now we consider that, firstly:

$$\int_0^{2\pi} d\phi'\cos\phi' = 0$$

therefore the first addend in the definition of $\mathcal{G}_n(\theta,\theta',\phi,\phi')$ can be deleted. Secondly:

$$\begin{aligned}\int_0^{2\pi} d\phi'\cos\phi'\cos[m(\phi-\phi')] = &\Big(\int_0^{2\pi} d\phi'\cos\phi'\cos m\phi'\Big)\cos m\phi+\\ &+\Big(\int_0^{2\pi} d\phi'\cos\phi'\sin m\phi'\Big)\sin m\phi\end{aligned}$$

and thus, by applying the Werner's identities:

$$\cos\alpha\cos\beta = \frac{\cos(\alpha+\beta)+\cos(\alpha-\beta)}{2} \tag{2.118}$$

$$\sin\alpha\cos\beta = \frac{\sin(\alpha+\beta)+\sin(\alpha-\beta)}{2} \tag{2.119}$$

one obtains the following result:

$$\int_0^{2\pi} d\phi'\cos\phi'\cos[m(\phi-\phi')] = \begin{cases}0, & m\neq 1\\ \pi\cos\phi, & m=1\end{cases}$$

By considering the equatorial symmetry of the system and that $P_n^1(\mu') = P_n^1(-\mu')$ only for odd values of $n\in\mathbb{N}$, we obtain the following integral form of equation 2.116:

$$\begin{aligned}\omega r\sin\theta = &-e^{(2\rho-\gamma)/2}\int_0^\infty dr'\int_0^1 d\mu'(r')^3\sqrt{1-(\mu')^2}S_\omega(r',\mu')\cdot\\ &\cdot\sum_{n=1}^{\infty} f_{2n-1}(r,r')\frac{P_{2n-1}^1(\mu)P_{2n-1}^1(\mu')}{2n(2n-1)}\end{aligned} \tag{2.120}$$

where $\mu,\mu' = \cos\theta,\cos\theta'$. For ease of reference, we report again in the following the obtained integral representation of the three elliptical equations, which are handled by the KEH scheme:

$$\begin{aligned}
\rho =& - e^{-\gamma/2}\int_0^\infty dr' \int_0^1 d\mu' (r')^2 S_\rho(r',\mu') \sum_{n=0}^\infty f_{2n}(r,r') P_{2n}(\mu) P_{2n}(\mu') \\
r\sin\theta\gamma =& -\frac{2}{\pi} e^{-\gamma/2}\int_0^\infty dr' \int_0^1 d\mu' (r')^2 S_\gamma(r',\mu') \sum_{n=1}^\infty \frac{f^1_{2n-1}(r,r')}{2n-1}\cdot \\
&\cdot \sin\left[(2n-1)\theta\right] \sin\left[(2n-1)\theta'\right] \\
\omega r\sin\theta =& - e^{(2\rho-\gamma)/2}\int_0^\infty dr' \int_0^1 d\mu' (r')^3 \sqrt{1-(\mu')^2} S_\omega(r',\mu') \cdot \\
&\cdot \sum_{n=1}^\infty f_{2n-1}(r,r') \frac{P^1_{2n-1}(\mu) P^1_{2n-1}(\mu')}{2n(2n-1)}
\end{aligned}$$

As a really important fact, the boundary condition of asymptotic flatness is automatically satisfied by these three equations. Indeed, the radial dependence of the functions $f(r,r')$ and $f^1(r,r')$ implies that $\rho \sim O(1/r)$, $\gamma \sim O(1/r^2)$ and $\omega \sim O(1/r^3)$ for $r \to \infty$. From the above equations one can note the radial integrals extended to infinity previously mentioned. On the original KEH scheme, these integrals are computed numerically by considering the radial range $[0, 2r_e]$ (where r_e is the coordinate equatorial radius). Moreover the expansion over the index n is done until the values $n = 18, 19$. We don't discuss here the fourth first-order PDE on the potential α because of its complexity. This equation, whose expression is like $\partial\alpha/\partial\mu = S_\alpha(r,\mu)$, is solved by an integration from the pole to the equator of models with the boundary condition of the local flatness on the rotation axis close to the pole.

In order to compute models one needs to solve the four above equations together with the three following hydrostationary equilibrium equations:

$$\begin{aligned}
H - \ln u^t + \int_{\Omega_c}^{\Omega} F(\Omega') d\Omega' &= const. \\
F(\Omega) = \frac{(\Omega-\omega) e^{2(\psi-\nu)} r^2 \sin^2\theta}{1-(\Omega-\omega)^2 e^{2(\psi-\nu)} r^2 \sin^2\theta} &= A^2(\Omega_c - \Omega) \\
P &= P(\epsilon)
\end{aligned}$$

Being based on the HSCF method, the KEH scheme manages the set of equations like a fixed point problem: by starting from an initial solution as guess, a number of iterations is done until the convergence is attained, namely when the difference between solutions of two successive iterations is below a certain threshold. Especially, the KEH scheme works as follows:

- initial guesses for the metric potentials ρ, γ, ω, α and for the mass-energy density ϵ, the pressure P and the spin frequency Ω are prepared[21]
- the three elliptical equations are solved through their integral representation and new values of $\tilde{\gamma}$, $\tilde{\rho}$ and $\tilde{\omega}$ are obtained

---

[21] We remember that the actual metric potentials are ν, ψ, α and ω and that $\gamma = \psi + \nu$, $\rho = \nu - \psi$. As initial guess one can choose for instance a model computed by solving the hydrostatic equations.

- by using the new potentials $\tilde{\gamma}$, $\tilde{\rho}$ and $\tilde{\omega}$ the first order PDE for α is solved and a new potential $\tilde{\alpha}$ is obtained
- the new potentials $\tilde{\gamma}$, $\tilde{\rho}$, $\tilde{\omega}$ and $\tilde{\alpha}$ are used to compute new profiles of Ω, ϵ and P from the three equations listed above

During the iterative process the three parameter A, r_p/r_e and ϵ_{max} are fixed. Thus in the KEH scheme, as in the HSCF method, the axis ratio is chosen as the rotational parameter. This choice is justified by two reasons. Firstly fixing r_p/r_e allows to compute models in a numerical stable manner[58]; secondly, as we saw during the study of the Maclaurin spheroids, if one decide to fix a value of the angular velocity as a parameter (for instance the central frequency Ω_c), thus a degeneracy on the models appears. There are two solutions with a single value of Ω for the Maclaurin spheroids. By fixing Ω we can obtain only one model of the two corresponding models but cannot do the other one. Therefore, a value of Ω is not a good parameter to probe all the models on equilibrium sequences[59]. Apart from fixing the parameter A, that is related on the degree of the differential rotation inside models, the numerical stability of the KEH scheme originates from the resolution of the hydrostationary equilibrium equations in terms of the other two parameters, ϵ_{max} and r_p/r_e. Three boundary points P, Q and W are adopted to model the objects: P is located at the pole ($r = r_p$ and $\mu = 1$), Q at the equator ($r = r_e$ and $\mu = 0$) and W at the location of the maximum value of the mass-energy density ($\epsilon = \epsilon_{max}$) on the equatorial plane ($\mu = 0$). Thus an appropriate change of the coordinates frame makes all the quantities dimensionless. In particular one defines the new frame in the following way:

$$\hat{s} = \frac{s}{r_e},\ \hat{t} = \frac{t}{r_e},\ \hat{r} = \frac{r}{r_e},\ \hat{\theta} = \theta,\ \hat{\phi} = \phi$$

and also the metric potentials, the parameter A and the frequencies are properly rescaled:

$$\hat{\alpha} = \frac{\alpha}{r_e^2},\ \hat{\nu} = \frac{\nu}{r_e^2},\ \hat{\psi} = \frac{\psi}{r_e^2},\ \hat{\omega} = \omega r_e,\ \hat{A} = \frac{A}{r_e},\ \hat{\Omega} = \Omega r_e,\ \hat{\Omega}_c = \Omega_c r_e$$

Within this new frame the points P, Q have new locations on the computational mesh[22]; in particular P is located at $(r_p/r_e, 1)$ and Q at $(1, 0)$. Since W is identified by the condition $\epsilon = \epsilon_{max} \wedge \hat{\mu} = 0$, fixing the two parameters r_p/r_e and ϵ_{max} within the new coordinates frame corresponds to locate uniquely all the three boundary points. During the iterative procedure, the equations of the hydrostationary equilibrium are calculated exactly at these points, applying the profiles of all the metric potentials known from the previous iteration. By using the EoS, the parametric form of $F(\Omega)$ and the expression of u^t (eq.2.47) in the Euler equation, one considers the following equation:

$$H(\epsilon) + r_e^2\hat{\nu} + \frac{1}{2}\ln\left[1 - (\hat{\Omega} - \hat{\omega})^2\hat{r}^2(1 - \hat{\mu}^2)e^{2r_e^2(\hat{\psi}-\hat{\nu})}\right] - \frac{1}{2}\hat{A}^2(\hat{\Omega}_c - \hat{\Omega})^2 = \text{const.} \quad (2.121)$$

---

[22] Each mesh point is denoted by the couple $(\hat{r}_i, \hat{\mu}_i)$, where $\hat{\mu}_i = \cos\hat{\theta}_i$. The integration of the equations is done bu considering a number of mesh points of 51x101. The three elliptical equations are integrated by using the Simpson's formula, instead the trapezoidal formula is used for the integration of the first order PDE.

and computes it at P, Q and W. In particular, since $\hat{\Omega}(P) = \hat{\Omega}_c$, $\hat{\mu}(P) = 1$ and $H[\epsilon(P)] = 0$ (because the mass-energy density vanishes at the pole), at the point P one finds that:

$$r_e^2 \hat{\nu}_P = \text{const.} \tag{2.122}$$

which fixes the value of the constant. Therefore, since $\hat{\mu}(Q) = 0$, $\hat{r}_Q = 1$ and $H[\epsilon(Q)] = 0$ (because the mass-energy density vanishes at the equator), at the point Q one finds that:

$$r_e^2 \hat{\nu}_Q + \frac{1}{2} \ln\left[1 - (\hat{\Omega}_Q - \hat{\omega}_Q)^2 e^{2r_e^2(\hat{\psi}_Q - \hat{\nu}_Q)}\right] - \frac{1}{2} \hat{A}^2 (\hat{\Omega}_c - \hat{\Omega}_Q)^2 = r_e^2 \hat{\nu}_P \tag{2.123}$$

Eventually, since $H[\epsilon(W)] = H(\epsilon_{max})$ and $\hat{\mu}(W) = 0$, at the point W we have:

$$H(\epsilon_{max}) + r_e^2 \hat{\nu}_W + \frac{1}{2} \ln\left[1 - (\hat{\Omega}_W - \hat{\omega}_W)^2 \hat{r}_W^2 e^{2r_e^2(\hat{\psi}_W - \hat{\nu}_W)}\right] - \frac{1}{2} \hat{A}^2 (\hat{\Omega}_c - \hat{\Omega}_W)^2 = r_e^2 \hat{\nu}_P \tag{2.124}$$

Once ϵ_{max} and $\hat{A}$ are fixed and the metric potentials are known from the previous iteration, the two equations 2.123-2.124 contain the four unknowns $\hat{\Omega}_c$, $\hat{\Omega}_Q$, $\hat{\Omega}_W$ and r_e. Thus other two equations are required to close the problem. These come from the following equation:

$$\frac{(\hat{\Omega} - \hat{\omega}) e^{2r_e^2(\hat{\psi} - \hat{\nu})} \hat{r}^2 (1 - \hat{\mu}^2)}{1 - (\hat{\Omega} - \hat{\omega})^2 e^{2r_e^2(\hat{\psi} - \hat{\nu})} \hat{r}^2 (1 - \hat{\mu}^2)} = \hat{A}^2 (\hat{\Omega}_c - \hat{\Omega}) \tag{2.125}$$

which is computed at the points Q and W (in P the equation is $0 = 0$). The equations 2.123-2.124 and the above computed at Q and W are all solved through the Newton-Raphson method. They give the values of $\hat{\Omega}_c$ and r_e, which are used to compute the Ω profile from eq.2.125. The obtained distribution of Ω is applied to determine the profile of ϵ (and of P through the EoS) from eq.2.121. The obtained profiles of ϵ and Ω are used to restart the iterative procedure, computing new metric potentials from the integrals of the Einstein equations.

We report now numerical results obtained with the `RNS` code. All of them represent uniformly rotating relativistic stars computed with a single barotropic equation of state, the EoSA described before. Several sequences of equilibrium models are plotted, in particular the Keplerian sequence (namely, the mass-shedding limit in the figures). This is computed by the code making use of eq.2.85. Together with the static configurations, it represents a boundary sequence for the stable solutions space of uniformly rotating objects. However, the Keplerian limit alone is not enough to determine the stability of models. As we discussed before, hydrostatic barotropic equilibria are dynamically (and also secularly) unstable beyond the point of maximum gravitational mass along the equilibrium sequence. In the case of uniformly rotating models the situation is quite different. In particular when dealing with rotating fluids one has to study the stability against both axisymmetric and non-axisymmetric modes, looking at the dynamical and the secular stability at the same time. A really important and analytical result concerning the axisymmetric stability is the **Turning-Point Theorem**[96]: *along an equilibrium sequence of barotropic and uniformly rotating relativistic models with constant angular momentum, models located beyond an extremum of the mass are secularly unstable.* The proof also shows that: *along an equilibrium sequence of barotropic and uniformly rotating relativistic models with constant baryonic mass, models located beyond an extremum of the angular momentum are secularly unstable.* This represents a *sufficient* condition for the secular stability, in the sense that the theorem provides stable models *if* they are located on a certain side of the sequence, but *it doesn't ensure their stability when they are not located there.* More recently[97] it has been shown that actually the secular instability of models starts just before the turning-point along the equilibrium sequence. By using fully general relativistic simulations, it has been found that the dynamical instability line coincides with the turning-point line[23] for spherical stars and it departs from the latter for uniformly rotating models, providing 5% central mass-energy density less in the case of rapid rotations. Because of this, in order to probe the actual secular and dynamical stability of uniformly rotating NS models one needs also numerical simulations together with the analytical theorem. However, the difference between the dynamical instability line and the turning-point line is quite small; thus we only applied the analytical theorem to study the stability of models plotted on the following figures. Eventually, for the secular and dynamical stability against non-axisymmetric modes one can appeal to the parameter β. During the introduction we saw that Newtonian stars are dynamical unstable when $\beta \gtrsim 0.27$, while they are secular unstable for $\beta \gtrsim 0.14$ via gravitational radiation or viscosity. Fore relativistic stars the situation is more complex. At a sufficiently high rotation rates ($\beta \gtrsim 0.27$ in the case of Maclaurin spheroids) NSs present dynamical instability driven by hydrodynamics and gravity; this instabilities deform stars into a bar shape causing the emission of strong GWs with frequencies in the KHz regime[61]. Instead, at lower rotation rate, NSs can become unstable to secular non-axisymmetric instabilities, driven by GWs or viscosity. It is clear that the onset of gravitational-radiation-driven secular instabilities does not coincide with the onset of the viscosity-driven ones, which occur at larger β[98]. Bar-modes instabilities are related to triaxial equilibrium configurations of NSs. Very recently, some authors have probed the dependence on the EoS of the properties of these extreme equilibria. For instance, it has been shown[99] that quark stars generally have a longer triaxial sequences of solutions than NSs; quark stars can reach a larger triaxial deformation before terminating the sequence at the mass-shedding limit. Moreover, when considering similar triaxial configurations, quark stars are (slightly) more efficient GW sources than NSs. However, in order to reveal interesting results from non-axisymmetric instabilities of compact stars one often needs relativistic simulations. In this thesis we will not focus on these aspects and we will consider the model with $\beta = 0.14$ as the starting point of the secular instability. Thanks to the `RNS` code we are able to compute models by fixing the central mass-energy density ϵ_c as a first parameter[24] and not only r_p/r_e as second parameter, but we can choose for example the baryonic mass or the angular momentum or even others instead of r_p/r_e. This

---

[23] This is the line connecting turning-points which belong to different equilibrium sequences of constant angular momentum or constant baryonic mass.

[24] It should be noted that here we are not using ϵ_{max}, that is the first parameter in the KEH scheme. For slowly rotating configurations one can consider that $\epsilon_c \approx \epsilon_{max}$ but the two values are quite different when rotation becomes fast. For instance, quasi-toroidal rapidly differentially rotating models show $\epsilon_{max} > \epsilon_c$[100]. However we will not go so much in detail in this thesis and we will assume $\epsilon_c \equiv \epsilon_{max}$ for all the models computed with `RNS`.

allows to build easily sequences of models with fixed values of the bulk quantities.

In Figure2.10 we report the diagram gravitational mass versus central energy density for several uniformly rotating models. Here, the thick-solid black line is the static sequence and the blue line is the Keplerian sequence. The last define the maximum mass attainable by the uniformly rotating models. In the figure we report also with thin-solid black lines sequences of constant angular momentum and with dashed-black lines sequences of constant baryonic mass. The extrema of both these classes of sequences match with each other, defining the turning-point line labeled with an arrow in the figure. On the right side of that line secularly unstable models are located. We can clearly see that the uniform rotation yields higher gravitational masses and also baryonic masses for a fixed ϵ_c with respect of static models. This increase on both the masses is an effect of the rotation. Like Newtonian stars, the rotation allows NSs to hold more baryonic mass within an equilibrium configuration; this comes by the presence of centrifugal forces which lower the effective gravity of the star. Moreover, only in the case of relativistic star we can note also the increase of the total mass-energy (the gravitational mass) because of the contribute of the rotational kinetic energy. Generally, *the maximum gravitational mass of stable uniformly rotating NSs is much higher than* M_{TOV}. By denoting this value as M_{max}, several works[73, 53, 101, 102] have shown that $(M_{max} - M_{TOV})/M_{TOV} \approx 20\%$ and also that this increment is quite universal among different EoSs and it can be describe with a relation $M_{max} \approx (1.203 \pm 0.022)M_{TOV}$. Moreover we can see that for a fixed gravitational mass rotating models show lower central mass-energy density than the non-rotating ones. Therefore, *the rotation of relativistic stars bring to higher gravitational masses, lowering their central mass-energy density at the same time*. Eventually in the figure, models with baryonic masses higher than those lying on the sequence with constant baryonic mass $M_B = 2.05M_\odot$ represent NSs which are called *supramassive*[73]. Supramassive NSs are stars that cannot reach a stable static configuration when losing angular momentum along a sequence of constant baryonic mass. They become secularly and after dynamically unstable before to dissipate all the kinetic rotational energy. After the overcoming of the turning-point line they collapse promptly to a BH. As a last consideration, all the models plotted here are stable against non-axisymmetric modes, in the sense that all the models have $\beta < 0.14$, even those on the Keplerian sequence (i.e. the most rapidly rotating models).

In Figure2.11 we report the diagram gravitational mass versus (equatorial) radius. With the respect of Figure2.10, here the sequences with constant baryonic mass are identified by dotted-black lines and the turning-point line with a dashed green line. Moreover, in this plot also sequences of constant axis ratio r_p/r_e are shown. We can clearly note that like Newtonian stars *the rotation makes relativistic stars oblate, the axis ratio being more small for higher rotation rates*. The Keplerian sequence has the smallest axis ratio among the equilibrium models. The other relevant result which is evident in the figure is that *the rotation yields less compact NSs with the respect of non rotating configurations for the same baryonic mass*. Generally, the increase in radius of uniformly rotating NSs is about $30-40\%$[61]. In Figure2.12 we report the diagram moment of inertia versus angular velocity. Lots of information are contained within this plot. Here, the blue line identifies Keplerian models and the solid-black line the sequences of uniformly rotating NSs with constant baryonic

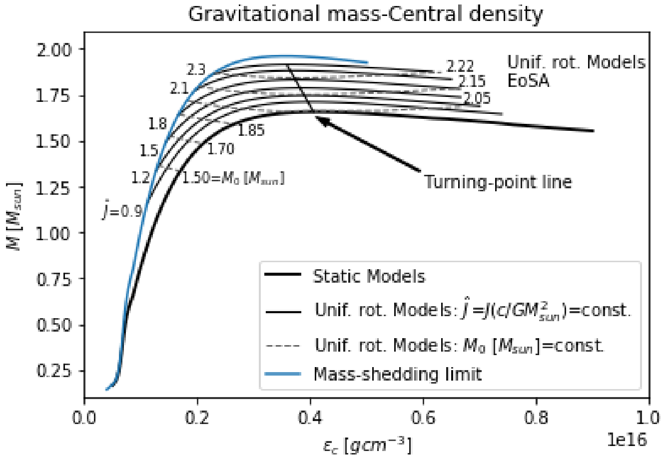

Figure 2.10: Plot of the relation between the gravitational mass and the central mass-energy density. Static and uniformly rotating models of NSs are plotted. The non-rotating sequence is represented with a thick-solid black line, the mass-shedding limit with a blue line. Also sequences with constant baryonic mass M_B (dashed-black lines) and sequences with constant dimensionless angular momentum $\hat{j}$ (solid-thin black lines) are reported; these are labeled in the plot with the corresponding values of the constant quantities. Eventually the turning-point line is identified with a solid black line pointed by the arrow.

mass and which are stable against axisymmetric modes. Models with axisymmetric secular instabilities (i.e. beyond the turning-point along the sequence of constant baryonic mass) are indicated with dotted-black lines. Firstly we can note that models with baryonic masses below $2.0-2.05M_\odot$ (i.e. not supramassive stars) are the most slowly rotating ones, that is correct because high masses cannot be provided by a slow rotation. Especially, we can see that within the smallest spin frequencies, $\sim [0,500]$Hz, the moment of inertia is quite independent on Ω. This is the slow-rotation regime (to the first order on Ω) provided by the Hartle's method. We remember that the fastest rotating NS currently known is PSR J1748-244, which has a spin frequency of about 716Hz. Therefore almost all the observed NSs, whose frequency has been measured, lie along the I-constant sequences on the plot. However, it is also evident that models deviates from the I-constant regime when Ω becomes enough high ($\Omega/2\pi \approx 700$Hz). Close to these frequencies models approach the blue line, that is their Keplerian limit. It is clear that the Hartle's approximation is no more valid here because $\Omega \approx \Omega_K$. At these frequencies the models are not more slowly rotating. In particular, now the moment of inertia increases as Ω increases. Moreover, not supramassive NS sequences of constant baryonic mass start from models close to the static limit ($\Omega \approx 0$) and, by increasing the angular velocity, they end at the mass shedding limit, where the higher moments of inertia and angular momentum are attained. This sequences never reach turning points, i.e. models never become secularly and dynamically unstable for axisymmetric modes. The evolution of a not-supramassive NSs that slows down because of the dissipation of angular momentum, moving along a sequence of constant baryonic mass, ends at the static limit without becoming unstable. Instead, rapidly rotating NSs have a completely different behaviour. The sequences of supramassive NSs plotted on the

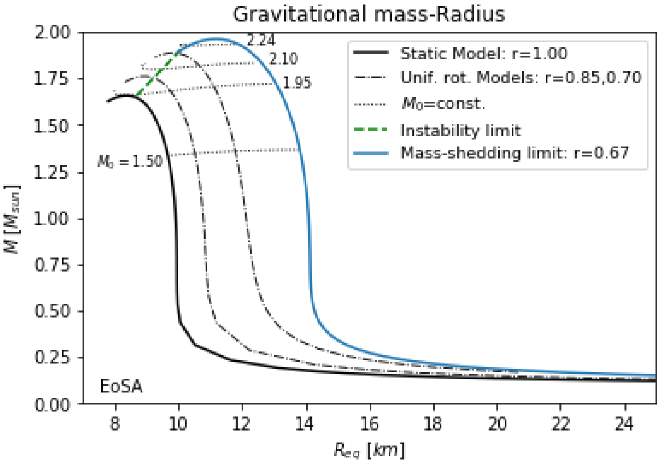

Figure 2.11: Plot of the relation between the gravitational mass and the equatorial radius. Static and uniformly rotating models of NSs are plotted. The non-rotating sequence is represented with a thick-solid black line, the mass-shedding limit with a blue line. Also sequences with constant baryonic mass M_B (dotted-thin black lines) and sequences with constant axis ratio r_p/r_e (dot-dashed black lines) are reported; these are labeled in the plot with the corresponding values of the constant quantities. In particular, the value of the axis ratio decreases from left to right on the plot. Eventually, the turning-point line is identified with a dashed green line.

figure seem very complex. We can distinguish two classes of supramassive NSs. The first one concerns stars with baryonic masses within the range $[2.0-2.05, 2.1]M_{\odot}$. These models move towards the static limit when slowing down, but they reach the turning point before of the configurations with $\Omega = 0$. In particular we can note that there is a spin-up of the models before they become unstable and collapse to a BH. This characteristic spin-up may be an observable precursor to black hole formation following the collapse of massive, rapidly rotating NSs[73]. The second class concerns stars with $M_B \in [2.15, 2.27]M_{\odot}$. These high-masses stars would only spin-up by reducing the moment of inertia because of the leak of angular momentum. More interesting is that this stars seem to be able to reach values of angular velocity more high than the Keplerian frequency before they become unstable. We highlight again the fact that all the models plotted here are β-stable ($\beta_{max} \approx 0.12 < 0.14$). We will see that bar-modes instabilities become relevant for stiffer EoSs, particularly in the case of quark stars.

2.4.3 ”Exact” solutions (2): the LORENE/rotstar code (hints)

The KEH scheme represents a powerful exact approach allowing to probe rapidly rotating relativistic objects. Nevertheless, some numerical issues are also present. Firstly, errors related to the so-called ”Gibbs phenomena” come out when one compute the surface of models. Physical variables like the baryonic density, the pressure and the energy density show large discontinuities near the surface of compact stars. The Gibbs phenomenon becomes very severe particularly in the case of incompressible fluids (i.e. with constant density within them and null outside, like Maclaurin

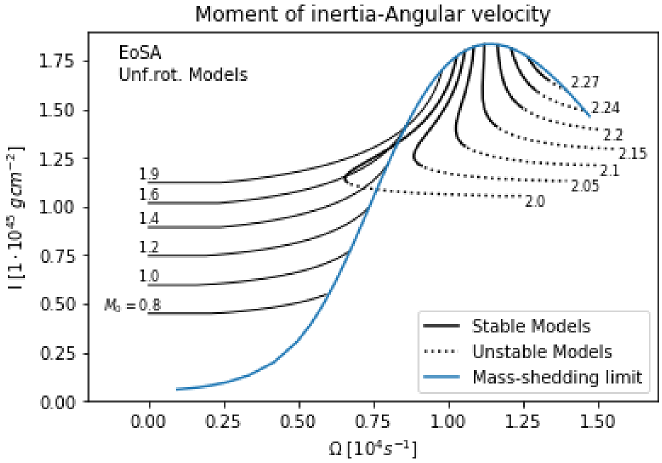

Figure 2.12

spheroids) or even in the case of EoSs of quark matter[25]. An other problem of the KEH scheme concerns the resolution of the Einstein's field equations. As we saw before, there is a first order ODE with a form like $\partial\alpha/\partial\mu = S_\alpha(r,\mu)$ which is not solved through the Green's functions but with a numerical integration from the pole to the equator of models, applying appropriate boundary conditions. We didn't report its expression because of its great length (8 lines). However it can be shown that inside this expression there are second order radial and angular partial derivatives. The first ones, especially, are related to an oscillatory behaviour of numerical solutions of the α-ODE[103]. This is particularly pronounced inside the star and generates errors of 1-2% in the bulk properties of models, like the mass and the radius. In the `RNS` code this problem has been solved by using a grid spacing two times bigger of the original one in the finite difference formula used for the evaluation of the second-order radial derivative. In this way, oscillations are completely damped and improvement in accuracy of up to 2% for some equilibrium properties of models with maximum mass has been obtained[94]. A third numerical issue comes from the use of $\mu = \cos\theta$ as second variable of the numerical grid. It has been noted that when the symmetry axis is approached some terms of the field equations are sensitive to division of small numbers. This produces an oscillatory behaviour of the angular derivatives generating numerical errors. Moreover, as we saw before, in the original KEH scheme the radial integration of the equations was cut off at a distance $2r_e$ because of the impossibility of extending it numerically to infinity. The CST compactification allowed to manage this problem. Eventually, the KEH scheme and also the `RNS` code can deal only with perfect fluids. This because of the α-ODE, which comes out from two identities of the Ricci tensor that are valid only in the case of a perfect stress-energy tensor. This represents a great limitation when one wants to probe situations where the tensor anisotropies become relevant; for instance, in the NS magnetosphere or even in the case of NSs with solid crust or solid interiors.

---

[25] As we will see after in this thesis, quark stars are characterized by a great jump in the baryonic density close to the surface. This is due properly to the EoS applied to describe strange-quark matter.

In order to overcome these problems we can appeal to an other exact approach developed by Bonazzola-Gourgoulhon-Salgado-Marck[104, 105], the so-called BGSM scheme. This is a different formulation of the problem of computing stationary axisymmetric rotating relativistic stars with respect of the KEH scheme. It is based on the so-called "3+1 formalism", that is the Hamiltonian formulation of the general relativity developed by Arnowitt-Deser-Misner[106]. Briefly, it consists on writing the second order Einstein PDEs into a system of first order PDEs, with respect on the coordinate t, in a form of a Cauchy problem subject to certain constraints. This is done through a foliation of the spacetime $\mathcal{S}$ in a family of spacelike hypersurfaces Σ_t, labelled by the coordinate time t (which is constant on each Σ_t) and where a system of three spatial coordinates $\{x^1, x^2, x^3\}$ is given, such that $\mathcal{S} = \mathbb{R} \times \Sigma_t$. By defining the future pointing unit vector n_μ as done in eq.2.71 and the induced metric tensor $h_{\mu\nu} = g_{\mu\nu} + n_\mu n_\nu$ on Σ_t, the spacetime metric tensor is defined by the following line element:

$$\begin{aligned} ds^2 = g_{\mu\nu}dx^\mu dx^\nu &= -N^2dt^2 + h_{ij}(dx^i + N^i dt)(dx^j + N^j dt) = \\ &= -(N^2 - N_i N^i)dt^2 - 2N_i dt dx^i + h_{ij}dx^i dx^j \end{aligned} \tag{2.126}$$

where N and $N^\mu = (0, N^i)$ are the *lapse function* and the *shift vector* respectively, which are defined by the condition:

$$t^\mu = Nn^\mu + N^\mu \tag{2.127}$$

where $t^\mu = (\partial_t)^\mu = \delta^\mu_t$ is the future pointing 4-vector tangent to the world line and $N^\mu n_\mu = 0$. In particular, Ndt is the time lapse along the direction of n^μ between the coordinate times t and $t+dt$, and $N^i dt$ is the i-component of the spatial shift between a path of length dt along n^μ and the path with the same length along t^μ. Therefore N is related to time evolution on the system orthogonally to the spacelike hypersurfaces Σ_t. Instead, N^i is related to the frame dragging phenomenon. Under the hypothesis of a stationary axisymmetric spacetime, without meridional circulation, a coordinate system $\{t, r, \theta, \phi\}$ can be chosen so that the form of the metric tensor becomes the following:

$$ds^2 = -N^2dt^2 + B^2r^2\sin^2\theta(d\phi - N^\phi dt)^2 + A^2(dr^2 + r^2d\theta^2) \tag{2.128}$$

where N, N^ϕ, A and B are functions of the only variables r, θ. Within this formalism the Einstein equations become a set of four elliptical equations on the above metric potentials. In particular they take the following form[104]:

$$\Delta_f u = \sigma_u^{fields} + \sigma_u^{quad} \tag{2.129}$$

where Δ_f is a flat space elliptic operator (the two or three dimensional flat space Laplace operator), u is a metric potential formed from the metric coefficients, σ_u^{fields} is the source term involving *all* the fields (gravitational, magnetic, etc.) and σ_u^{quad} is an expression containing only non linear quadratic terms in the metric potentials. All the equations are not obtained with the assumption of a isotropic stress-energy tensor. Therefore one can probe more realistic configurations of NSs, considering the presence of magnetic fields, solid crust or other. This was not possible within the

KEH scheme. We don't discuss here the equations of motion obtained for a perfect fluid in which an electric current is circulating, generating magnetic field (see [104] for references about this problem). However, in the particular case of a perfect fluid we can obtain a new set of equations which is quite different compared to that listed on the KEH scheme. The new set is the following[107]:

$$\begin{aligned} 4\pi A^2(E+3P+(E+P)U^2)+\frac{B^2r^2\sin^2\theta}{2N^2}(\partial N^\phi)^2-\partial\nu\partial(\nu+\beta) &= \Delta_3\nu \\ -16\pi\frac{NA^2}{B}(E+P)U-r\sin\theta\partial N^\phi\partial(3\beta-\nu) &= \tilde{\Delta}_3(N^\phi r\sin\theta) \\ 16\pi NA^2BPr\sin\theta &= \Delta_2[(NB-1)r\sin\theta] \\ 8\pi A^2[P+(E+P)U^2]+\frac{3B^2r^2\sin^2\theta}{4N^2}(\partial N^\phi)^2-(\partial\nu)^2 &= \Delta_2(\nu+\alpha) \end{aligned} \tag{2.130}$$

where $\nu = \ln N$, $\alpha = \ln A$, $\beta = \ln B$, and:

$$\begin{aligned} \Delta_2 &= \frac{\partial^2}{\partial r^2}+\frac{1}{r}\frac{\partial}{\partial r}+\frac{1}{r^2}\frac{\partial^2}{\partial\theta^2} \\ \Delta_3 &= \frac{\partial^2}{\partial r^2}+\frac{2}{r}\frac{\partial}{\partial r}+\frac{1}{r^2}\frac{\partial^2}{\partial\theta^2}+\frac{1}{r^2\tan\theta}\frac{\partial}{\partial\theta} \\ \tilde{\Delta}_3 &= \Delta_3-\frac{1}{r^2\sin^2\theta} \\ \partial a\partial b &= \frac{\partial a}{\partial r}\frac{\partial b}{\partial r}+\frac{1}{r^2}\frac{\partial a}{\partial\theta}\frac{\partial b}{\partial\theta} \end{aligned}$$

and also U, P and E are respectively the fluid 3-velocity, the pressure and the energy density measured on the ZAMO's frame: $U = A^2Br\sin\theta(\Omega-N^\phi)/N$, $E = \Gamma^2(E+P)-P$, $\Gamma^2 = 1/(1-U^2)^{1/2}$. In order to compute models, the four elliptical equations are supplemented by the first integral of motion:

$$H(r,\theta)+\nu(r,\theta)-\ln\Gamma(r,\theta)+\int_{\Omega_0}^{\Omega(r,\theta)}F(\Omega')d\Omega' = const. \tag{2.131}$$

where H is the enthalpy of the fluid defined previously and $F(\Omega)$ is the same function seen in the KEH scheme but here with a quite different expression because of the new formalism:

$$F(\Omega) = \frac{A^4B^2r^2\sin^2\theta(\Omega-N^\phi)}{N^2-A^4B^2r^2\sin^2\theta(\Omega-N^\phi)^2} \tag{2.132}$$

Clearly, as in the KEH scheme, one has to define the form of $F(\Omega)$. Also in the BGSM scheme we can choose the parametric form reported in eq.2.68. This new formulation of the problem has lots great advantages. Firstly, all the equations for the metric potentials are in an elliptical form and thus a first order PDE is no longer present. This allows to overcome the issue concerning the integration of that PDE due to the presence of second order partial radial derivatives, increasing the accuracy of the method overall. Secondly, the equations are solved using a spectral method[94]: all the functions are expanded in terms of a set of basis functions in both the angular and radial directions and a fast Fourier transform is used to obtain coefficients. Outside the star the new radial variable $u = 1/r$ is used in order to maps infinity to a finite distance. This allows to handle numerically infinity with respect of the KEH scheme. Moreover this spectral method has been improved[105], allowing for several domains of integration. The whole space is divided into three domains: the first is inside the star, starting from its origin and having boundary on the star surface; the second is an intermediate domain, whose inner boundary is the star surface and the outer is a sphere located at $\sim 2r_e$; the third is an external domain whose inner boundary is the outer boundary of the second domain and which extends up to infinity, because of the compactification through the new radial variable $1/r$. As a really important fact, at the star surface (the boundary of the first domain), a regularization procedure is applied to the discontinuity of physical variables in order to make the numerical computation nearly free of Gibbs phenomena. The accuracy of the BGSM approach has been greatly improved by this multi-domain spectral method. All these updates and also many others developed over the years are currently located inside the `LORENE` library, which is available as a public domain software[108]. The LORENE/rotstar code allows us to compute sequences of static, uniformly and also differentially rotating NSs. In this code an equilibrium configuration is computed once the central enthalpy[26] H_c and the central angular velocity Ω_c are fixed, together with a given EoS. Sequences of models can be obtained once two ranges for the two parameters are specified.

In [109] there is a direct comparison of three different representative numerical codes for constructing models of rapidly rotating neutron stars in general relativity. One is based on the original KEH scheme, one is the `RNS` code (in which the original KEH scheme has been improved by applying the CST compactification and the issue concerning the second order partial radial derivative has been solved) and the latest is a code based on the original BGSM scheme. In all three codes, the same physical parameters, equations of state and interpolation method are used. A typical agreement better than $0.01 - 0.1\%$ is found for most models, which are calculated with high accuracy especially in the case of polytropic EoSs and also realistic equations of state without phase transitions. A certain difference in the accuracy, with relative values of $\sim 10^{-3} - 10^{-2}$, between the first code and the others two is noted for stiff polytropic EoSs. This may be related to the application of the boundary conditions only approximately at a finite distance from the star, which characterizes the code based on the original KEH scheme. Moreover, the accuracy of all these codes becomes lower in the extreme case of uniform density stars, where the Gibbs phenomena at the discontinuous surface affect the models. A great improvement in this direction is done within LORENE/rotstar thanks to the multi-domain spectral method. Because of its high accuracy when dealing with large discontinuities on the surface of stars, which appear for instance when considering EoSs of strange-quark matter, we will use LORENE/rotstar to obtain models of differentially rotating quark stars.

---

[26] Actually, the definition in gravitational units $H = \int_0^P dP'/[P' + \epsilon(P')]$ is referred by some authors[104] to the so-called *heat function*. It can be shown that $H = \ln h$, where $h = (\epsilon + P)/\rho$ is the *relativistic enthalpy per baryon*. Therefore, in LORENE/rotstar actually one fixes the central value of $\ln h$.

2.4.4 Relevant comparison between the codes

During the numerical computations of NSs models executed by applying the two codes previously discussed, `RNS` and LORENE/rotstar, we have noted a relevant result that is illustrated in Figure2.13. Some hints about this fact have been also reported in other works (for instance see [107]). When dealing with ordinary NSs, the two codes give very similar estimates of the bulk properties of compact stars, like the gravitational and the baryonic masses. There are very small discrepancies between them in these cases (about $\sim 1\%$ of difference). Anyway, for traditional EoSs (i.e. hadron EoSs) the two codes are consistent. This is shown in the plot, where the black and magenta curves describe static models of NSs computed applying the previously discussed EoSB and using the `RNS` and LORENE/rotstar codes respectively. However, the things change a lot when one deals with strange-quark stars. As shown in the plot, for the EoSs describing these objects, the two codes give similar gravitational masses but, concerning the baryonic masses, the differences as big as $\sim 20-30\%$ between the two codes!

According to the analysis reported in [107], the different measurements of baryonic masses between several codes used for studying rapidly rotating compact stars would be due to the Gibbs phenomenon. Indeed, since quark stars are characterized by a large discontinuity of the mass density field at the surface, there is a strong evidence of the effects of this phenomenon. In particular, we can note from the eq.2.76 that the computation of the baryonic mass in these codes is directly dependent on the mass density field. Therefore, such a discontinuity strongly affects the estimates. Clearly, because of the previous considerations, correct estimates can be obtained only with the LORENE/rotstar code and not with `RNS` in these situations.

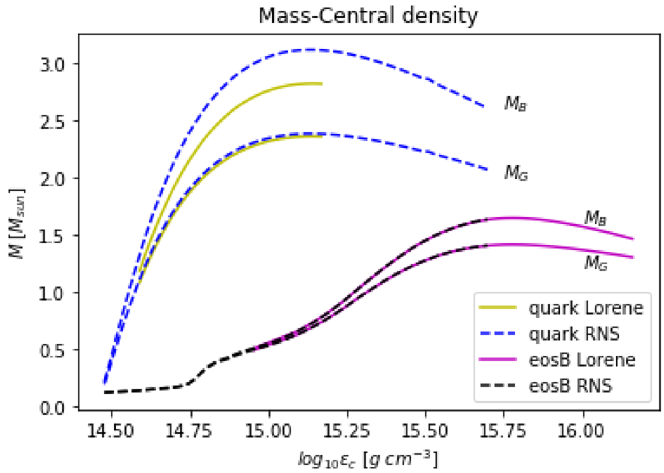

Figure 2.13: Direct comparison between the estimates of gravitational and baryonic masses of non rotating compact stars models, which are obtained with the two codes used in this thesis: `RNS` and LORENE/rotstar.

Chapter 3

The Nuclear Equation of State

The study of the inner structure of NSs represents a big challenge for relativistic astrophysics and nuclear physics. Although there have been great advances in the observational and theoretical researches, the complete picture of compact matter that composes NSs remains an unsolved mystery till today. Nevertheless, our knowledge on the main properties of this extreme objects has been improved over the years. Firstly, we know that it is possible to distinguish four principal regions inside a NS, whose properties are partially understood. The inner structure of a NS can be sketched in the following way, starting from the star edge towards the core:

- a very thin atmosphere ($\sim$cm of thickness), mainly composed by photons, accreted hydrogen and helium, and traces of heavy nuclei of the iron group

- an outer crust, which can be subdivided into two main regions. An outer one constituted by WD-like matter, i.e. characterized by a lattice of atomic nuclei interacting with a Fermi sea of electrons, the latest becoming relativistic when the density reaches the value of $\sim 10^6$ gcm^{-3}. An inner one, where the energies of electrons are sufficiently high to trigger electron capture processes. This makes the nuclei more rich of neutrons up to the density of $\sim 10^{11}$ gcm^{-3}, where the neutron-drip begins

- an inner crust with a density spanning the range of $\sim (10^{11}, 2.7 \cdot 10^{14})$ gcm^{-3}, where the matter is constituted by a mixture of neutron-rich nuclei, completely degenerate relativistic electrons and free neutrons, possibly in a superfluid state. Close to the density of $\sim 10^{14}$ gcm^{-3}, i.e. of the order of the nuclear saturation density, the nuclei dissolve into a mixture of free electrons, protons and neutrons in chemical equilibrium

- a central core composed by ultra-dense matter, i.e. with a density larger than the nuclear saturation density. Completely degenerate relativistic electrons, a neutron superfluid and a superconductive proton superfluid are expected at least in the outer part of this region. Free muons can also be present here. The components of the matter inside the inner region of the core are still unknown. Hyperons, Δ-resonances, pion and kaon condensates or even deconfined quarks could fill it together or without the nucleon-electronic fluid

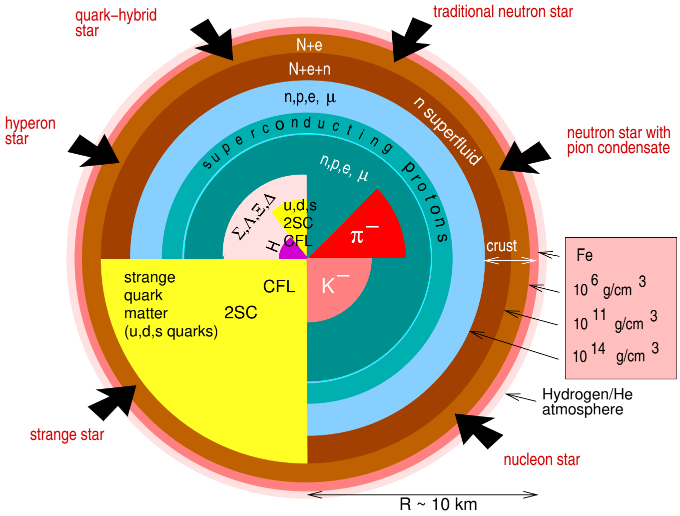

Figure 3.1: Picture of several NSs inner structures according to different models; from the most traditional ones, in which the standard hadron NS model is predicted (with or without hyperons), to the most exotic ones, in which hybrid NSs (i.e. hadron NSs with a quark core) or even strange-quark stars are conceived. The image is taken from [110].

The EoS which describes the matter inside NSs is quite well known below the nuclear saturation density. As we have just listed, we know what kind of matter constitutes the regions out of the core of NSs. The big open question concerns the ultra-dense matter that can be found in their cores. However, as we discussed during the introduction, although we are not able to reproduce this high densities in the terrestrial laboratories we can test them through the observations of the bulk properties of NSs, mainly their gravitational masses and radii. Concerning the mass, observational data has been obtained with considerable accuracy, yielding both small and big mass values. We know NSs with masses spanning the range $\sim (1.17, 2.01)M_\odot$. The radii measurements, instead, remain still quite questionable up to now. Generally, their estimates are affected by several systematic errors (for instance, errors on the distance) and often the analyses are model dependent. As we have seen in the introduction, in a few papers radii in the range $\sim (9.8, 11.2)$km have been suggested; still, larger radii cannot be excluded. We will see later that a few papers [111] have derived radii in the range $(12.00, 13.45)$km from the observations of GW170817, and by using state-of-the-art EoSs of pure hadronic matter. New and more precise radii measurements are needed to probe definitely the EoS of NSs. For instance, the new NASA mission NICER launched aboard a SpaceX Falcon 9 rocket on June 3, 2017, will be able to estimate NSs radii reaching a precision of $\sim$ 1km. Numbers of candidates of EoSs have been suggested so far. At the beginning, the value of about $1.4M_\odot$ was generally considered the canonical upper limit for NSs. However, the most recent observations of masses of the order of $2M_\odot$ seem to indicate that ordinary NSs have masses around $1.4M_\odot$, but NSs with more high masses are possible at the same time. Because of the estimated high values of M_{TOV}, several soft EoSs have been ruled out, promoting more stiff ones. The problem of reaching such high masses has been investigated by numbers of authors. We are able to obtain different stiff EoSs satisfying these constraints. Nevertheless, even if a $M_{TOV} \sim 2M_{\odot}$ can be reached by the models, severe issues arise from the uncertainties on the radii measurements. In particular, concerning the radius $R_{1.4}$ of the ordinary NS with mass $M = 1.4M_{\odot}$, one can imagine three possibilities: $R_{1.4} \gtrsim 13$km, 11.5km$\lesssim R_{1.4} \lesssim 13$km or even $R_{1.4} \lesssim 11.5$km[112]. This represents a great problem. Indeed, the stiffer is the EoS the bigger will be the maximum mass and the larger will be the radius of NS models. Consequently, a big an still open question turns up: does it exist an EoS for nuclear matter that allows to build NS models which reach maximum masses $\sim 2M_{\odot}$ and at the same time provides a $1.4M_{\odot}$ NS whose radius is smaller than ~ 11.5km? In the following we discuss some proposed recent schemes which are trying to answer this question.

3.1 Traditional models: the hadron EoS

According to the traditional model, NSs are composed by baryons and leptons in chemical equilibrium. A big problem concerns the presence of hyperons in the most inner regions. The first theoretical indication for the appearance of hyperons in the core of a neutron star dates back to the 60s[113]. It's known that at ordinary densities these particles are unstable and decay quickly into nucleons. Nevertheless, at the densities expected inside the NSs cores the situation can be different. The energy of nucleons is so high that their chemical potentials can reach the value of the hyperons rest masses, allowing to produce them within a stable state. Notice that the complete degeneracy limits the phase space available to nucleons, thus preventing the decay of hyperons. The appearance of these more massive baryons reduces the Fermi pressure of the system, implying a softer EoS and thus smaller values for the maximum mass of NSs. Within this scenario, the existence of hyperons inside NSs whose masses are $\sim 2M_{\odot}$ could seem improbable. But the situation is a little more complicated. As a first important point, the softening of the EoS and the lowering of M_{TOV} due to the hyperons are strictly related to the density's value at which these particles begin to be produced. This density depends on the kind of interactions that enable the conversion of nucleons into hyperons. Since a violation of the strangeness is required to create hyperons from nucleons, the latter ones must interact with each other through weak interactions[1]. Moreover, one needs also to consider the strong interactions to describe the dynamics of the system. Treating these ones still represents a big problem. Indeed, compared to the electroweak interactions, close to the nuclear saturation density the strong coupling constants are so much larger that we cannot apply a perturbative analysis. A phenomenological treatment of baryons interactions is generally used. There are several models which model the observed attractive and repulsive components of the nuclear strong interaction, taking into account several contributions: the spin coupling, the spin-orbit interaction, tensorial forces, central potentials and others. In particular, non relativistic many-body approaches and relativistic mean field theories have been applied. The first ones predict the appearance of hyperons at around 2-3 times the nuclear saturation density, causing a great softening of the nuclear equation of state. On the

---

[1] In the Standard Model of particles, the weak interactions are the only interactions which can violate the conservation of the strangeness.

other hand, relativistic nuclear models indicate much weaker effects as a consequence of the presence of strange baryons in the core of a NS[114]. The problem concerning the existence of these particles inside NSs is called *hyperon puzzle*.

3.1.1 Non-relativistic many-body approach

In a recent investigation reported in [114], the authors have studied the effects of different phenomenological constructions of hadrons interactions on the properties of NSs, modeling those through a non relativistic many-body approach. In particular, they have considered only Λ hyperons coupled to neutrons, and they have probed what happens when a three-body repulsive interaction is also included. Like in other non relativistic many-body approaches, baryon matter is described in terms of point-like neutrons and Λ-hyperons. The Hamiltonian of the particles system has the following expression:

$$H = \sum_i \frac{p_i^2}{2m_n} + \sum_\lambda \frac{p_\lambda^2}{2m_\Lambda} + \sum_{i<j} v_{ij} + \sum_{i<j<k} v_{ijk} + \sum_{\lambda,i} v_{\lambda,i} + \sum_{\lambda,i<j} v_{\lambda ij} \tag{3.1}$$

where the indices i, j are associated with neutrons and λ with Λ particles. The first two terms are simply the total kinetic energies of the two fluids of particles; the third is the nucleon-nucleon potential; the fourth is the potential associated to the three-nucleon interactions; the fifth represents the hyperon-nucleon potential; the sixth describes the three-body interaction between nucleons and hyperons. Several models have been applied to compute all these potentials. In particular the construction of the potentials has been done phenomenologically, in the sense that each potential must fit the scattering data about baryons interactions measured in the laboratories. The agreement with observational data guides the calculations in these approaches. In order to reproduce the numerous physical quantities related to the interaction processes, several parameter have been adopted. In particular the authors have investigated how different parametrizations of the three-body interactions can affect the EoS and the NS models itself. Hyperon-hyperon interaction has not been considered during the analysis: $\Lambda\Lambda$ scattering data are not available and the experimental information about double Λ hyperonculei are scarce[114]. Eventually chemical equilibrium between particles has been imposed, and this allowed to compute the hyperon fraction as a function of the baryon density: the threshold density for Λ, that is the density at which these hyperons start to be produced, is determined when that fraction becomes larger than zero. The results of their calculation are resumed in Figure3.2 and Figure3.3.

In Figure3.2 the plot of the several EoSs obtained for different kinds of particles and different types of interactions is reported. In the inset, the baryon fractions changing with the medium density are shown. We can clearly see that adding Λ hyperons makes the EoS softer. However, a very important role is played by the kind of interactions. In the case of a two-body interaction alone, hypernuclei turn out to be strongly overbound: the Λ threshold density is quite low (~ 0.24 fm^{-3}, less than 2 times the nuclear saturation density). In this case the formation of hyperons starts very soon, implying a great softening of the EoS. Nevertheless, when the three-body interaction is added and their repulsive contribution taken into account, a stiffer EoS

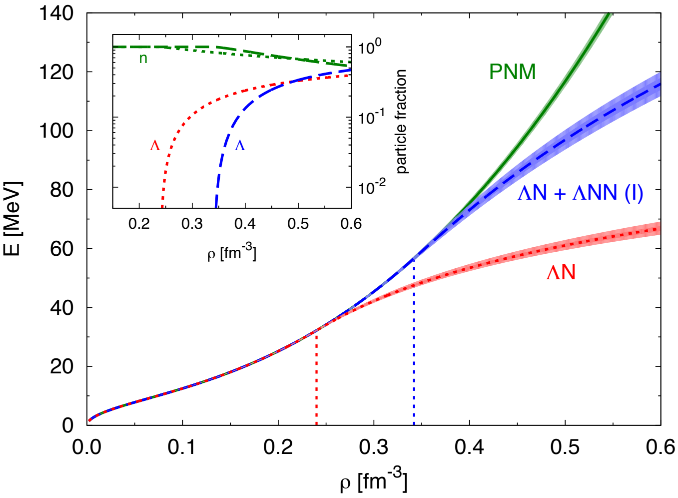

Figure 3.2: Plot of different EoSs. The green curve describes the pure neutron matter. The blue an the red ones contain also Λ particles. The former provides two and three-body Λ-neutron interactions; the latter the two-body force alone. In the inset, neutron and Λ fractions are plotted for each EoS. In particular, the blue curve has been obtained making use of the "parametrization I" (see details in the original paper [114]).

is obtained and the Λ threshold density is pushed up to ~ 0.34 fm^{-3} (larger than 2 times the nuclear saturation density). In this case the appearance of hyperons is unfavorable until high densities. In Figure3.3 the mass-radius diagram obtained by computing static models of NSs in equilibrium is shown. Here with full dots the configurations with maximum masses are marked. Four equilibrium sequence are reported: the green one is that computed with the EoS of pure neutron matter; the blue one corresponds to the EoS with neutrons and hyperons interacting through two and three body forces; the red one describes neutrons and hyperons coupled through two-body forces; the black one is similar to the blue curve but with an other parametrization of the three-body interaction. The plot reveals that in order to reach masses of the order of $2M_{\odot}$, compatibly with the current measurements of the masses of PSR J1614-2230 ($1.928M_{\odot}$) and PSR J0348+0432 ($2.01M_{\odot}$), one needs to prevent the production of hyperons at least up to sufficiently high densities. This is possible if one considers strong three-body repulsive interactions. By applying the "parametrization II" (see the details in [114]) of these forces the energy balance favors the onset of hyperons only for densities out of the the domain that has been considered during the analysis ($\rho \leq 0.56$ fm^{-3}). In conclusion, we stress that this choice allows to obtain NSs models with high masses, but also with large radii (i.e. $\sim$ 13km). This scenario cannot explain the smaller values estimated for NSs radii, which range from 9km to 12km. Actually, beyond the upper limits on M_{TOV} and the uncertain limits on the NSs radii, there are numbers of others empirical constraints on the EoS which come from microphysical and astrophysical observations. In particular, severe constraints come from to the so-called *Urca-processes.* These are nuclear reactions, which can release a great amount of neutrinos. Among these, the *direct* Urca-processes, for instance the reaction $n \to p + e + \bar{\nu}_e$, are the simplest ones and they are thought to be the most efficient cooling processes happening in NSs. If

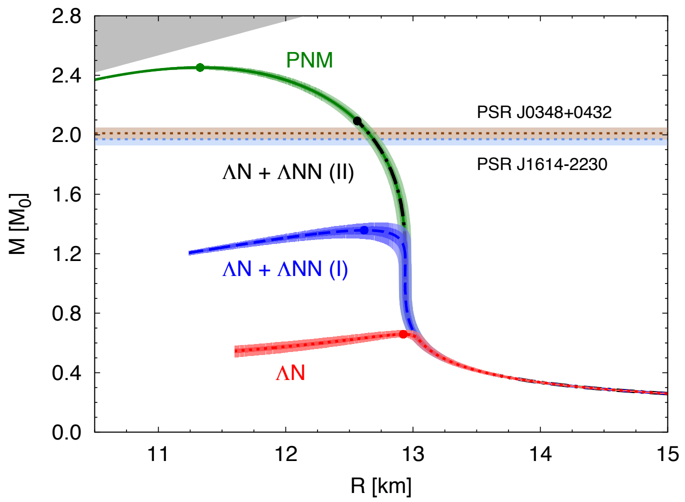

Figure 3.3: Gravitational mass versus radius diagram for the three different EoSs reported in Figure3.2. Full dots represent the predicted maximum masses. Horizontal bands at $\sim 2M_{\odot}$ are the observed masses of the most massive pulsars currently known, PSR J1614-2230 and PSR J0348+0432. With the dashed-dotted black curve the equilibrium sequence obtained with the "parametrization II" of the three-body interaction is plotted (see details in the original paper [114]).

triggered, such reactions should generate a fast cooling of NSs, making them invisible for thermal detections within few years[115]. The NS cooling data concerning isolated NSs seem to indicate that the mass at which Urca-processes can be triggered is larger than $\sim 1.5M_{\odot}$ (the so-called *strong direct-Urca constraint*)[116]. The hyperon puzzle complicates strongly this situation. Indeed, together with a great softening in the EoS, the appearance of hyperons can also trigger others direct-Urca processes, for instance the reaction $\Lambda \rightarrow p+e+\bar{\nu}_e$. Therefore, hyperons could promote the fast cooling of NSs, especially within those schemes for which their production starts at quite low densities (for instance, at $\sim$ 2 times the saturation density, like the previous model with only two-body interactions). In order to overcome this difficulties a good scheme is that recently proposed in [117]. There a relativistic mean filed method has been considered.

3.1.2 Relativistic mean field approach

Relativistic mean field (RMF) theories represent a theoretical approach developed within the framework of the QFT (Quantum Field Theory). Particles are described in terms of quantum-states of fields (scalar, vector or spinor) which fill the Minkowsky spacetime, and their interaction are defined through appropriate coupling terms. Especially, these mixing fields terms are multiplied by coupling constants, whose value is related to the strength of interactions. Following the general scheme of QFTs, a Lorentz covariant Lagrangian theory of nuclear matter is provided. This is the so-called *Quantum Hadrodynamics*, that has been firstly advanced in [118, 119, 120]. It is an effective theory, in the sense that the fields of the theory are not associated with elementary particles. Indeed, each field describes hadrons (baryons and mesons) but not their constituents: quarks and gluons. Moreover, nuclear interactions between baryons are expressed in terms of exchanges of mesons. Mainly, three kind of mesons are taken into account: a scalar meson σ, that is associated with the attractive component of nuclear forces; a vector meson ω^μ, that is related to the repulsive component of nuclear forces and a vector isospin-triplet meson ρ_i^μ $(i = 1, 2, 3)$, which is used to take into account the so-called *nuclear symmetry energy*[2]. By using appropriate symmetries one writes the Lagrangian density function of the nuclear system, where all the particle fields and the coupling terms are included in a dimensionally correct way. Since Quantum Hadrodynamics is not a fundamental theory, the coupling constants cannot be determined experimentally. These constants are parameters that one has to adjust properly in order to fit the observational data describing nuclear matter. In particular, some empirical properties of nuclear matter are quite well measured in the laboratories[60]. The first one is the nuclear saturation number density, $n_0 = 0.153\text{fm}^{-3}$, which is obtained experimentally from electron-nucleus scattering processes. The second one is the binding energy per nucleon, that is defined as:

$$\frac{B}{A} = \frac{M(A,Z) - [Zm_p + (A - Z)m_n]}{A} \tag{3.2}$$

where m_p and m_n are the proton and neutron masses respectively, Z is the nuclear atomic number, A is the nuclear mass number and $M(A,Z)$ is the mass of the nucleus. It can be obtained that, neglecting Coulomb interactions, the binding energy per nucleon of infinite $(A \to \infty)$, symmetric $(A = 2Z)$, nuclear matter is $B/A = -16.3\text{MeV}$ [60]. In the same conditions one can measure also another quantity, that is the symmetry energy coefficient, $a_{sym} = 32.5\text{MeV}$. Eventually, at the saturation, other two empirical quantities are measured: the compression modulus, $K \approx 234\text{MeV}$, and the nucleon effective mass, $m^*/m \approx 0.7 - 0.8$. All these quantities constrain strongly the EoS of nuclear matter. In particular, n_0 and B/A define the normalization of the EoS, in the sense that they set the behaviour of the EoS at intermediate densities, close to the nuclear saturation point. At this point, the agreement with a low-density EoS (like the BPS) is required. K, m^*/m and a_{sym} constrain the EoS at high density regimes; especially, the higher is the compression modulus the stiffer becomes the EoS, and the bigger is the value of effective nucleon mass the softer is the EoS. The computation of the EoS within the framework of the RMF theory is done in the following standard way. The hadronic density Lagrangian function of the system of particles is firstly defined. For instance in the case of a system composed of nucleons and hyperons interacting through σ, ω and ρ mesons, and also of leptons (which are needed for the charge neutrality), the Lagrangian

---

[2] This is an unbinding energy contribute observed in asymmetric nuclei, i.e. nuclei which have a number of neutrons larger than the number of protons $(A > 2Z)$. This happens for atomic numbers beyond the value $Z \approx 20$. When $Z > 20$ stable nuclei start having a neutron excess.

function of the Quantum Hadrodynamics has the following expression[60]:

$$\begin{aligned}\mathcal{L} =& \sum_B \bar{\psi}_B(i\gamma_\mu\partial^\mu - m_B + g_{\sigma B}\sigma - g_{\omega B}\gamma_\mu\omega^\mu - \frac{1}{2}g_{\rho B}\gamma_\mu\tau^i\rho_i^\mu)\psi_B + \\ &+ \frac{1}{2}(\partial_\mu\sigma\partial^\mu\sigma - m_\sigma^2\sigma^2) - \frac{1}{4}\omega_{\mu\nu}\omega^{\mu\nu} + \frac{1}{2}m_\omega^2\omega_\mu\omega^\mu - \frac{1}{4}\rho_{\mu\nu}^i\rho_i^{\mu\nu} + \frac{1}{2}m_\rho^2\rho_\mu^i\rho_i^\mu + \\ &- \frac{1}{3}bm_N(g_\sigma\sigma)^3 - \frac{1}{4}c(g_\sigma\sigma)^4 + \\ &+ \sum_\lambda \bar{\psi}_\lambda(i\gamma_\mu\partial^\mu - m_\lambda)\psi_\lambda \end{aligned} \tag{3.3}$$

where the baryon spinors[3] are denoted by ψ_B, while $\bar{\psi}_B \equiv \gamma_0\psi^\dagger$, and the leptons fields by ψ_λ. In particular, the first ones are summed over all the baryonic states B (p, n, hyperons and eventually also Δ-resonances) according to the kind of particles that one wants to include in the system. Instead, the last ones are summed over the electrons and muons states ($\lambda = e, \mu$)[4]. The first line contains the free baryon Lagrangian density:

$$\mathcal{L} = \sum_B \bar{\psi}_B(i\gamma_\mu\partial^\mu - m_B)\psi_B \tag{3.4}$$

and the remaining mixing fields terms are the baryon Lagrangians associated with the nuclear interactions, which are described through the mesons fields (σ, ω and ρ) and the coupling constants ($g_{\sigma B}$, $g_{\omega B}$ and $g_{\rho B}$, each one specified for each baryon species). The second line contains the free meson Lagrangians for each meson field:

$$\mathcal{L}_\sigma = \frac{1}{2}(\partial_\mu\sigma\partial^\mu\sigma - m_\sigma^2\sigma^2) \tag{3.5}$$

$$\mathcal{L}_\omega = -\frac{1}{4}\omega_{\mu\nu}\omega^{\mu\nu} + \frac{1}{2}m_\omega^2\omega_\mu\omega^\mu \tag{3.6}$$

$$\mathcal{L}_\rho = -\frac{1}{4}\rho_{\mu\nu}^i\rho_i^{\mu\nu} + \frac{1}{2}m_\rho^2\rho_\mu^i\rho_i^\mu \tag{3.7}$$

where:

$$\omega_{\mu\nu} = \partial_\mu\omega_\nu - \partial_\nu\omega_\mu \tag{3.8}$$

$$\rho_{\mu\nu}^i = \partial_\mu\rho_\nu^i - \partial_\nu\rho_\mu^i + g_\rho\epsilon^{ijk}\rho_{j,\mu}\rho_{k,\nu} \tag{3.9}$$

The third line contains scalar-self interactions between the fields σ, where b and c are the coupling constants, and m_N is the nucleon rest mass. Eventually, the last line represents the total free lepton Lagrangian. As we can see, for a fixed baryon species, there are five coupling constants (g_σ, g_ω, g_ρ, b and c). These are used to define five parameters related to the five empirical properties of nuclear matter. In order to

---

[3] Since baryons are fermions, spinor fields are associated with them. It's important to note that each spinor is actually an isospin multiplet, in the sense that it contains different isospin states for the same particle. For instance in the case of nucleons we have two isospin state: $\psi_N = (\psi_p, \psi_n)$, where ψ_p represents the proton state with isospin charge equal to 1/2, and ψ_n represents the neutron state with isospin charge equal to $-1/2$.

[4] The leptons τ are not expected to be found inside NSs, since because the charge chemical potential in these stars never exceed the tau lepton rest mass[60].

do this, one puts the Lagrangian density3.3 inside the relativistic Euler-Lagrange equations, that is the dynamical equations of the system:

$$\sum_{\phi}\Big[\frac{\partial\mathcal{L}}{\partial\phi}-\partial_{\mu}\frac{\partial\mathcal{L}}{\partial(\partial_{\mu}\phi)}\Big]=0 \tag{3.10}$$

splitting all the terms relative to each field ϕ (in the above case ψ_B, ψ_λ, σ, ω^μ and ρ_i^μ). Therefore, the *mean-field approximation* is applied. This represents the "heart" of the RMF theories. Briefly, it consists in computing the ground-state expectation values of all the terms in the equations of motion. The ground-state of the system is defined by a static and uniform matter distribution and all the mesons fields are substituted by their mean values in this state. This means to treat the interaction field like a classical field, whose quantum fluctuations in the Minkowsky spacetime are negligible. In such a representation, all the interacting baryons belonging to the many-body hadron system are described each one like single particles interacting with an effective mean field. Therefore the new meson mean fields $\langle\sigma\rangle$, $\langle\omega\rangle$ and $\langle\rho\rangle$ are treated like classical fields and the quantum treatment is restricted to the only baryons and leptons. By doing this approximation in all the equations of motions, one compute the expression for each mean meson field. Then, the homogeneity of the Minkowsky spacetime[5] allows to define the following current:

$$T^{\mu\nu}=-\mathcal{L}\eta^{\mu\nu}+\sum_{\phi}\Big[\frac{\partial\mathcal{L}}{\partial(\partial_{\mu}\phi)}\partial^{\nu}\phi\Big] \tag{3.11}$$

which is conserved on the spacetime $\partial_\mu T^{\mu\nu}=0$. This is the *canonical* stress-energy tensor of the theory. One can compute the ground-state expectation value of this tensor in the rest frame of the nuclear matter, applying the mean field approximation. In this frame, by assuming a perfect fluid configuration, it has the well known diagonal form obtained from eq.2.25. Thus the mean local pressure and mass-energy density of the ensemble of hadrons are defined as:

$$\epsilon=-\langle\mathcal{L}\rangle+\Big\langle\frac{\partial\mathcal{L}}{\partial(\partial_{0}\phi)}\partial^{0}\phi\Big\rangle \tag{3.12}$$

$$P=\langle\mathcal{L}\rangle+\frac{1}{3}\Big\langle\frac{\partial\mathcal{L}}{\partial(\partial_{i}\phi)}\partial^{i}\phi\Big\rangle \tag{3.13}$$

The above equations define the EoS of nuclear matter within the RMF approach. It can be shown that the five empirical quantities characterizing saturated matter can be obtained algebraically in terms of combinations of the coupling constants of the theory[60]. Two important points need to be highlighted. Firstly, to describe correctly the nuclear system, it is required to combine the EoS with the equations of the chemical equilibrium and of the charge neutrality. The firsts are relations between the chemical potentials of the different kind of particles, allowing the system to be populated by baryon species beyond the nucleons at sufficiently high densities. The second ones guarantee a total null charge of the system. Eventually, the relations between the empirical quantities and the coupling constants within the RMF approach

---

[5] The Minkowsky metric $\eta_{\mu\nu}$ is invariant under spatial and temporal translations, that is they are isometries of the spacetime of the Special Theory of Relativity.

are formulated also in terms of the masses of mesons, when considering the case of infinite nuclear matter. This implies that by changing the mesons masses, one can change the fit of the bulk properties of nuclear matter and thus the EoS itself. In the RMF scheme proposed in [117] the authors include the nucleons (n and p), the hyperons Λ^0, $\Sigma^{\pm,0}$ and $\Xi^{-,0}$, and the mean meson fields σ, ω, ρ and ϕ, the latter being another vector meson field applied to fix more precisely the stiffness of the EoS. As for the masses of these particles, they consider the values m_N=938 MeV, m_Λ=1116 MeV, m_Σ=1193 MeV, m_Ξ=1318 MeV, neglecting the small mass splitting in isospin multiplets. The lepton masses are instead m_e=0.5 MeV and m_μ=105 MeV. The method developed by the authors consists in writing the baryon-meson coupling constants and the masses of all the hadrons in terms of the mean scalar field σ, through an appropriate dimensionless variable (see the details of the calculation in the original paper[117]). They consider the system as composed by cold nuclear infinite matter, in chemical equilibrium and neutrally charged. Moreover, the parameters of the nucleon sector are fixed in order to reproduce the five bulk properties of saturated matter discussed before. Since the values of the compression modulus and the nucleon effective mass are not exactly known, if not with some large uncertainty, the fitting values can be changed in order to better satisfy the constraints on the NS equation of state. A big repulsive potential is obtained for the Σ hyperons, preventing their appearance in most of the computed models. Equilibrium configurations of non rotating NSs are computed by solving numerically the system of static equations already discussed in this thesis. Finally, within the low density range $n \lesssim (0.6-0.8)n_0$, the EoS of nuclear matter computed with the RMF approach matches the BPS EoS.

As the main result of their work, the authors suggest three models of NS equation of state (called KVORH, MKVORHϕ and MKVORH$\phi\sigma$), for nuclear matter with hyperons, each one obtained by adjusting in different ways the parameters of the theory and satisfying as much as possible the observational constraints on the EoS. They provide a possible solution of the hyperon puzzle. In particular, changing the parameter allows to modify the hyperon population in the nuclear matter. Especially, the MKVORHϕ shows a reduced hyperon population with respect to the KVOR model, and in the MKVORH$\phi\sigma$ model the appearance of Λ and Ξ^0 hyperons is even prevented. The threshold density of the Ξ^- appearance is shifted to higher values. In this way one can prevent the beginning of direct-Urca processes at lower densities (thus for small NS masses) due to hyperons. Moreover, the models KVORH and MKVORHϕ don't exceed the neutron threshold for the direct-Urca process $n \rightarrow p + e + \bar{\nu}_e$ for densities lower than n_Λ, where n_Λ is the threshold density at which the Λ-direct-Urca process begins. For central densities higher than n_Λ the process $\Lambda \rightarrow p + e + \bar{\nu}_e$ starts. Instead in the MKVORH$\phi\sigma$ model Λ-hyperons don't appear at all and the direct-Urca processes occur only for higher densities, i.e. bigger than the neutron direct-Urca threshold[117]. In Figure3.4 the obtained gravitational mass-radius diagram for the three models of EoS is shown. In the diagram several constraints are also reported. The green region represents constraints on NS masses and radii obtained from observational data about the quasi-periodic brightness oscillations of the low-mass X-ray binary 4U 0614+091 (the data are taken from[121]). The choice of this particular NS comes from the fact that it shows a high maximum

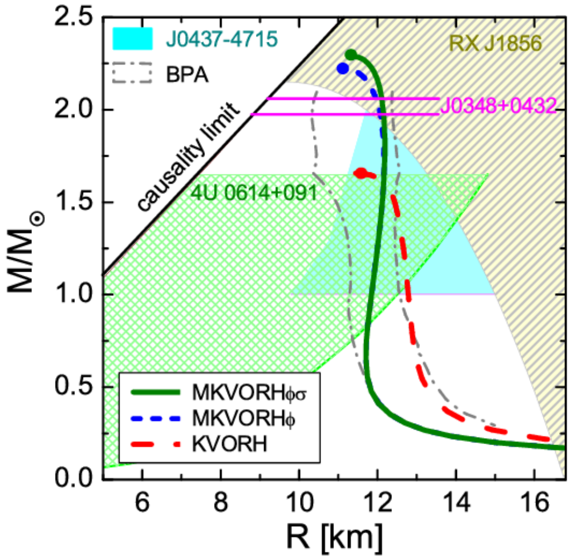

Figure 3.4: Gravitational mass-radius diagram obtained in[117]. Three sequences of equilibrium NSs models are reported, which have been computed by using three different EoSs. Several observational constraints are also plotted. See details in the text and in the original paper.

frequency of oscillations, allowing to tighten the limits on NSs masses and radii. The brown region represents the probable intervals for the mass and the radius of the isolated NS RX J1856.5-3754, estimated by measurements of its thermal radiation (also these data are taken from[121]). Here uncertainties come mainly from the distance measures. The cyan region describing more recent constraints obtained from the X-ray spectroscopy of PSR J04374715, together with the Bayesian probability analysis of several X-ray burst sources, are also reported in the plot (see references in[117]). Eventually, strong constraints on the NS masses comes from the observations of the binary pulsar PSR J0348+0432; these are reported in the plot with purple horizontal lines. It is clear that the KVORH model is not able to reproduce the high mass estimated for PSR J0348+0432, instead the MKVORHϕ and MKVORH$\phi\sigma$ models provide M_{TOV} big enough to satisfy this constraint. Moreover these two models of EoS are also able to reproduce NS configurations within the several colored regions. The high stiffness of these EoSs is mainly due to the choice of the parameters within the RMF approach. This allows to reproduce the high masses observed for NSs in a well manner. However, one must to respect the causality limit; we can see that all the models provided by the authors satisfy this limit. Eventually, even if the presence of hyperons, the MKVORHϕ and MKVORH$\phi\sigma$ models are able to obtain NS configurations with high masses and also quite small radii, that is of the order of 12km. This could be a good advancement respect to the others models of hadron EoSs listed before. However radii of the order of 10-11 km together with high masses are still very difficult to obtain, also within the RMF approach.

3.2 Strange-quark matter in compact stars

The so-called "strange-quark matter hypothesis", formulated by Witten and anticipated by Bodmer[122, 123], states that the actual ground-state of strongly interacting matter is a deconfined state of quark matter, consisting of an approximately equal proportion of up, down and strange quarks. This was named "strange matter". It implies that the confined state of quarks into hadrons would not be the *absolute* ground-state of strong interactions, but "nuclear" systems with a larger binding energy per nucleon than in iron (B/A = 8.8MeV) could exist in nature. However, although there is presently no evidence that the ground state of matter *must* be that of confined quarks, free quark particles have not been observed till today. The strange matter remains an hypothesis so far. Nevertheless, ultra-relativistic heavy-ions experiments have provided many indications of the existence of a new phase characterized by strongly interacting matter, which is obtained by heating up hadronic matter to temperatures $\sim$ 100MeV[124]. This is the so-called "quark-gluon plasma": a hot ensemble of free gluons and quarks strong-interacting with each other. But also another kind of quark matter could exist, not satisfying the rather extreme Bodmer-Witten hypothesis: it consists in a deconfined state formed at very large baryon density and small temperatures, when matter is highly degenerate. The large density regime could make energetically favorable the transition process of quarks from nuclei to the deconfined state. In particular, this kind of matter would be in agreement with the asymptotic freedom regime predicted by QCD. Such a degenerate matter is likely searched inside the core of NSs, where densities can be higher than nuclear saturation density. As a surprising fact, many attractive outlooks turn up when ones analyzes quark matter, either satisfying the Bodmer-Witten hypothesis or not, within the relativistic astrophysical context. In particular, the recent large mass measurements of NSs can be obtained in a more easy way by considering the presence of free quarks inside them (at least in their cores). Several different schemes have been developed during the last decades in order to probe the possibility of quark matter inside NSs. In particular, the main problem was to define an EoS for the strange matter and, above all, to combine it together with the hadron EoS which characterizes lower densities regions. All the different approaches have shown that another branch of equilibrium configurations of compact stars is likely to exist for very high masses. This new branch is composed partially (no BW hypothesis) or even totally (BW hypothesis) by quark matter; the former are named "Hybrid Stars" (HSs), the latter "Quark Stars" (QSs). In particular, hybrid stars should contain free quarks within their most inner regions, because of their higher densities compared to the envelope. This possibility modifies in a dramatically the way we represent NSs. At the beginning they were thought to be formed mainly by neutrons, with small fractions of protons and leptons. Later, the evidence of an hyperon puzzle significantly complicated the view and some models of hadron (nucleons+hyperons) EoSs have been obtained, satisfying as much as possible the observational constraints. Now, the new scenarios are suggesting that quark matter could exist inside these stars. Because of these considerations all these stellar systems, as highlighted in the title of this thesis, are likely called "Compact Stars" (CSs). In the following we briefly discuss two proposed different schemes which deal with hybrid and quark stars. They are called ”Twins-stars scenario” and ”Two-families scenario” respectively.

3.2.1 Twin-stars scenario

The twin-stars scenario has been developed by several authors in many papers, for instance in [125, 126]. The main feature of this scenario is that, once the low-density hadron EoS (only with nucleons or also with hyperons) and the EoS of quark matter are specified, the hybrid EoS is obtained by matching the two through an appropriate phase transition region, whose parametrization (under certain conditions) can generate via an *unstable* branch another disconnected family of compact stars in equilibrium. In particular, this new branch can describe configurations having equal or even higher masses than the most massive stars belonging to the hadronic branch, but with *smaller* radii. Because of the appearance of different families of equilibrium stars having equal masses, the authors refer to them as twin stars. As an example, in [126] the authors have studied hybrid stars configurations by considering for the hadronic part two models of EoSs called BHF and DBHF. The former is obtained through a non relativistic approach and the latter with a relativistic one. Their trends are very similar until quite high densities ($\sim 0.3\text{fm}^{-3} \approx 2n_0$) from where DBHF starts to be slightly stiffer. The two EoSs don’t contain hyperons. For the high density region the authors have applied a common technique, that is called ”constant speed of sound” (CSS) parametrization. This consists in considering a sharp interface[6] between nuclear matter and a high-density phase region, for instance a quark matter phase. A first-order phase transition is considered and a constant speed of sound in the high density region is assumed. In particular, in the case of a cold EoS, the square of sound velocity is defined as:

$$c_s^2 = \frac{dP}{d\epsilon} \tag{3.14}$$

A first-order transition phase is characterized by a constant pressure during the transition. However, because of the hydrostatic equilibrium condition, a region with constant pressure inside these stars cannot exist. Then, from the Maxwell construction, such a phase transition can be realized thanks to a discontinuity on the mass-energy density profile. Called this discontinuity $\Delta\epsilon$ andP_{trans} the value of the pressure at the phase-transition, if c_s^2 is constant in the high density region, it is easy to show that the overall EoS $\epsilon(P)$ for the hybrid stars can be written as follows:

$$\epsilon(P) = \epsilon_{NM}(P)\Theta(P_{trans} - P) + \left[\epsilon_{NM}(P) + \Delta\epsilon + \frac{1}{c_s^2}(P - P_{trans})\right]\Theta(P - P_{trans}) \tag{3.15}$$

where $\epsilon_{NM}(P)$ represents the EoS of the hadronic matter (purely nucleonic). Therefore, the EoS can be parameterized by three parameters: $P_{trans}/\epsilon_{trans}$, $\Delta\epsilon/\epsilon_{trans}$ and c_s^2 (where $\epsilon_{trans} = \epsilon_{NM}(P_{trans})$). It is very important to note that the authors have not specified the nature of the matter constituting the high density region. One can assume that this region is composed by quark matter. However, the conditions for

---

[6] This means that there is not a mixed-phase region between the low-density and the high-density regions. This is valid when assuming the case of a Maxwell phase transition.

the chemical equilibrium have been not considered here. The choice of a constant speed sound EoS for the high density region is based on the fact that this assumption is valid for a large class of models of quark matter. In particular, CSS EoS fits very well quark EoSs obtained via the field correlator method[126]. We report some results of the authors' analysis in the following.

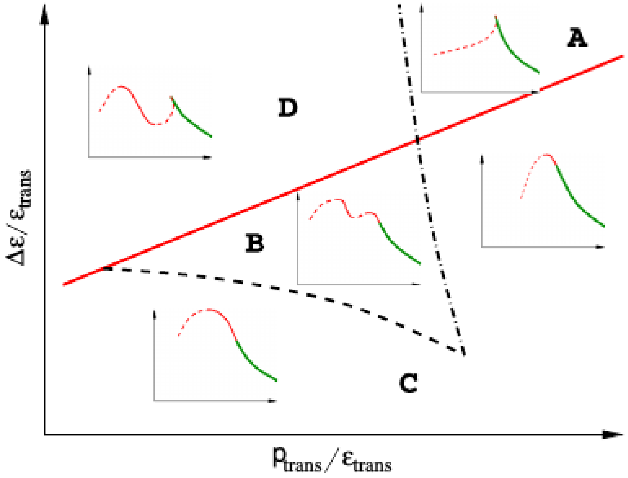

Figure 3.5: Schematic phase diagram for hybrid star branches in the mass-radius relation of compact stars. This is a representative plot obtained for a fixed value of the constant square speed of sound c_s^2. Different topologies of mass-radius diagram are shown in the inset. These are collected within four classes in the plot, each one identified by different values of the parameters $\Delta\epsilon/\epsilon_{trans}$, $P_{trans}/\epsilon_{trans}$. See details in the text and in the original paper [126].

In Figure3.5 several models of hadron and hybrid stars are shown. In particular, mass-radius diagrams are depicted in inset plots. Here, green lines represent equilibrium sequences of static hadron stars; red lines models of static hybrid stars. In particular, the solid-thin red curves are related to stable equilibrium models, instead the dashed ones to unstable equilibria. This fact follows from the stability principle of static solutions discussed in the previous chapter. Moreover in the plot, different topologies of mass-radius diagrams are located in different regions. These ones are defined by the values of two parameters ($\Delta\epsilon/\epsilon_{trans}$, $P_{trans}/\epsilon_{trans}$) and for a fixed constant speed of sound c_s. In particular two specific lines constrain them: the solid-thick red one is defined by the threshold values of $\Delta\epsilon/\epsilon_{trans}$ below which there is always a stable hybrid star branch connected to the neutron star branch; the dashed and dot-dashed ones mark the border of regions where a disconnected hybrid star branch exists. The different topologies of mass-radius diagrams are classified in four classes. The class C contains sequences of models in which the hybrid branch connects continuously to the hadron branch; therefore, there is only a unique branch of compact stars. Within the class D, the two branches appear disconnected, i.e. the connecting sequence is composed by unstable equilibria. Class B contains models of hybrid stars which are both connected and disconnected with the hadron branch. Eventually, within the class A, no stable equilibria of hybrid stars appear. Once the two EoSs are specified, i.e. the hadron one and the CSS EoS, changing the

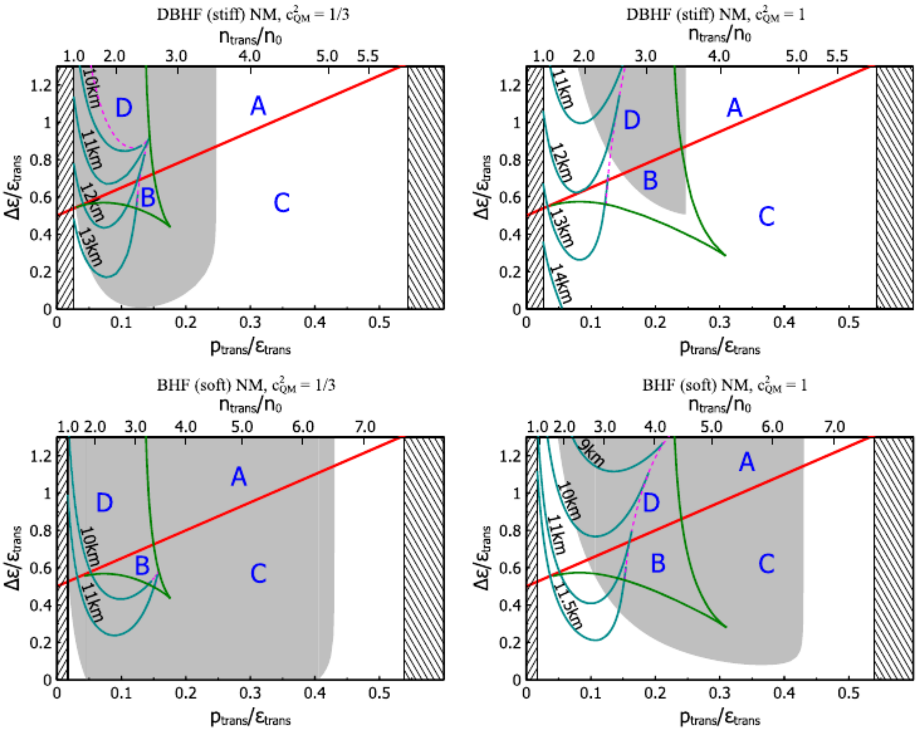

Figure 3.6: Sequences of hybrid stars with $M = 1.4M_\odot$ and constant radii as functions of the CSS parameters. The two upper plots contain models computed by using the stiffer hadron EoS (DBHF), in the lower two the softer one (BHF) is applied. The two plots on the left are characterized by $c_s^2 = 1/3$, the two on the right side buy $c_s^2 = 1$. See more details in the text and in the original paper [126].

values of the two parameters $(\Delta\epsilon/\epsilon_{trans}, P_{trans}/\epsilon_{trans})$ for a fixed c_s corresponds to locate models in this plot. This allows to know to what kind of class they belong, thus indicating also what sort of hybrid branches will be present. Eventually, by changing the value of the third parameter c_s, one can modify the classes' location on the plot. In particular, it can be shown that c_s affects only the two black curves but not the solid-thick red one. By looking at the inset mass-radius diagrams in Figure3.5, we can clearly note that, for a fixed gravitational mass, stable solutions belonging to different branches with the same mass but different radii are possible. These are the so-called twin-stars. However, even in the absence of twin-stars, when a stable hybrid branch exist for a fixed set of parameters, the models belonging to it will have *always* smaller radii than hadron stars. Eventually, when the two branches coexist, the highest mass values allowed are reached by hybrid configurations.

In Figure3.6 static models of hybrid stars with a fixed gravitational mass of $1.4M_\odot$ and computed for different constant values of radius are collected within four diagrams. In particular, for a fixed radius, different sequences of models are obtained by changing the variables of the method: the three parameters of the CSS parametrization and the EoS of the hadron matter. Each of the four diagrams is identified by a specific choice of the hadron EoS and of the values of the parameter c_s. In particular, the two upper diagrams are obtained with the stiffer hadron EoS (DBHF), the lower two with the softer hadron EoS (BHF). On the left hand side, plots with $c_s^2 = 1/3$ are reported and, on the right hand side, the two plots with $c_s^2 = 1$ are shown. Moreover, inside each diagram, sequences of models with fixed radius (and $M = 1.4M_\odot$) are computed as functions of the other two parameters ($\Delta\epsilon/\epsilon_{trans}$ and $P_{trans}/\epsilon_{trans}$). Within each plot the four classes A, B, C and D are also reported, together with the red and black boundary curves (here the dashed and dot-dashed black curves are substituted by a single solid-green line). Different values of the ratio n_{trans}/n_0 are also listed in the diagrams, where n_0 is the nuclear saturation number density and n_{trans} the number density of hadron matter at the transition phase. In particular, the hatched band at low density (where $n_{trans} < n_0$) represents an excluded region. Indeed, here the bulk nuclear matter would be metastable since the transition to quark matter would occur below nuclear saturation density. There is also another hatched band at high density, which is related to another excluded region. This is excluded since here the transition pressure would be above the central pressure of the heaviest stable hadronic star. In this case no transition towards stable hybrid stars would happen. Clearly, for a fixed transition pressure P_{trans}, an hydrostatic equilibrium hybrid configuration with stiffer hadron EoS will have a smaller number density at which the phase transition occurs. We can note this trend by looking at the values of n_{trans}/n_0 on the diagrams: n_{trans}/n_0 is lower for the two upper plots, where a stiffer EoS is applied. Therefore, the right side excluded region begins at lower values of n_{trans}/n_0 for the two upper plots compared to the lower ones. Moreover within all the diagrams a grey dashed region is also plotted. This contains all the sequences of models whose maximum mass is smaller than $2M_\odot$, thus they are excluded by the observed existence of a $2M_\odot$ NS. Eventually, the dashed-magenta lines delimit sequences which extends only up to moderate transition pressure. A part from the behaviour showed by the sequences according different values of the parameters, that we will not investigate here, an important result turns up from this plot. Models of hybrid stars obtained with this scheme can allow $R_{1.4} \sim 11$km *only* when one considers a constant speed of sound equal to (or of the order of) the speed of light in vacuum, that is a request very difficult to justify. Observational data about NS masses and radii can be explained within the twin-stars scenario only if extreme conditions are considered. From the plot we can note that this result is almost independent on the EoS for the low density regime. This means that, even if slightly smaller radii can be obtained with a softer hadron, the main change on the models radii is due to the choice of c_s^2, i.e. by the EoS applied for the high density matter phase.

3.2.2 Two-families scenario

The two-families scenario is a scheme in which the strange-matter hypothesis is tested on NSs. It has been proposed in many papers[112, 127, 8, 128]. Similarly to the twin-stars scenario, it predicts the existence of another branch of massive compact stars distinguished from the traditional family of hadron stars. Nevertheless, now the second branch is provided in a new, different fashion. Firstly, the two populations of stars appear always as disconnected branches. Therefore, one actually distinguishes two different kinds of compact objects: the hadron stars and the quark stars, i.e. two populations of stars which depict indeed the so-called "two-families scenario". The disconnection between them is provided by the fact that there is a rapid transition process from hadron stars to quark stars, i.e. hybrid stars appear only within timescales which are very short compared to the lifespan of stars. In particular, the formation of a quark star from a hadron star is characterized initially by a fast burning of the most inner part of the hadron star. Inside very high densities regions, when a sufficiently amount of strangeness is formed and appropriate microphysical conditions are satisfied (see details in [127]), a small drop of quark matter can be produced, pulling the trigger of the nuclear burning. The conversion of hadron matter into quark matter happens through a adiabatic and turbulent mechanism, which involves most of the stellar core. The adiabaticity of the process is guaranteed by its very short timescales ($\sim$ms), which don't allow the system to dissipate outwards its energy by neutrino emissions. Since the process is exothermic, the system warms up and a hybrid configuration with a hot EoS is generated. After the fast initial burning of the core, the envelope of the newborn hybrid star is deconfined through a diffusive mechanism, that is characterized by longer timescales ($\sim$ 10s). During this process the system can release the internal energy into the environment, cooling down by the neutrino flows. Notice that the amount of energy dissipated by the cooling corresponds exactly to the binding energy acquired by the system when deconfinement is ultimated. At this point a cold quark star is formed. Unlike the twin-star scheme, in the two-families scenario the transition from hadron stars towards quark stars is always obtained via a stable process; moreover, extreme values of the speed of sound are never required. In particular, the authors have provided a detailed microphysical analysis, taking into account of all the equations for the chemical equilibrium and the charge neutrality of the system. Within this approach the speed of sound is always smaller than the speed of light in vacuum.

Concerning the EoSs applied by the authors, some interesting points need to be highlighted. Firstly, for the hadron family they have considered the relativistic mean filed approach. Here, hyperons Λ, Σ, Ξ and also Δ-baryons have been considered together with the nucleon-electronic fluid. The Δ-baryons are heavy baryons composed only by up and down quarks, and they have spin number 3/2. Because of this their equation of motion is not the usual Dirac equation; the latter indeed describes fermions whose spin number is equal to 1/2. This implies that for the Δ-particles one needs a different Lagrangian compared the hadronic one within a RMF theory. According the mean-field scheme considered by the authors, the Lagrangian density associated with the Δ-particles is the following:

$$\mathcal{L} = \bar{\psi}^{\nu}_{\Delta}[i\gamma_{\mu}\partial^{\mu} - (m_{\Delta} - g_{\sigma\Delta}\sigma) - g_{\omega\Delta}\gamma_{\mu}\omega^{\mu} - g_{\rho\Delta}\gamma_{\mu}I_{3}\rho_{3}^{\mu}]\psi^{\nu}_{\Delta} \tag{3.16}$$

where ψ^{ν}_{Δ} is the Rarita-Schwinger spinor for the Δ-isobars (Δ^{++}, Δ^{+}, Δ^{-}, Δ^{0}) and I_3 =diag(3/2,1/2,-1/2,-3/2) is the matrix containing the isospin charges of the Δs. The other coupling terms are related to the strong nuclear interactions mediated by mesons. There are numbers of studied which have suggested the existence of Δ-baryons in the core of neutron stars[129, 130, 131, 132]. By considering these particles, some very important results turn up. Firstly, in the two-families scenario, the early appearance of Δ-baryons, the first being the Δ^{-}, considerably shifts the onset of hyperons which start to form at densities as large as $5n_0$ [112]. In this way, the large amount of strangeness in the core of hadron stars needed for the beginning of the quark deconfinement is reached only for quite massive stars ($M \sim 1.5 M_\odot$ [112])[7]. Moreover, the Δ-resonances produce a considerable softening of the hadron EoS. Particularly, the two-families scenario predicts that the most massive hadron stars have masses $\sim 1.5 - 1.6 M_\odot$ and radii $\sim 10.5 - 11$km, thus interpreting the estimates of $R_{1.4} < 11.5$km as the radii of massive hadron stars. Eventually, within the two-families scenario, the presence of Δs should not be a problem for the NSs fast cooling caused by Urca processes. Indeed, it has been shown[133] that if the nucleon Urca process is forbidden (which observations show to be triggered only for NSs masses bigger than $\sim 1.5 M_\odot$[116]), the Urca-processes $\Sigma^- \to n + l + \bar{\nu}_l$ and $\Delta^- \to n + l + \bar{\nu}_l$ (where l is a lepton) are also forbidden. Under these circumstances, the only Urca processes that could still be allowed are those involving Λ hyperons: $\Lambda \to p + l + \bar{\nu}_l$, $\Sigma^- \to \Lambda + l + \bar{\nu}_l$ and $\Delta^- \to \Lambda + l + \bar{\nu}_l$. The two-families scheme predicts the formation of the Λs only at very high densities ($\sim 5n_0$), where models are close to the end of the hadron branch, at densities close to the ones triggering quark deconfinement.

Concerning the EoS of quark matter, several models have been discussed by the authors, some applying the so-called "MIT Bag-model" or slightly modified versions of it[134], and others based on perturbative-QCD calculations[112] or even on chiral models. Basically, the actual EoS of quark matter is still unknown. As we saw during the discussion of the twin-stars scenario, generally one models it making use of some parameters which are fixed in order to reproduce the observational properties of massive compact stars. However, within the two-families scenario, more detailed microphysical considerations are done. In particular, we consider here the model of quark matter's EoS reported in [134]. We will apply it later for the modeling of the post-merger phase of GW170817. This EoS belongs to the class of bag-models, which are developed in order to describe the quark confinement observed for strong-interactions at the non-perturbative regime. Their usual approach is to collect all the non-perturbative effects of strong interactions into a bag constant B. In particular, the quark fluid is described here by an appropriate formulation of its Grand-canonical potential. This is defined as follows:

$$\Omega_{QM} = \sum_{i=u,d,s,e} \Omega_i + \frac{3\mu^4}{4\pi^2}(1 - a_4) + B_{eff} \tag{3.17}$$

where Ω_i are the Grand potentials for the up, down and strange quarks, and the electrons. The last ones are treated as non interacting particles. Moreover, μ is the baryon chemical potential of quarks. The two quantities a_4 and B_{eff}, eventually, represent the parameters of the model which allow to include non-perturbative QCD effects. Also the chemical equilibrium and the charge neutrality conditions are assumed in this model. Therefore several static configurations of quark stars are computed and the whole parameter range of a_4 and B_{eff} is explored. In particular, the smaller is a_4 the more effective are QCD corrections. The authors have probed how the maximum non rotating mass M_{TOV} of quark stars change by varying the two parameters. Values $2.2 M_\odot \lesssim M_{TOV} \lesssim 2.4 M_\odot$ of quark stars can be reached

---

[7] This is due to the fact that Δ-baryons don't contain strange quarks. Therefore the presence of hyperons is needed to produce strangeness in the core of NSs.

in this scheme. Some microphysical constraints concerning chemical potentials turn up beyond values $\sim 2.4M_{\odot}$. In this thesis we have considered the quark matter EoS characterized by the values $a_4 = 0.65$ and $B_{eff} = 129$ of the parameters. By using the `RNS` code we have computed the static sequence of quark stars and we have obtained a maximum mass of $M_{TOV} = 2.38M_{\odot}$. Again, with this code, we have computed static sequences of hadron stars and hybrid stars making use of the corresponding EoSs provided within the two-families scenario. The obtained mass-radius diagrams are reported in Figure3.7. Here both the gravitational mass

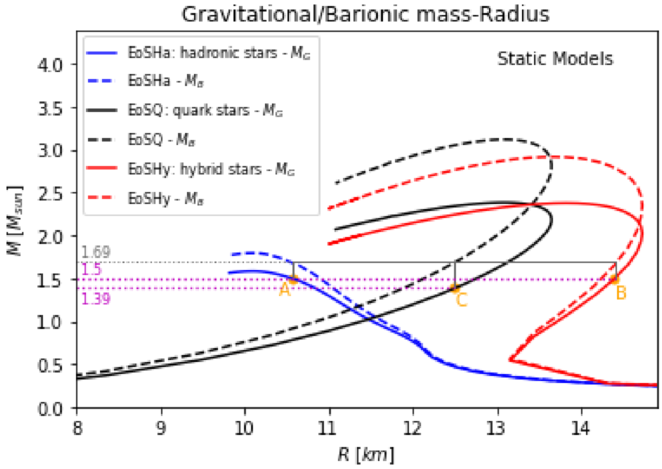

Figure 3.7: Gravitational/baryonic mass-radius diagram. Sequences of static models are computed by applying three different EoSs developed within the two-families scenario. The blue curves represent sequences of hadron stars; the red curves sequences of hybrid stars; the black ones sequences of quark stars. The gravitational mass-radius diagrams are plotted with solid lines, the baryonic mass-radius diagrams with dashed lines. See the text for the other details.

and the baryonic mass are plotted as functions of the stellar radius. In particular, the gravitational mass-radius diagrams are depicted with solid curves, the baryonic mass-radius ones with dashed curves. We stress here that this is just a rough analysis of the features of compact stars within the two-families scenario. Indeed, as we have noted in the previous chapter, the `RNS` code presents some troubles when evaluating the baryonic masses of stars composed by quark matter. Therefore the numbers that we report here are not exact, but concerning the hybrid and quark models some corrections on the baryonic mass should be made. However, here we are just interested on the general behaviour of such stars. Therefore, even by using the `RNS` code, we can figure these typical properties.

In the plot, the blue lines represent the sequences of hadron models, the red ones the sequences of hybrid stars and the black curves configurations of quark stars. Schematically, we report here the evolutionary track of a hadron star with gravitational mass $M = 1.5M_{\odot}$, labeled with the point A in the plot, whose core undergoes the quark nucleation process. During the entire process the baryonic mass is conserved. Its value is established by the gravitational mass of the initial hadron star. In the case discussed here, this is $1.69M_{\odot}$. Firstly the hadron star (A) evolves towards the hybrid star (B). The conservation of the baryon mass is underlined by the horizontal grey line painted in the plot. The horizontal magenta lines, instead, connect models with the same gravitational mass, that is models with the same amount of mass-energy. We can note that the two models A and B have both equal baryonic masses and equal gravitational masses. This is correct since we have seen before that this process is realized within very short timescales ($\sim$ms), therefore via an adiabatic mechanism. The absence of dissipation of energy together with the conservation of the baryonic mass implies also the conservation of the gravitational mass. Once the hybrid configuration B is attained, this evolves within longer timescales ($\tau \sim 10$s) towards the quark model C by conserving again the baryonic mass. Since now the transition is no more adiabatic, some energy will be lost by the star. Indeed when the quark configuration is attained, the gravitational mass is smaller ($M_C = 1.39 M_\odot$). In particular, because of the efficiency of the neutrino cooling during this transition, the $0.11 M_\odot$ mass loss corresponds to the amount of thermal energy lost by the star. This causes necessarily the cooling of the EoS itself. Another very important result can be noted from the plot. The two long-life families of compact stars[8], that is the blue-hadron and the black-quark sequences, appear completely disconnected and with mass-radius diagrams showing absolutely different behaviours. Unlike the twin-stars scheme, we can see from the plot that the two-families scenario predicts quark configurations which have both higher masses and larger radii than the hadron ones. In particular, within these scheme, the maximum masses of quark stars still satisfy largely the observational constraint $M \sim 2M_\odot$. The trend of the black sequence in the plot is due to the fact that the construction of the quark EoS is done by considering the microphysical implications of the Bodmer-Witten hypotesis. According this one, the absolute energy minimum of the strong interactions is reached for a certain amount of strangeness in a mixture of quarks up, down and strange, and at a finite value of density (slightly larger than the nuclear saturation density). This is the value of the quark matter density in equilibrium, i.e. when $P = 0$. Since the condition of null pressure defines the edge of a star, we will have quark stars with a edge characterized by a density of the order of the nuclear saturation density. This implies that compared to ordinary NSs, where the density profile inside the star decreases monotonically and continuously with the pressure from the high central densities until the value of the nuclear matter density in equilibrium (e.g. $n_{P=0} \sim 5 \cdot 10^{-15}\text{fm}^{-3} \ll n_0$, in the case of matter composed by iron nuclei), quark stars present a density discontinuity at the surface $\Delta n \gtrsim n_0$: strange-quark stars have probably the hardest smoothest surface of any object in the universe[60]. A behaviour $M \propto R^3$ along the equilibrium sequence of these compact objects is thus expected. We can clearly note that this is the trend of the black curves in the plot. Actually, the behaviour changes for very massive quark stars. Indeed in these cases the gravity is so strong that it is able to increase the density of the quark matter at the center of stars. This growth of the density explains the stiffer increase of the mass with the radius.

It is very important to underline the fact that the two-families scenario is currently the only scheme which could satisfy both the constraints on the measured NSs masses and radii without invoking a sound velocity close to that of light in vacuum.

---

[8] This means that the lifespan of hadron stars and quark stars is much longer compared that of hybrid stars, as the two-families scenario predicts.

Clearly, more precise measurements on the radii are needed to draw final conclusions. However, we can also note that the hyperon puzzle is easily solved within this scenario: hyperons and deltas do reduce the maximum mass of compact stars to values significantly smaller than $2M_\odot$ but this fact does not represent a puzzle since the most massive objects are actually quark stars[112]. Eventually, concerning double-NS mergers, a new kind of event is allowed within the two-families scenario: the coalescence of a hadron star and a quark star.

Chapter 4

Phenomenology of GW170817/GRB170817A/AT2017gfo

On August 17, 2017, at $12^h41^m04^s$ UTC the Advanced LIGO and Advanced Virgo gravitational-wave detectors made their first observation of gravitational waves from the coalescence of two compact objects whose estimated masses were in agreement with masses of known neutron stars. The GWs signal (GW170817) allowed to localize the binary system within the host galaxy NGC4993, constraining a sky region of $31deg^2$ and a distance of 40^{+8}_{-8} Mpc. This represented the first direct detection of a double neutron star merger[135]. Moreover, GW170817 was associated with the short γ-ray burst GBR170817A observed independently by the Fermi Gamma-ray Burst Monitor and the Anti-Coincidence Shield for the Spectrometer for the International Gamma-Ray Astrophysics Laboratory[9]. The short-GRB was delayed by about 1.7s with respect to the coalescence time. Eventually, the two detections were followed by multiple observations which revealed the existence of an electromagnetic transient counterpart in the same location of the GRB and GW signals. The electromagnetic signal covered a large range of spectral frequencies, from the X-rays, to UV, optical, IR and finally even the radio bands. The optical transient was detected about 10^h52^m after the coalescence. The blue one faded within 48 hours. The X-ray and radio signals were observed at the transient's position about 9 and 16 days, respectively, after the merger. No ultra-high-energy gamma-rays and no neutrino signals consistent with the source were found during follow-up searches. The electromagnetic observations clearly enforced the hypothesis that the gravitational-wave event was produced by the merger of two compact stars. All these observations marked the beginning of the so-called *Multi-messenger Astronomy*[136].

4.1 GW170817

The GW signal detected by LIGO and VIRGO has allowed to infer the so-called *chirp mass* of the binary system as $M_c = 1.188^{+0.004}_{-0.002} M_\odot$. This quantity is defined in terms of the mass of the two stars m_1, m_2; precisely, $M_c = (m_1 m_2)^{3/5}/(m_1 + m_2)^{1/5}$. General Relativity makes detailed predictions for the inspiral phase. However, although we can constrain the chirp mass very well, concerning the component masses there is a degeneracy between mass ratio $q = m_2/m_1$ (here we assume $m_2 \leq m_1$) and the aligned spin components of the two stars. Therefore, the evaluation of q is done by making some assumptions about the spins. Under the hypothesis that the two stars have spins compatible with those observed in ordinary binary neutron star systems (the so-called "low spin case"), it has been inferred that $q \geq 0.7$. Therefore the masses of the two components belong to the range $(1.17, 1.60)M_\odot$ and we can measure the total gravitational mass before the merger as $M = 2.74^{+0.04}_{-0.02}M_\odot$[137]. During most of the inspiral phase the two stars can be treated as point like sources. However when the distance between them becomes sufficiently small, i.e. the length-scale of the process becomes of the order of the stars radii, the GW signal is affected by the sizes of the two stars. During this phase, particularly relevant are the tidal forces, which perturb the stars structure and accelerate the process. The parameter that quantifies the action of the tidal forces and thus the deviation of the GW signal from the case of point like sources is the so-called *tidal parameter* $\tilde{\Lambda}$. This strongly depends on the properties of the two stars. In particular, for fixed masses, the larger are the radii of the two stars the bigger is the tidal deformability and thus the parameter $\tilde{\Lambda}$ too. If one knows the mass of the system during the inspiral phase, a precise measurement of $\tilde{\Lambda}$ can allow to constrain the radius of NSs and thus the underlying EoS. During the GW170817 event it has not be possible to follow the gravitational-wave signal up to the merger. Nevertheless, an upper limit on the value of the tidal parameter has been set. In [138], under minimal assumptions about the nature of the compact objects, the authors have obtained the constraint for the tidal deformability parameter $70 \lesssim \tilde{\Lambda} \lesssim 720$. Moreover, in [139] by using a generic family of NS EoSs interpolating state-of-the-art theoretical results at low and high baryon densities and applying the constraints about the tidal deformability, the authors have obtained for the $1.4M_\odot$ NS an upper limit on the radius of NSs: $R_{1.4} \lesssim 13.4$km.

The possibility that GW170817 has led to a prompt collapse seems to be very improbable because of the following observation of an electromagnetic counterpart. In particular, in the case of a delayed collapse, several different outcomes are possible. Full general relativity simulations have shown that in this situation an initial differentially rotating object is formed[72]. More recent investigations have also revealed that the rotational profile of the remnant is quite complicated, but it is almost universal for several different EoSs[140]. This object could be stable only as long as differential rotation is present (hypermassive star), or it could evolve to a rapidly uniformly rotating compact star which is stable as long as rigid rotation is present (supramassive star), or it could evolve to a totally stable non-rotating stable object. These different scenarios depend mainly on the dissipative mechanisms affecting the remnant, like magnetic fields or the GW emission itself. In all these cases we expect a GW signal during the post-merger phase, whose spectral features are quite different from the signal detected during the inspiral phase and also depend on the kind of rotation which governs the remnant dynamics. Indeed, the initial differentially rotating configuration can last no longer than about 1s, while the rigid rotation phase can last from $\sim 10^4$s up to $\sim 10^6$yr[141]. Therefore, if an hypermassive NS is formed, a big amount of energy would be released through GWs within very short timescales (< 1s). Instead, in the case that a uniformly rotating NS is formed, a long-life signal should be detected.

The absence of an extended emission (EE) both in the GW and electromagnetic wave (EMW) signals, together with the subsequent observation of an electromagnetic transient, promotes a hypermassive NS as the outcome of the event, which survived at least some milliseconds after the merger. This would imply that the gravitational mass of the system at the merger was higher than the maximum mass of supramassive NSs (M_{max}). Since the latter is estimated $\sim 1.20 M_{TOV}$ quite universally, from the total mass at the merger (M) one can constrain the value of M_{TOV}. By assuming a gravitational binding energy of the binary to be $\approx 0.06 M_\odot \sim 2\% M$, which is lost through GWs during the merger, and considering also the mass ejection mechanisms involved during the event, which allow to loose a maximum amount of mass of $\approx 0.1 M_\odot \sim 4\% M$ (as we will see later), the total mass at the beginning of the post-merger phase is $\sim 94\% M \approx 2.58 M_\odot$. Therefore, the constraint $M_{max} \lesssim 2.58 M_\odot$ implies that $M_{TOV} \lesssim 2.15 M_\odot$. We stress here that, in this calculus, we have assumed that the collapse to BH takes place when the object is still rapidly rotating with a frequency of ~kHz. This assumption is based on the two considerations previously mentioned: the absence of an EE in the GW signal and the absence of a large EMW emission in the environment. This result has been investigated also in [142] where the authors have provided the range $2.01^{+0.04}_{-0.04} M_\odot \leq M_{TOV} \leq 2.16^{+0.17}_{-0.15} M_\odot$. Here, the lower limit is derived from accurate observations of massive pulsars in binary systems and the error bars on the upper limit take into account some uncertainties, which are associated with the leak of knowledge about the post-merger phase. For instance, as reported in the introduction, in [1] a weak EE in GWs could has be revealed after the merger. In this case, other evolutionary scenarios should be considered.

A delayed collapse would also imply that the mass of the differentially rotating NS was smaller than the threshold mass $M_{threshold}$. This quantity correspond to the maximum gravitational mass sustainable by the remnant of the double-NS merger. In [86] it has been shown that $M_{threshold}$ scales with M_{TOV} by a relation containing the compactness (M/R) of the non rotating configuration with maximum mass. Therefore, the information $M < M_{threshold}$ allows to constrain the mass and the radius of the object, and thus to probe the EoS. According the result of [143], the constraint $M_{threshold} \gtrsim 2.74 M_\odot$ would suggest $R_{1.6} \gtrsim 10.7$km.

4.2 Electromagnetic signals

4.2.1 GRB170817A

The indication of a short-GRB after the GW signal strongly suggested that the merger involved two NSs. This has been named as GRB170817A and it has been detected ~ 2s after the merger, appearing particularly weaker than ordinary short-GRBs. In particular, none EE has been detected. The faintness of the signal could be explained by assuming an intrinsically sub-luminosity or even quasi-isotropy of it[144]. An other possibility is that it was actually an ordinary short-GRB but observed off-axis[145]. Future investigations about the time-evolution of the γ-emission will allow us to distinguish between these two possibilities.

Generally, two different types of short-GRBs can be observed. The first ones present only a strong prompt emission (PE) within short timescales ($\sim$ 10s); the second ones present a PE together with a following extended emission (EE), which is a quasi-plateau emission lasting about $10^3 - 10^4$s[146]. Lots of doubts are still present about the inner engine of short-GRBs. In the presence of a PE alone, a short-GRB could be explained with a post-merger phase consisting in a prompt collapse to a BH[147]. In particular within this scenario, a rapidly rotating BH would be formed with a hot and strongly magnetized torus surrounding it. The toroidal distribution of matter would emit promptly the GRB (PE) in the case of a rapid ablation caused by the central BH. Instead, in the presence of an accretion process towards the BH, the timescale of the γ-emission would be longer and thus an EE would be observed[148]. An other completely different scenario considers a proto-magnetar as the inner engine of the two types of emission observed in short-GRBs. In particular, the EE is identified with a pulsar-like emission generating by a long-lived rotating NS. Within this scenario, several schemes have been proposed. One considers the short-GRBs with only PE as the result of a delayed collapse to a BH. If a supramassive NS is formed after the merger, since the rotation can last for timescales $\sim 10^4$s, a delayed collapse is expected. In the presence of an EE, this scheme requires a ”time-reversal” mechanism[149]. The EE should be generated by the star formed after the merger before the collapse to a BH, but observed after the PE because of the time needed by the soft EE signal to leak out the thick cocoon surrounding the star. The PE would be emitted immediately after the BH formation and would exit the cocoon along the rotation axis. This would allow it to be detected before the EE, since the torus is less thick in that direction. Within this scheme the time delay between the moment of the merger and the PE is of the order of the lifespan of the supramassive star (i.e. $\sim 10^4$s). An other scheme considers that a stable rotating NS is formed after the merger. In particular, the final outcome of the event is not a BH but rather a quark star. Therefore, the light curve observed during the EE would be provided by a pulsar-like emission coming from a long-lived quark-proto-magnetar with surface magnetic fields $\sim 10^{15} - 10^{16}$G and spin frequencies $\sim$ 1kHz. In particular, the EE would have timescales of the order of the lifespan of the rotating quark star. Concerning the PE, the quark deconfinement reaching the stellar surface could allow it. In this case the time separation between the merger and the PE would be $\sim$ 10s, that is the timescale required to the quark deconfinement for reaching the star surface. This timescale is different from that predicted by the other scheme. Therefore from the observations we would be able to differentiate them.

4.2.2 AT2017gfo

Although the absence of an EE in GRB170817A, a prompt collapse scenario cannot be invoked. Indeed an electromagnetic signal has been detected after the short-GRB. This signal corresponds to a transient signal spanning a large range of wavelengths within a quiet long time interval. Firstly, a blue component has been observed, involving the X and UV bands. Then a rapid evolution towards redder wavelengths has been noted: at 1.5 days after the merger the signal had peak at about 5000Å, and already at about 4.5-7.5 days it left the optical regime. By 10 days the wavelength was bigger than 15000Å. In particular, the decline of the signal was more rapid in the blue component, making the red the dominant component of the spectrum during the last observations. The electromagnetic signal extended in time from about 0.47 to 18.5 days after the merger, overall. The data in the UV, optical and NIR bands were consistent with a Kilonova signal expected after a NS merger[137]. The signal has been called AT2017gfo. Being based on the observational data, this signal has been modeled in the following way. A first component with wavelength within the UV and blue optical bands, characterized by the highest luminosities ($\sim 5 \cdot 10^{41}$ ergs^{-1}) and the shortest timescales (~ 1), has been identified as the so-called *Blue Kilonova*. This kind of emission was modeled for the first time in [150]. It is related to mass ejections with very low opacity. The Blue Kilonova signal is likely to be associated with r-processes involving the formation of nuclei lying between the first and the second peaks. Comparison to models have provided that $M_{ej} \sim (0.01 - 0.03)M_{\odot}$, $\beta_{ej} \sim 0.3$ and a Lanthanide fraction of $\sim 10^{-5} - 10^{-4}$ were associated with this component of the Kilonova[151, 152]. Moreover, by modeling the entire electromagnetic data set, it has been found that models with heating from radioactive decay of ^{56}Ni, or those with only a single component of opacity from r-process elements, failed to capture the rapid optical decline and red optical/NIR colors of the signal. Therefore, an other model has been required to fit the red component of the Kilonova. This has was called *Red Kilonova*[152]. It represents the late and less luminous component of the signal ($\sim 5 \cdot 10^{40}$ ergs^{-1}). In particular, it is characterized by a higher opacity; then, this component is associated with an ejected material containing r-process heavy nuclei filling the third peak ($A > 140$). This data have been fitted by considering $M_{ej} \sim 0.04M_{\odot}$, $\beta_{ej} \sim 0.1$ and a Lanthanide fraction of $\sim 10^{-2}$[152, 153].

These observations have shown that in principle a not unique value of the opacity and thus of Lanthanide fraction can be used to describe Kilonovae associated with NS-mergers. In particular, the existence of at least two components of the ejecta, a Lanthanide poor (Blue Kilonova) and a Lanthanide rich (Red Kilonova), is needed. The evidence of two not overlying components is likely related to two different matter ejections, which come from two different regions of the remnant, with varying opacity, and moving along two different angles of emission. A deep investigation on the opacity estimated from the analysis of the Kilonova would allow to infer information about the ejection mechanism and, in particular, about the nuclear equation of state of NSs. The blue component of AT2017gfo, characterized by a very low opacity, has been related to a dynamical mass-ejection mechanism, particularly to a shock-wave mechanism. Concerning the Lanthanide richer Red Kilonova, a dynamical mechanism of tidal ejection along the equatorial plane seems to be the better one to explain the signal origin. In particular, by considering that $M_{ej}^{Red} > M_{ej}^{Blue}$, it seems that the tidal mechanism dominated the mass ejection during the merging.

Two important results about the Kilonova signal turn out. Firstly, the M_{ej} estimated to explain the blue component of the signal seems to indicate quite small NS radii. Indeed, it can been shown that the shock-wave mechanism associated with this component becomes more efficient in the case of softer EoSs, i.e. small radii. By applying these considerations, the GW170817 blue ejecta mass can be reached by nearly-equal mass binaries and soft EOSs with very small NS radii ($< 11 - 12$km).

This estimate for the radius of NSs is particularly crucial. Such small radii would be in fact difficult to explain together with the observed NS masses $\sim 2M_\odot$ within a one-family scenario. Nevertheless, these measurements could be easily explained by considering a two-families scenario. Other recent studies [154] have considered also the existence of a disk of matter surrounding the outcome of the merger. These have estimated a mass of the disk $\approx 0.04M_\odot$. In particular, from the analysis of the EMW signal, the authors have inferred a lower limit on the tidal deformability $\tilde{\Lambda} \gtrsim 300 - 400$. According them, this would imply the constraint on the radius $R_{1.4} = 12.2^{+1.0}_{-0.8} \pm 0.2\text{km}$.

4.3 Possible post-merger GW signal

In the analysis reported in [1] the authors have look for a post -merger GW signal finding an extend emission started before the short-GRB, i.e. during the gap of 1.7s between the coalescence time inferred from LIGO observations ($t_c = 1842.43\text{s}$) and the onset of GRB170817A. They have revisited the LIGO H1, L1 and V1 data from the LIGO Open Science Center (LOSC) by applying a model-independent analysis which uses matched filtering over chirp-like templates, allowing the detection of ascending and descending chirps with phase-coherence within appropriate time scales. The obtained data are shown in Figure4.1.

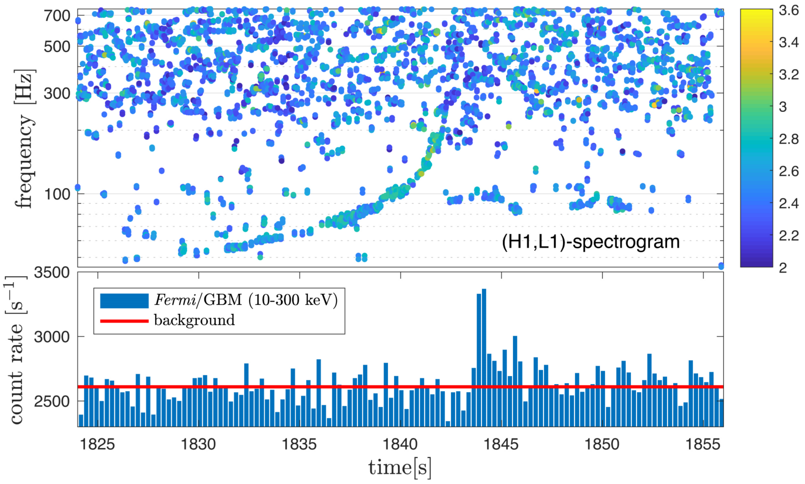

Figure 4.1: Ascending-descending chirp in the (H1,L1)-spectrogram produced by the double neutron star merger GW170817 concurrent with GRB170817A past the coalescence. Color coding (blue-to-yellow) is proportional to amplitude defined by butterfly output of time-symmetric chirp-like template correlations to data. See more details in the text and in the original paper[1].

Their analysis has yielded the following results:

- the relative loud merger signal of GW170817 with binary coalescence at the time $t_c = 1842.43\text{s}$, as estimated by LIGO, is described by an ascending chirp in GW frequency identified up to 260Hz before the coalescence ($t < t_c$). In particular, the luminosity in GWs at the highest detected frequency would be $L_{GW} \simeq 1.35 \cdot 10^{50}\text{ergs}^{-1}$

- there is continuation of GW170817 with an exponentially descending chirp during GRB170817A and lasting few seconds, whose initial frequency is about 700Hz identified at the time $t_s = t_c + 0.67s$, and the final frequency is about 300Hz

This chirp would start in the 1.7s gap between GW170817 and GRB170817A. In particular, from the exponential track the authors have estimated the frequency of the GW signal at the coalescence time as 774Hz, stressing that this value of frequency is below the orbital frequency at which the stars approach the Inner Most Stable Circular Orbit (ISCO) of the system as a whole, i.e. ∼1100 Hz at ∼16km according to the Kerr metric[1]. Since in the case of a prompt collapse to a $\sim 3M_\odot$ Kerr BH any gravitational-radiation from remaining debris orbiting about the ISCO would be above 2 kHz, the <1kHz descending chirp would be related to the GW emission of a *long-lived* rotating hyper-massive neutron star or magnetar induced by dynamical and secular instabilities that may include magnetic fields[1]. From the measured frequencies one can estimate the amount of energy released through GWs during the descending chirp:

$$E_{GW} \simeq 0.2\% M_\odot c^2 \approx 3.6 \cdot 10^{51}\text{erg}$$

All of these results would support the idea that the outcome of the merger was an hypermassive NS. Up to now, this is the only suggested evidence of a post-merger GW emission. It is worth noticing that in [3] no evidence of such an emission has been found.

Chapter 5

Modeling the post-merger phase

The event of August, 2017, is routinely described as the merger of two neutron stars, forming in the post merger a hypermassive configuration, which collapses to a BH on a timescale from tens of milliseconds up to about one second. This interpretation is rather successful, but it faces at least one difficulty when used to describe the Kilonova signal (KN): from one side, in order to be able to describe the blue component it is necessary to assume radii for the stars undergoing the merger smaller than $\sim (11-12)$km. On the other side, in order to describe the red (or purple [155]) KN a large amount of mass should be ejected from the disk and this indicates a not too small value for the tidal polarisability, $\tilde{\Lambda} > 300-400$. These two requests are conflictual [128] and a possible way out is offered by the two-families scenario in which the merger was not of two neutron stars, but of a neutron star and of a strange quark star. In that way the limit on $\tilde{\Lambda}$ can be respected while the radius of the neutron star participating to the merger was of the order of 11 km or smaller. Notice also that radii of 11 km for NSs having a mass of about (1.3-1.4) $M_{\odot}$ are difficult to obtain if only one family of compact stars exist, as described in Chapter 3.

It is also important to remark that since the total gravitational mass estimated for the system at the merger ($\sim 2.74 M_{\odot}$) is bigger than the threshold mass of binary hadron star systems in the two-families scenario, i.e. $\sim (2.52-2.72)M_{\odot}$ as estimated in [156], the hypothesis that the binary system involved during GW170817 was a HS-HS system is disfavored. In the following we will therefore assume that the merger was of a NS (first family) with a QS (second family). This possibility is particularly relevant for binaries having at least a moderate mass asymmetry, because in that way the probability that the most heavy component is a QS is maximized. In the following we will consider $q = 0.85$. As described in De Pietri et al. (to be published) the product of the merger in that case is a compact object whose central region is entirely made of quarks, while the external region is still made of hadrons. This configuration is reached a few milliseconds after the merger and it takes a significantly longer time, of the order of seconds, for the quark deconfinement process to be completed [157].

In the following we first evaluate the total baryonic mass during the post-merger phase and then we describe the evolution of the remnant in three temporal steps: $t \lesssim$ a few ms; a few ms$\lesssim t \lesssim (10-20)$ms; $t \gtrsim (10-20)$ms.

5.1 Estimate of the baryonic mass after the merger

The evaluation of the baryonic masses of the binary stars from their gravitational masses is done by applying two different EoSs previously discussed (see Figure3.7), i.e. the hadron and the quark EoSs. It's known from GW170817 that: $M_{tot} = (m_1 + m_2) \approx 2.74M_\odot$, which is the total gravitational mass before the merger. Therefore, by considering that $q = 0.85$ and that the most massive compact object of the binary system is the quark star (i.e. $m_1 = m_Q$ and $m_2 = m_H$, with $m_1 > m_2$), we obtain that:

$$\frac{m_2}{m_1} = 0.85 \;\wedge\; m_1 + m_2 = 2.74M_\odot$$
$$\implies m_2 = m_H = 1.26M_\odot \; m_1 = m_Q = 1.48M_\odot$$

The calculation of the corresponding value of the hadron star's baryonic mass we use the results plotted in Figure3.7, which are obtained applying the `RNS` code. Instead, the baryonic mass of the quark star is estimated by using the LORENE/rotstar code, since it is more accurate than other codes for treating stellar objects characterized by a strong density discontinuity at the surface (as well discussed in the Chapter 2). Also, LORENE/rotstar gives $M_{TOV} = 2.36M_\odot$ instead of the value $2.38M_\odot$ estimated by `RNS`. The calculation gives $m_H^B = 1.38M_\odot$ for the hadron star and $m_Q^B = 1.66M_\odot$ for the quark star. Therefore, the total baryonic mass of the system before the merger is easily estimated as:

$$M_{tot}^B = m_H^B + m_Q^B = 3.04M_\odot$$

During and immediately after the merger the mass-ejection mechanisms can reduce slightly this value. This mass loss can be estimated from the Kilonova signal. As we have discussed before, concerning the Blue-KN it has been estimated $M_{ej} \sim (0.01 - 0.03)M_\odot$. Instead, for the Red-KN a larger amount of ejected mass is estimated: $M_{ej} \sim 0.04M_\odot$. Therefore, we can consider here a maximum amount of mass-ejection of $0.1M_\odot$. The total baryonic mass after the merger, which characterizes the hypermassive star formed as outcome, is then:

$$M_{tot,fin}^B \equiv M^B = (3.04 - 0.1)M_\odot = 2.94M_\odot$$

This quantity must be conserved during the entire evolution of the remnant.

5.2 Evolution for $t \lesssim$ a few ms

Numbers of numerical simulations in full general relativity of binary NS mergers have been realized probing the differential-rotation law of the outcome of such events, when a prompt collapse to BH doesn't occur. The analysis reported in [140] have studied the angular velocity profile for a large set of EoSs, finding that there is a quasi-universal behaviour characterized by a central slowly and almost uniformly rotating core, surrounded by a differentially rotating "disk". This disk is characterized by a rapidly rotating inner part, whose frequency is larger than the core's frequency,

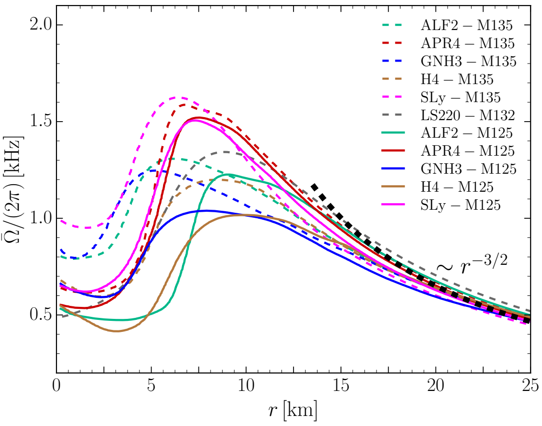

Figure 5.1: Time and azimuthally averaged rotational profiles obtained from the simulations of binary-NS mergers, applying different EoSs. Solid curves describe the profiles in the case of low-mass binaries, whereas dashed curves refer to the case of high-mass binaries. See more details in the text and in the original paper [140].

and an outer part with a velocity profile scaling like $\sim r^{-3/2}$. The transition between the slower inner core and the rapidly rotating exterior takes place across a narrow region which is only $3-4$ km wide. This behaviour has been obtained for both stiff and soft EoSs. It's important to stress that this trend of the frequency is largely different from that depicted by the already discussed "j-constant law". Although its several applications in studying rotating compact stars developed over the years, such a simple rotational law is not the correct one to investigate post-merging configurations, which are very chaotic and complex systems. However, we will see soon that it could still be useful to treat more quietly differentially rotating objects. Although its quasi-universality, the profile law obtained in [140] changes a little between the several EoSs investigated. The authors have considered five nuclear-physics EoSs: the APR4 and SLy ones belong to the class of variational-method EOSs and they describe a composition consisting mainly of neutrons, with little admixtures of protons, electrons and muons; the GNH3 and H4 ones are computed by applying a RMF approach, in which hyperons are included at high densities; the last one ALF2 describes hybrid nuclear matter, since it contains a phase transition. All these EoSs satisfy the observational constraint $M_{TOV} \sim 2M_\odot$. Moreover, the merger between the binary compact stars has been simulated for two different choices of the total gravitational mass of the system[1] $M = 1.25M_\odot$ and $M = 1.35M_\odot$. It has been found that the spatial size of the slow inner core depends both on the EOS and on the initial mass of the binary; in particular the small-mass binaries ($M = 1.25M_\odot$) generate a remnant with larger core with respect the case of high-mass binaries. Eventually, the maximum frequency reached in the core weakly depends on the EoS: stiffer EoSs are associated with lower central angular velocities than softer EoSs. We can note that all the central frequencies are of the order of $\sim$ 1kHz, spanning the range $\sim (0.5, 1.0)$kHz. The results obtained by the authors are showed in Figure5.1. We can expect that, during the event of August 2017, the hypermassive compact star formed after the merger had an inner rotational profile like this.

---

[1] The two binary stars are assumed to have equal masses.

5.3 Evolution for a few ms$\lesssim t \lesssim (10-20)$ms

Here we first discuss the evolution of the differential rotation profile inside the remnant due to the presence of viscosity, by applying the analysis reported in [158]. We then discuss properties of the final configuration assuming for simplicity that it corresponds to a quark star.

5.3.1 Effects of the viscosity

Several simulations show that during the first milliseconds after the merger the viscosity plays a relevant role for the evolution of the outcome, when a prompt collapse doesn't occur. In order to study these first stages of the life of our hypermassive star, we can apply the analysis reported in [158]. Here the authors have performed long-term general relativistic neutrino-radiation hydrodynamics simulations for a canonical remnant formed after the binary NS merger. The simulations have been done in full general relativity, applying the 3+1 formalism, where also non-isotropic stresses in the stress-energy tensor have been considered. Concerning the microphysics context, the authors have applied a hadron hot EoS[2] built with a RMF approach, in which Λ hyperons and also light and heavy nuclei have been included.

It's known that in a differentially rotating medium the tangential stresses between adjacent layers, which are connected with the existence of magnetic field, turbulence (*eddy*) and molecular (*shear*) and radiative viscosities, are the mechanisms of transport of angular momentum[159]. Generally, the last two viscosities can be neglected in compact stars. In particular, in [160] it has been pointed out that the Reynolds number estimated for quark stars is very big ($\sim 10^{14}$), implying a very small share viscosity. Concerning the effects of the magnetic field and the turbulence, in the Newtonian approximation, one can estimate the total stress as follows[159]:

$$w_{r\phi} = \mu \frac{\partial v_\phi}{\partial r} = -\Big[\rho c_s^2 \Big(\frac{v_t}{c_s}\Big) + \rho c_s^2 \Big(\frac{B^2}{4\pi\rho c_s^2}\Big)\Big] \tag{5.1}$$

where $w_{r\phi}$ is the tangential stress, μ is the viscosity coefficient, v_ϕ is the circular Keplerian velocity, v_t the turbulent velocity, c_s the speed of sound, ρ the density of the medium and B the strength of the magnetic field. The first right hand side term describes the stress generated by the turbulence, instead the last one represents the magnetic stress. Usually one applies the parametrization for the total stress $-w_{r\phi} \equiv \alpha\rho c_s^2$ where α is a viscosity parameter. This one in the case of a turbulent mechanism is always smaller than 1 [159]. Since the simulations have been done through a neutrino-radiation-viscous hydrodynamics code, the authors have studied the general evolution of the massive NS-binary merger determined only by the eddy neutrino-radiation-driven viscosity, without considering magnetic fields. Being the eddy viscosity defined also as $\eta_t = \rho v_t L$, where L is the maximal scale of the turbulent cell [159], from the eq.5.1 the authors have chosen the following prescription for the

---

[2] The dependence of the EoS on the temperature must be taken into account to probe the first moments after the merger.

kinematic viscosity ν:

$$\nu = \frac{\eta_t}{\rho} = \alpha c_s L \tag{5.2}$$

where they have put $L = 10$km, because it should be approximately equal to the size of the remnant. As the fiducial model they have considered $\alpha = 0.02$, which is in agreement, at least for the outer part of the remnant, with some recent high-resolution global magneto-hydrodynamical simulations for a binary neutron star merger[158]. The simulations have shown that within the first $\lesssim$ 20ms, the viscosity plays a relevant role in the angular momentum redistribution. In particular, the angular momentum of the high angular-velocity disk located out of the star's core (see Figure5.1) is transported towards low angular-velocity regions, especially spinning-up the central core. This quite rapid process produces a mostly uniformly rotating object with a central spin frequency of the order of 1kHz. These results are shown in Figure5.2. We consider such an evolution for the remnant of the HS-QS merger.

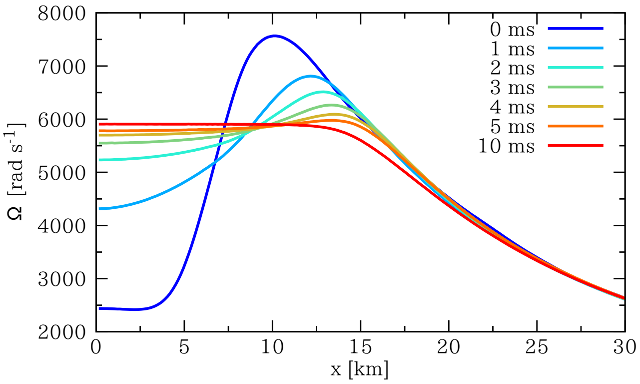

Figure 5.2: Angular velocity profiles on the equatorial plane at different times. The evolutionary track has been obtained for the fiducial model DD2-135135-0.02-H. See more details in the text and in the original paper [158].

5.3.2 Stability of a uniformly rotating QS

During the earliest stages of the post-merger phase, a large number of quark-nucleation processes take place inside the remnant. Indeed, due to the high masses involved in this phase ($M^B_{tot} = 3.04 M_\odot$), a quark deconfinement in the core of the star is well expected. Within timescales ∼ms mostly of the inner part of the remnant is composed of quark matter. Moreover, since one of the two binaries before the merger was already a QS, lots of quark-drops should be located also in the star's envelope. In this way, the slow ($\sim$ 10s) diffusive mechanism converting hadron matter into quark matter in the outer regions of the star, predicted by the two-families scenario, should be accelerated because of the decrease of the lengthscales of the process. In fact, like ordinary diffusive processes, the time involved during the deconfinement scales with the distances like $\tau \sim d^2$. Because of these considerations, we expect that the process of quark deconfinement is completed in $\lesssim$ 1s. For simplicity we assume in the following that a quark star is already formed after few tens of ms.

Therefore at the end of the evolution depicted in Figure5.2, a 1kHz mainly uniformly rotating quark stars is formed. The main features of uniformly rotating quark stars are investigated in Figure5.3.

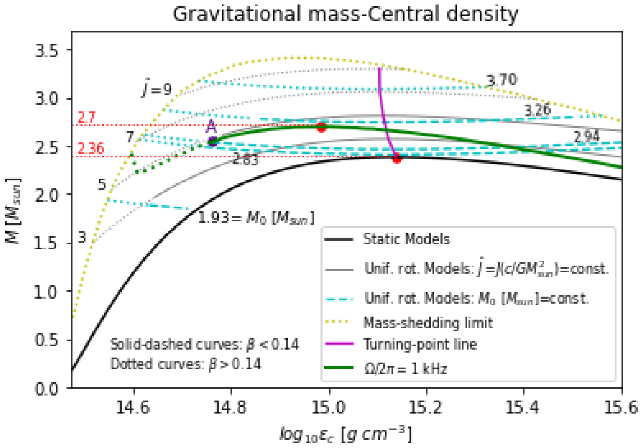

Figure 5.3: Gravitational mass-radius diagram obtained with LORENE/rotstar applying the quark matter EoS. Here, the point A represents our model of 1kHz uniformly rotating model quark star, with baryonic mass of $2.94M_\odot$, which we expected to be formed $\sim$ 10ms after the coalescence. See more details in the text.

Here we report the gravitational mass vs central mass-energy density diagram computed by using the LORENE/rotstar code and applying the quark-matter EoS. In the plot, the thick-solid black line represents the sequence of non-rotating models, the thin-grey curves instead represent sequences of uniformly rotating models with constant angular momentum (whose values are indicated on the left side of the diagram) and the green curve describes models with constant spin-frequency of 1kHz. Moreover, the sequences of uniformly-rotating stars with constant baryonic mass are represented with cyan lines; each value of the mass is reported in the plot. We can note that supramassive quark star configurations have baryonic masses bigger than $2.83M_\odot$. The yellow curve is the Keplerian sequence and the magenta curve is the turning-point line. Eventually, all the solid/dashed curves are related to models which are secularly stable against non-axisymmetric instabilities (i.e. $\beta < 0.14$); instead, all the dotted curves are associated with unstable models. We have indicated in the plot with the point A the quark star that we assumed to be formed $\sim$ 10ms after the merger, whose baryonic mass is equal to $2.94M_\odot$. It is a supramassive star. Therefore if it loses angular momentum along a sequence with constant baryonic mass it will pass the turning-point line, collapsing to a BH within dynamical timescales. An other important result turns up from the plot: the triaxial secular-instability is a very common feature of rapidly rotating quark stars. This is in agreement with others recent studies previously discussed, in which it has been shown that quark stars can reach large triaxial deformations before terminating the sequence at the mass-shedding limit[99]. There are several works which have noted that the values of β are generally higher in quark stars compared to others NSs. These values are high for rapidly rotating quark stars also with moderate masses (for which cases one could expect more stable objects since $|W|$ is bigger); for instance, $\beta \sim 0.2$ for a rotational period of 0.86ms and a baryonic mass of $1.60 M_\odot$ [107]. Therefore, this seems to indicate that triaxial instabilities could develop more easily in rotating strange stars. This is probably due to the fact that QSs are strong-self-bound objects, and not self-gravity bound systems like ordinary NSs. Here we have just reported a rough analysis of the triaxial instability in quark stars. Indeed we have based it on the Newtonian limit for the secular bar-mode instabilities, i.e. $\beta \lesssim 0.14$, which corresponds to the bifurcation point between the Maclaurin and the Jacobi sequences. Actually, for relativistic compact stars the bifurcation point depends on the compactness of the star (M/R) and it differs slightly from the classical value. However, we can consider an other recent result. As shown in [99] the bifurcation point to triaxial sequence of QSs happens at a spin period of ~ms, corresponding to a GW emission due to the instability with frequencies ~kHz. Our model labeled with the point A in Figure5.3 has a spin frequency of 1kHz and it is correctly located very close to the edge of the β-stable region. In fact, models on the right of A are all stable against bar-mode instabilities. We can expect that β-instabilities have played an important role during its early evolution. Actually, in Figure5.3 we have report only the secularly-unstable/stable models. For bigger values of β dynamical bar-modes instabilities allow to dissipate a great amount of energy within very short timescales (~ms). In our plot these β-instabilities concern models with the same baryonic mass of A $(2.94 M_\odot)$ and higher frequencies, which are closer to the mass shedding limit. In particular, on the Keplerian curve $\beta \approx 0.25$. Therefore, we can expect that the considerable amount of rotational kinetic energy of the quark star has been dissipated mainly through dynamical bar-mode instabilities during the early times after the merger. The secular-stable configuration labeled by A would be the end-point of this early evolution, where the dissipation of energy through bar-mode instabilities is over. In our scheme the stellar remnant formed after GW170817 has not collapsed rapidly to a BH once a Keplerian configuration with maximum mass has been reached (as predicted in [161]), but it has dissipated enough rotational-energy to attain a 1kHz uniformly rotating configuration within timescales $\sim (10-20)$ms. This object is far from the mass-shedding limit, as we can see from Figure5.3. The energy dissipation happening during the first tens of milliseconds after the merger has restored the β-stability of the object at this point. Therefore it should be an axially-symmetric β-stable quark star, uniformly rotating at 1kHz frequency.

5.4 Evolution for $t \gtrsim (10-20)$ms

In this section we discuss the ultimate evolution of the QS, lasting up to some seconds. At the end of the previous step we have considered that a 1kHz uniformly rotating QS was formed. We now discuss the possibility of emitting GWs due to a deformation of the star's shape induced by an internal toroidal magnetic field. The braking due to the GWs will slow down the region deformed by the toroidal field. While we assume that the most inner region of the star preserves its initial angular momentum during the evolution. Initially we discuss the strength of the toroidal field needed to generate such a deformation. We also show that there can be an external poloidal field strong enough to generate a short-GRB but at the same time sub-leading respect to GWs in the braking of the rotation. Finally, we illustrate the evolution of the differentially rotating QS down to its collapse to a BH.

5.4.1 Toroidal and poloidal magnetic fields

Until this point our scheme provides a possible evolutionary scenario for the first $\sim$(10-20)ms of the post-merger phase. This early phase is characterized by a great dissipation of energy through GWs, due to β-instabilities, whose frequencies are expected to be $\sim$kHz. This is confirmed by numerical simulations showing a strong GW emission during the post-merger. Nevertheless, the comparison of this scenario with the observational data represents a great challenge for us, since GW170817 has been detected only during the inspiral phase and no signals have been observed during the merger and in the ring-down phase.

However as we have previously reported, in [1] the evidence of a GW post-merger signal has been proposed. While this observation has been challenged in the analysis of [3], here we ask ourselves how this emission could be explained. In particular, an interpretative scheme has to include: a mechanism that is able to explain the descending chirp starting at frequencies of $\approx$ 700kHz and ending at $\approx$ 300Hz, through a sequence of configurations which are dynamically stable during the entire evolution; the emission of $\sim 3.6 \cdot 10^{51}$erg by GWs; a mechanism that allows to generate the short-GRB observed after the merger.

It's known that NSs are generally characterized by very strong poloidal magnetic fields, since the conservation of the magnetic flux during the core collapse SNe which form them. This field is frozen into the stars and it can couple with the rotational field inside them. A differential rotation in the star would create an inner toroidal field from the poloidal component thanks to the so-called ω-process. This is a well known mechanism described within the classical one-fluid Magneto-Hydrodynamics. In our scheme the best moment to generate the differential rotation is during the process of quark deconfinement driven by the diffusive mechanism. This phase that can last up to $\sim$ 1s in our scenario and it is characterized by the presence of two components which rotate with different velocities. The inner toroidal field could reach strengths $\sim 10^{17}$G inside NSs, as reported in some recent analysis (e.g. [162]). In particular, one may estimate the maximum interior magnetic field to be as high as 10^{18}G. With such a mechanism the star looses part of its rotational kinetic energy increasing the strength of the toroidal field. This would happen within a not steady process but oscillating: when much of the available kinetic energy of the differential rotation has been transformed into toroidal magnetic energy, the magnetic tension forces react back and reverse the motion, developing a torsional, standing, Alfvén wave in the star [162]. This wave is not damped inside NSs because their very low shear and bulk viscosities, above all in the case of quark stars. In this way the system starts to oscillate like a torsion pendulum. This oscillation generates a quadrupole-mass moment, allowing the star to emit GWs.

We consider the process above described as the guiding mechanism of the dynamical evolution of our quark star model. In particular, we can estimate the strength of the inner toroidal magnetic field by considering the amount of energy emitted through GWs during the descending chirp. The module of the rate of the energy emission due to the mechanism is [163]:

$$\dot{E}_{GW}^{B_\phi} = \frac{32G}{5c^5}(I\epsilon_B)^2\Omega^6 \tag{5.3}$$

where $I \approx 0.2MR^2$ is the star's moment of inertia, ϵ_B is the ellipticity induced by the magnetic field and $\Omega/2\pi$ is the spin frequency of the object, which is equal to half of the emission frequency of the GWs (this fact is well demonstrated in [163]). The ellipticity is given by[164]:

$$\epsilon_B = -k_e \times 10^{-12} R_{10}^4 M_{1.4}^{-2} B_{\phi 12}^2 \tag{5.4}$$

where k_e is a parameter depending on the internal magnetic field configuration, $B_{\phi 12}$ is the toroidal magnetic field (in units of 10^{12}G) and $M_{1.4}$ is the mass (in units of $1.4M_\odot$) and R_{10} is the radius (in units of 10km) of the star. By combining the above equations and writing the emitted energy as $\dot{E}_{GW}^{B_\phi} \approx xM_\odot c^2\tau^{-1}$ (where $\tau \sim 1$s as inferred from [1]), one finds that:

$$B_{\phi 12} \approx 7 \times 10^8 \Big(\frac{M_{1.4}\sqrt{x}}{k_e R_{10}^6 \Omega_{100}^3}\Big)^{1/2} \tag{5.5}$$

where Ω_{100} is the angular velocity in units of 100Hz. In our case, at the beginning of the chirp, from the data in [1] and the results of LORENE/rotstar we have that: $M \approx 2.5M_\odot$ and $R \approx 16$km, $\Omega/2\pi \approx 350$Hz and $x \simeq 2 \times 10^{-3}$. Moreover, $k_e \simeq [0.5-5]$ [164]. We take the mean value $k_e \approx 2$. Therefore, the strength of the inner toroidal field is:

$$B_\phi \approx 3 \times 10^{17} G \tag{5.6}$$

which is in agreement with the estimates reported in [162] and, above all, it is well below the maximum field $\sim 10^{18}$G. This is the inner field required to our quark star for emitting the amount of energy estimated in [1] through GWs. Moreover, concerning the strength of the external poloidal field B_θ, we can estimate it by considering a magnetic-dipole emission of EMWs at a rate $\lesssim \dot{E}_{GW}^{B_\phi}$. This is comparable with the typical luminosity of short-GRBs ($\sim 10^{51}$ergs^{-1}). We can apply the well known "magnetic-dipole model" of pulsars [163]. In the case of a NS rotating uniformly in vacuum at a frequency Ω and which possess a magnetic dipole moment m, the energy radiated by the time-varying dipole moment at the frequency $\Omega/2\pi$ (half of the frequency of GW signals) can be estimated from:

$$\dot{E}_{EMW}^{B_\theta} \sim -\frac{B_\theta^2 R^6 \Omega^4}{6c^3} \tag{5.7}$$

By taking the module of the above equation and considering again that $\dot{E}_{EMW}^{B_\theta} = xM_\odot c^2\tau^{-1}$ with $\tau \approx 1$s, we obtain that:

$$B_\theta \approx 1.7 \times 10^{21} G \frac{\sqrt{x}}{R_{10}^3 \Omega_{100}^2} \tag{5.8}$$

Now by using the above values for the radius and the spin frequency of the star, the condition $\dot{E}_{EMW}^{B_\theta} \lesssim \dot{E}_{GW}^{B_\phi}$ gives $B_\theta \lesssim 3.8 \times 10^{16}$G. This strength is comparable with some estimates provided by recent works, in which the authors have modeled the observed X-ray light curves of several short-GRBs by assuming a proto-magnetar as the inner engine of such events (e.g.[165]).

From this calculus we have pointed out a very important result. By assuming an external poloidal magnetic field of $\approx 1 \times 10^{16}$G, we can easily power a short-GRB via the proto-magnetar model and at the same the rotational energy emitted via EMWs is one order of magnitude smaller than the energy emitted via GWs. Notice that in our discussion we are considering values of the poloidal magnetic field one order bigger than those reported in [166].

Eventually, we discuss the effects of the viscosity during the conversion process of the poloidal field into the inner toroidal field. As we have previously argued the shear viscosity is largely negligible inside quark stars. However, as reported in [162], the energy of the torsional oscillation could leak out of the star because of the presence of a second viscosity due to the magnetic field. In [162] this is named as *bulk* viscosity. The Alfven wave, being non-compressive, is not damped by bulk viscosity at the linear approximation. Nevertheless, the Alfvén torsional oscillation is not linear and, because of a non-resonant coupling, magnetic-pressure gradients make compressive the oscillation. Therefore, the bulk viscosity acts on this compressive part of the non-linear oscillation, damping it within a few time. The calculation of such a damping is done by solving the MHD equations perturbatively to second order. In [162] a more simple and approximate estimate is proposed, treating the specific case of a strange-quark star. Here it's shown that for normal quark stars the time-scale of the damping process is about:

$$\tau = 4.8 \times 10^{10} T_9^2 m_{s100}^{-4} \text{ s} \tag{5.9}$$

where T_9 is the equilibrium temperature of the medium (in units of 10^9K) and m_{s100} is the mass of the quark strange (in units of 100MeV). Clearly, this time is very long. Therefore, during the evolution of our quark star model, lasting about few seconds, we can assume that the effects of the bulk viscosity are largely negligible. This guarantees the efficiency of the process of GW emission driven by the magnetic field during the entire descending chirp.

We suggest that the descending chirp in GWs observed in [1] would be due to the coupling between the rotation of the star and magnetic field frozen into the plasma of quarks. In particular, as shown in [164], with the growth of the internal toroidal field the ellipticity of the star becomes dominated by the magnetically induced, prolate deformation. This deformation is particularly relevant in the outer regions of the star, slowing them down together with the GW emission. Therefore, we assume here a bi-component structure of the quark star: an outer slowly-rotating matter distribution, strongly deformed by the toroidal field; a inner central core still rapidly-rotating at a $\sim$ 1kHz frequency. Since the weakness of the viscosity forces, such a differential rotation coupled with the magnetic field inside the star is maintained for a sufficiently long time ($\gtrsim$ 1s), i.e. up to the collapse to a BH.

Modeling the descending chirp

We depict here our interpretative scheme of a post-merger extended emission in GWs, based on the detection of the descending chirp reported in [1]. During its evolution towards the collapse our supramassive quark star looses rotational energy by emitting GWs, according the mechanism previously discussed. It also preserves its baryonic mass. In particular, since the last detected frequency of the descending chirp is $\approx$ 300Hz, the evolutionary track in our scheme starts from the 1kHz uniformly rotating object and ends at a differentially rotating configuration with equatorial spin frequency of $\approx$ 150Hz and central frequency still of 1kHz. Eventually, part of the rotational energy is also dissipated via EMWs in order to generates the short-GRB.

In our analysis we make use of the LORENE/rotstar code, without employing full general relativity time-dependent simulations. Therefore, we figure the entire evolution through stationary equilibrium configurations characterized by different degrees of differential rotation. We need to verify if *stable* differentially rotating objects with equatorial frequency as small as $\approx$ 150Hz can be obtained with our EoS. As shown in [167], we can apply the turning-point line criterion to study the stability of differentially rotating compact stars with good accuracy. We use it to determine both the secular and the dynamical stability against axially-symmetric modes of the several configurations. Therefore, along the sequence of constant baryonic mass of $2.94M_{\odot}$, the model with the minimum angular momentum represents the last stable equilibrium model. The secular and dynamical stability against non-axially symmetric modes are studied here by considering again the criterion $\beta \leq 0.14$. Eventually, we apply the well discussed "j-constant law" for defining the differential rotation inside the star. Clearly, this represent a remarkable limit for our evolutionary scenario; however, it ensures the Rayleigh local stability for each configuration during the track. A representation of the typical rotation profile inside our configurations is reported in Figure5.4.

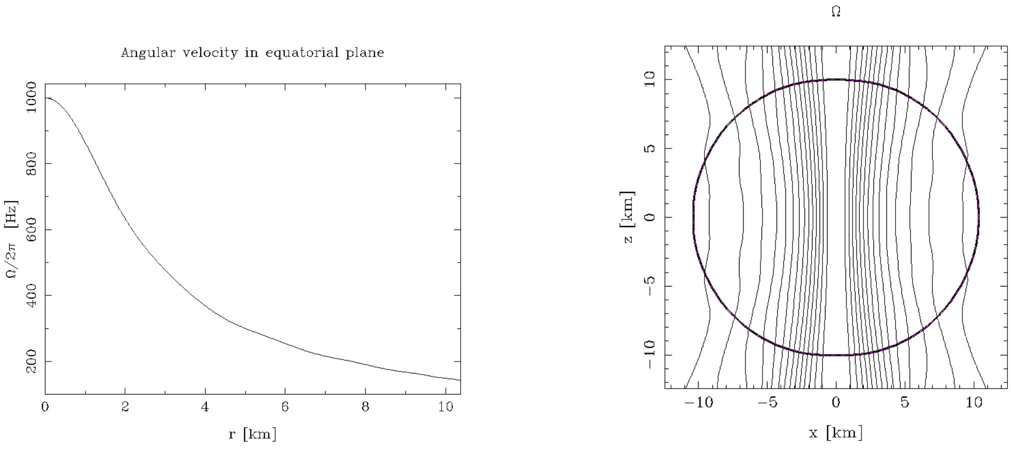

(a) 1-dimensional plot of the rotational profile on the equatorial plane obtained with the "j-constant law".

(b) 2-dimensional plot of the rotational profile obtained with the "j-constant law".

Figure 5.4

The results of our analysis are shown in Figure5.5. Here we report the gravitational mass vs central mass-energy density diagram for several equilibrium configurations together with the track of the differentially rotating QSs during the descending

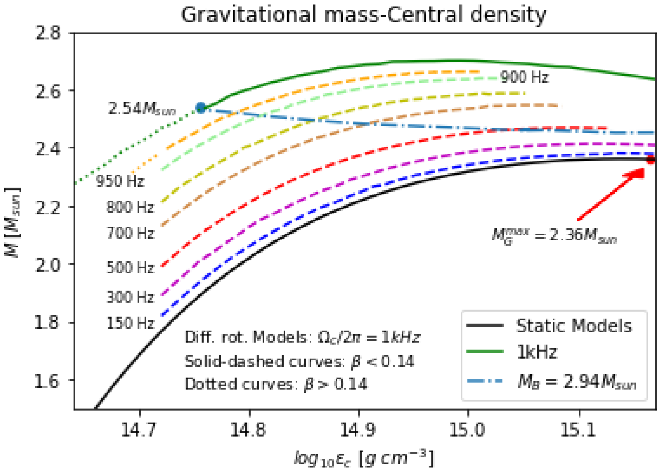

Figure 5.5: Gravitational mass-central mass-energy density diagram for several models of QSs computed with the LORENE/rotstar code. Here, both static and uniformly and also differentially rotating objects are probed. The dashed-dotted light-blue line is the evolutionary track proposed to explain the descending chirp in GWs reported in [1]. See more details in the text.

chirp. In the plot, the black curve represents the sequence of static models, instead the green one is the Keplerian sequence. With different colours and dashed curves we mean differentially rotating QSs, whose central frequency is fixed at $\Omega_c/2\pi$ =1kHz and the equatorial frequency changes among them. In particular, the value of $\Omega_e/2\pi$ for each curve is reported in the plot. For all the sequences, the dotted branches are associated with models having $\beta \gtrsim 0.14$. Eventually, the dashed-dotted light-blue curve describes the sequence of models with constant baryon mass of $2.94M_{\odot}$. This is the evolutionary track of our quark star. A first important point that turns up from the plot is that the model evolves through configurations which become more and more $\beta-$stable as the equatorial frequency decreases. Therefore, the differential rotation acts for the stability of the star against non-axisymmetric modes. This can be explained by considering that $\beta = T/|W|$ and along the track the model preserves its baryonic mass decreasing the mean angular velocity. In particular, we have that:

$$\frac{T}{|W|} = \frac{T}{|M_G - M_B - T - U|} = \frac{1}{|(M_G - M_B - U)/T - 1|} \tag{5.10}$$

Since M_B is conserved and also M_G doesn't change very much along the track (the relative change is $\sim 10\%$, as inferred from the plot), we need to know the variation of the internal energy U during the decrease of the mean angular velocity of the star ($\delta T < 0$). From the plot we can note that the mass-energy density increases as the envelope of the model slows down. This is due to the weakening of the centrifugal forces on the ourter regions during the evolution. Because we are treating a cold EoS, which describes a completely degenerate quark matter's fluid, the increasing of the density implies $\delta U > 0$. Together with $\delta T < 0$, this provides the decreasing of the β parameter as the star slows down. Eventually, our results show that the turning point of the sequence with constant baryonic mass is very close to the maximum gravitational-mass configuration of the sequence with equatorial frequency of 500Hz.

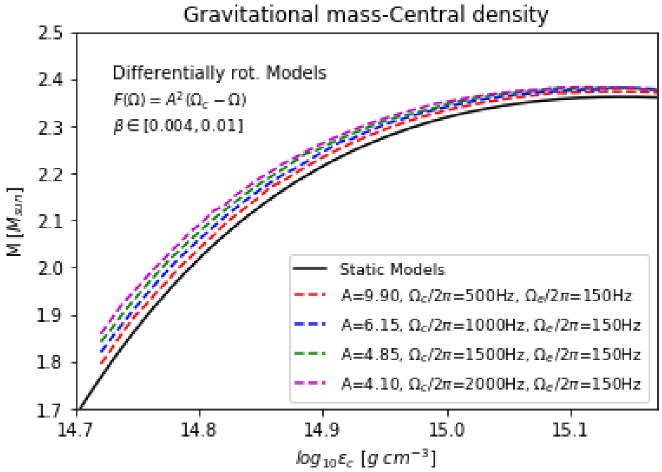

Figure 5.6: Gravitational mass-central mass-energy density diagram for several models of QSs computed with the LORENE/rotstar code. Here, the black line is the sequence of static models. Sequences of differentially rotating QSs are represented by the dashed-curves; these have a fixed equatorial frequency of 150Hz and different central frequencies, from 500Hz to 2kHz. As reported on the plot, all the models compute are β-stable.

Unfortunately, our quark star never reaches an equilibrium configuration with equatorial spin frequency of ~ 150Hz, but it overcomes the last stable configuration thus collapsing to a BH within dynamical timescales. The problem is that with such a small frequency at the equator, the gravitational mass of a compact star cannot be quite bigger than M_{TOV}. In particular in Figure5.6 we note that this behaviour is almost independent on the value of the central spin frequency. Indeed, even considering $\Omega_c/2\pi = 2$kHz for a fixed $\Omega_e/2\pi = 150$Hz, the increasing on the gravitational mass is very small. Unfortunately, our scheme seems not able to explain correctly the descending chirp in GWs reported in [1]. Nevertheless, one could investigate how the results change by taking for instance a more stiff EoS for the quark matter, i.e. a more high M_{TOV}. This would allow the sequence with $\Omega_e/2\pi \sim 150$Hz to be closer to our evolutionary track. An other possibility could be the changing of the rotational law. Indeed in our models only the inner part of the core rotates fast, as it can be easily noted in Figure5.4. It is clear that a rotational law involving a more large rapidly rotating core at frequencies ~ 1kHz, satisfying the Rayleigh local stability criterion at the same time, would allow sequences with more high gravitational masses because of the strengthening of the centrifugal forces.

Conclusions

Our analysis have pointed out that in order to explain a possible extended emission in GWs as suggested in [1] three ingredients are required: a value of M_{TOV} at least of the order of $2.3 - 2.4 M_{\odot}$; a differential rotation lasting at least few seconds, indicating a very small viscosity; a very strong internal toroidal field generating the deformation at the origin of the post-merger GW signal.

All these requests somehow support that a strange-quark star was formed during the post-merger phase. Indeed, within a one-family scenario, such large a value of M_{TOV} is in tension with the upper limit on the tidal deformability $\tilde{\Lambda} < 720$: as reported in [139] the parameter space allowing that value of M_{TOV} is rather limited. Instead, in this thesis, we have explicitly built an example of a model, basing on the two-families scenario and satisfying both the request on M_{TOV} and the limit on $\tilde{\Lambda}$. Moreover, a very low value of viscosity is also compatible with quark matter as indicated in [162]. Finally, the formation of a very strong internal toroidal magnetic field is facilitated by the presence of a relevant differential rotation. Within the two-families scenario, at t$\lesssim$ 1s the compact object is constituted by an inner part entirely made of quarks and an external hadronic layer: such a bi-component structure could be at the origin of the strong differential rotation. In the future the present analysis could be extended to a larger set of differential rotation profiles, in particular having a larger rapidly rotating inner core. In such a way a better interpretation of the post-merger signal reported in [1] could be obtained.

Bibliography

[1] M. H. P. M. van Putten and M. Della Valle, "Observational evidence for Extended Emission to GW170817," 2018.

[2] L. Piro, N. R. Butler, H. G. Khandrika, O. D. Fox, A. Rossi, T. Sakamoto, E. Troja, G. Ryan, S. B. Cenko, B. Zhang, H. van Eerten, R. Ricci, M. H. Wieringa, G. Novara, and A. Tiengo, "A long-lived neutron star merger remnant in GW170817: constraints and clues from X-ray observations," *Monthly Notices of the Royal Astronomical Society*, vol. 483, pp. 1912–1921, 11 2018.

[3] B. P. Abbott *et al.*, "Search for gravitational waves from a long-lived remnant of the binary neutron star merger GW170817," 2018.

[4] P. Haensel, A. Y. Potekhin, and D. G. Yakovlev, eds., *Neutron Stars 1 : Equation of State and Structure*, vol. 326 of *Astrophysics and Space Science Library*, 2007.

[5] W. Baade and F. Zwicky, "Remarks on Super-Novae and Cosmic Rays," *Physical Review*, vol. 46, pp. 76–77, July 1934.

[6] S. A. Colgate and R. H. White, "The Hydrodynamic Behavior of Supernovae Explosions," , vol. 143, p. 626, Mar. 1966.

[7] A. Hewish, S. J. Bell, J. D. H. Pilkington, P. F. Scott, and R. A. Collins, "Observation of a Rapidly Pulsating Radio Source," , vol. 217, pp. 709–713, Feb. 1968.

[8] P. Haensel, M. Bejger, M. Fortin, and L. Zdunik, "Rotating neutron stars with exotic cores: masses, radii, stability," *European Physical Journal A*, vol. 52, p. 59, Mar. 2016.

[9] B. P. A. et al. ., "Gravitational waves and gamma-rays from a binary neutron star merger: Gw170817 and grb 170817a," *The Astrophysical Journal Letters*, vol. 848, no. 2, p. L13, 2017.

[10] V. M. Kaspi, "Grand unification of neutron stars," *Proceedings of the National Academy of Sciences*, vol. 107, 04 2010.

[11] P. B. Demorest, T. Pennucci, S. M. Ransom, M. S. E. Roberts, and J. W. T. Hessels, "A two-solar-mass neutron star measured using Shapiro delay," , vol. 467, pp. 1081–1083, Oct. 2010.

[12] J. Antoniadis, P. C. C. Freire, N. Wex, T. M. Tauris, R. S. Lynch, M. H. van Kerkwijk, M. Kramer, C. Bassa, V. S. Dhillon, T. Driebe, J. W. T. Hessels, V. M. Kaspi, V. I. Kondratiev, N. Langer, T. R. Marsh, M. A. McLaughlin, T. T. Pennucci, S. M. Ransom, I. H. Stairs, J. van Leeuwen, J. P. W. Verbiest, and D. G. Whelan, "A Massive Pulsar in a Compact Relativistic Binary," *Science*, vol. 340, p. 448, Apr. 2013.

[13] A. Drago, A. Lavagno, G. Pagliara, and D. Pigato, "The scenario of two families of compact stars," *Eur. Phys. J.*, vol. A52, no. 2, p. 40, 2016.

[14] V. Kalogera and G. Baym, "The maximum mass of a neutron star," *The Astrophysical Journal Letters*, vol. 470, no. 1, p. L61, 1996.

[15] G. Srinivasan, "The maximum mass of neutron stars.," *Bulletin of the Astronomical Society of India*, vol. 30, pp. 523–547, Sept. 2002.

[16] P. Z. J. L. F. A. F. CHAMEL, N.; HAENSEL, "On the maximum mass of neutron stars," *International Journal of Modern Physics E*, vol. 22, 07 2013.

[17] B. D. Margalit, Ben; Metzger, "Constraining the maximum mass of neutron stars from multi-messenger observations of gw170817," *The Astrophysical Journal*, vol. 850, 11 2017.

[18] P. Haensel, J. L. Zdunik, and F. Douchin, "Equation of state of dense matter and the minimum mass of cold neutron stars," , vol. 385, pp. 301–307, Apr. 2002.

[19] F. Özel and P. Freire, "Masses, Radii, and the Equation of State of Neutron Stars," *Ann. Rev. Astron. Astrophys.*, vol. 54, pp. 401–440, 2016.

[20] R. A. Hulse and J. H. Taylor, "Discovery of a pulsar in a binary system," , vol. 195, pp. L51–L53, Jan. 1975.

[21] J. M. Weisberg and J. H. Taylor, "The Relativistic Binary Pulsar B1913+16: Thirty Years of Observations and Analysis," in *Binary Radio Pulsars* (F. A. Rasio and I. H. Stairs, eds.), vol. 328 of *Astronomical Society of the Pacific Conference Series*, p. 25, July 2005.

[22] M. Burgay, N. D'Amico, A. Possenti, R. N. Manchester, A. G. Lyne, B. C. Joshi, M. A. McLaughlin, M. Kramer, J. M. Sarkissian, F. Camilo, V. Kalogera, C. Kim, and D. R. Lorimer, "An increased estimate of the merger rate of double neutron stars from observations of a highly relativistic system," , vol. 426, pp. 531–533, Dec. 2003.

[23] A. G. Lyne, M. Burgay, M. Kramer, A. Possenti, R. N. Manchester, F. Camilo, M. A. McLaughlin, D. R. Lorimer, N. D'Amico, B. C. Joshi, J. Reynolds, and P. C. C. Freire, "A Double-Pulsar System: A Rare Laboratory for Relativistic Gravity and Plasma Physics," *Science*, vol. 303, pp. 1153–1157, Feb. 2004.

[24] C. Kim, "The double pulsar psr j0737-3039," *Journal of the Korean Physical Society*, vol. 65, 9 2014.

[25] L. Kuiper, W. Hermsen, F. Verbunt, D. J. Thompson, I. H. Stairs, A. G. Lyne, M. S. Strickman, and G. Cusumano, "The likely detection of pulsed high-energy gamma -ray emission from millisecond pulsar PSR J0218+4232," , vol. 359, pp. 615–626, July 2000.

[26] D. C. Backer, S. R. Kulkarni, C. Heiles, M. M. Davis, and W. M. Goss, "A millisecond pulsar," , vol. 300, pp. 615–618, Dec. 1982.

[27] R. N. Manchester, "Millisecond pulsars, their evolution and applications," *Journal of Astrophysics and Astronomy*, vol. 38, 9 2017.

[28] The NANOGrav Collaboration, Z. Arzoumanian, A. Brazier, S. Burke-Spolaor, S. Chamberlin, S. Chatterjee, B. Christy, J. M. Cordes, N. Cornish, K. Crowter, P. B. Demorest, T. Dolch, J. A. Ellis, R. D. Ferdman, E. Fonseca, N. Garver-Daniels, M. E. Gonzalez, F. A. Jenet, G. Jones, M. L. Jones, V. M. Kaspi, M. Koop, M. T. Lam, T. J. W. Lazio, L. Levin, A. N. Lommen, D. R. Lorimer, J. Luo, R. S. Lynch, D. Madison, M. A. McLaughlin, S. T. McWilliams, D. J. Nice, N. Palliyaguru, T. T. Pennucci, S. M. Ransom, X. Siemens, I. H. Stairs, D. R. Stinebring, K. Stovall, J. K. Swiggum, M. Vallisneri, R. van Haasteren, Y. Wang, and W. Zhu, "The NANOGrav Nine-year Data Set: Observations, Arrival Time Measurements, and Analysis of 37 Millisecond Pulsars," , vol. 813, p. 65, Nov. 2015.

[29] M. Bauböck, F. Özel, D. Psaltis, and S. M. Morsink, "Rotational Corrections to Neutron-star Radius Measurements from Thermal Spectra," , vol. 799, p. 22, Jan. 2015.

[30] C. O. Heinke, H. N. Cohn, P. M. Lugger, N. A. Webb, W. C. G. Ho, J. Anderson, S. Campana, S. Bogdanov, D. Haggard, A. M. Cool, and J. E. Grindlay, "Improved mass and radius constraints for quiescent neutron stars in ω Cen and NGC 6397," , vol. 444, pp. 443–456, Oct. 2014.

[31] J. M. Lattimer and A. W. Steiner, "Neutron Star Masses and Radii from Quiescent Low-mass X-Ray Binaries," , vol. 784, p. 123, Apr. 2014.

[32] E. F. Brown and L. Bildsten, "Deep Crustal Heating in Accreting Neutron-Stars: Quiescent Emission from Transients," in *19th Texas Symposium on Relativistic Astrophysics and Cosmology* (J. Paul, T. Montmerle, and E. Aubourg, eds.), p. 319, Dec. 1998.

[33] N. D. T. W. R. B. L. I. R. Marino, Alessio; Degenaar, "On obtaining neutron star mass and radius constraints from quiescent low-mass x-ray binaries in the galactic plane," *Monthly Notices of the Royal Astronomical Society*, vol. 479, 09 2018.

[34] C. O. Heinke, R. Wijnands, P. G. Jonker, and R. E. Taam, "New XMM Observations of the Accreting Millisecond X-ray Pulsar SAX J1808.4-3658 in Quiescence," in *American Astronomical Society Meeting Abstracts*, vol. 38 of *Bulletin of the American Astronomical Society*, p. 1065, Dec. 2006.

[35] N. A. Webb and D. Barret, “Constraining the Equation of State of Supranuclear Dense Matter from XMM-Newton Observations of Neutron Stars in Globular Clusters,” , vol. 671, pp. 727–733, Dec. 2007.

[36] C. O. Heinke, G. B. Rybicki, R. Narayan, and J. E. Grindlay, “A Hydrogen Atmosphere Spectral Model Applied to the Neutron Star X7 in the Globular Cluster 47 Tucanae,” , vol. 644, pp. 1090–1103, June 2006.

[37] S. Bogdanov, C. O. Heinke, F. Özel, and T. Güver, “Neutron Star Mass-Radius Constraints of the Quiescent Low-mass X-Ray Binaries X7 and X5 in the Globular Cluster 47 Tuc,” , vol. 831, p. 184, Nov. 2016.

[38] T. Güver, F. Özel, A. Cabrera-Lavers, and P. Wroblewski, “The Distance, Mass, and Radius of the Neutron Star in 4U 1608-52,” , vol. 712, pp. 964–973, Apr. 2010.

[39] A. Majczyna and J. Madej, “Mass and Radius Determination for the Neutron Star in X-ray Burst Source 4U/MXB 1728-34,” , vol. 55, pp. 349–366, Dec. 2005.

[40] J. J. E. Kajava, J. Nättilä, O.-M. Latvala, M. Pursiainen, J. Poutanen, V. F. Suleimanov, M. G. Revnivtsev, E. Kuulkers, and D. K. Galloway, “The influence of accretion geometry on the spectral evolution during thermonuclear (type I) X-ray bursts,” , vol. 445, pp. 4218–4234, Dec. 2014.

[41] T. M. Braje, R. W. Romani, and K. P. Rauch, “Light Curves of Rapidly Rotating Neutron Stars,” , vol. 531, pp. 447–452, Mar. 2000.

[42] D. Psaltis and F. Özel, “Pulse Profiles from Spinning Neutron Stars in the Hartle-Thorne Approximation,” , vol. 792, p. 87, Sept. 2014.

[43] D. Page, “Surface temperature of a magnetized neutron star and interpretation of the ROSAT data. 1: Dipole fields,” , vol. 442, pp. 273–285, Mar. 1995.

[44] F. Özel, “Surface Emission Properties of Strongly Magnetic Neutron Stars,” , vol. 563, pp. 276–288, Dec. 2001.

[45] K. Boshkayev, “Non-rotating and slowly rotating stars in classical physics,” *International Journal of Mathematics and Physics*, vol. 5, no. 1, pp. 69–80, 2014.

[46] G. Meynet and A. Maeder, “Stellar evolution with rotation. V. Changes in all the outputs of massive star models,” , vol. 361, pp. 101–120, Sept. 2000.

[47] A. Maeder and G. Meynet, “The Evolution of Rotating Stars,” , vol. 38, pp. 143–190, 2000.

[48] J. B. Hartle, “Slowly Rotating Relativistic Stars. I. Equations of Structure,” , vol. 150, p. 1005, Dec. 1967.

[49] J. B. Hartle and K. S. Thorne, "Slowly Rotating Relativistic Stars. II. Models for Neutron Stars and Supermassive Stars," , vol. 153, p. 807, Sept. 1968.

[50] S. Chandrasekhar, *Ellipsoidal figures of equilibrium.* 1969.

[51] A. R. Choudhuri, *The physics of fluids and plasmas : an introduction for astrophysicists /.* Nov. 1998.

[52] R. Wavre, *Figures planetaires et geodesie.* 1932.

[53] T. W. Baumgarte, S. L. Shapiro, and M. Shibata, "On the Maximum Mass of Differentially Rotating Neutron Stars," , vol. 528, pp. L29–L32, Jan. 2000.

[54] J. P. Ostriker and J. W.-K. Mark, "Rapidly rotating stars. I. The self-consistent-field method," , vol. 151, pp. 1075–1088, Mar. 1968.

[55] R. Kippenhahn and A. Weigert, *Stellar Structure and Evolution.* 1990.

[56] A. Maeder, *Physics, Formation and Evolution of Rotating Stars.* 2009.

[57] L. Rayleigh, "On the Dynamics of Revolving Fluids," *Proceedings of the Royal Society of London Series A*, vol. 93, pp. 148–154, Mar. 1917.

[58] I. Hachisu, "A versatile method for obtaining structures of rapidly rotating stars," , vol. 61, pp. 479–507, July 1986.

[59] H. Komatsu, Y. Eriguchi, and I. Hachisu, "Rapidly rotating general relativistic stars. I - Numerical method and its application to uniformly rotating polytropes," , vol. 237, pp. 355–379, Mar. 1989.

[60] N. K. Glendenning, ed., *Compact stars : nuclear physics, particle physics, and general relativity*, 2000.

[61] V. Paschalidis and N. Stergioulas, "Rotating stars in relativity," *Living Reviews in Relativity*, vol. 20, p. 7, Nov. 2017.

[62] H. Spruit and E. S. Phinney, "Birth kicks as the origin of pulsar rotation," , vol. 393, pp. 139–141, May 1998.

[63] R. N. Manchester, G. B. Hobbs, A. Teoh, and M. Hobbs, "The Australia Telescope National Facility Pulsar Catalogue," , vol. 129, pp. 1993–2006, Apr. 2005.

[64] D. R. Lorimer, "Binary and Millisecond Pulsars," *Living Reviews in Relativity*, vol. 11, Nov. 2008.

[65] D. K. Galloway, M. P. Muno, J. M. Hartman, D. Psaltis, and D. Chakrabarty, "Thermonuclear (Type I) X-Ray Bursts Observed by the Rossi X-Ray Timing Explorer," , vol. 179, pp. 360–422, Dec. 2008.

[66] J. W. T. Hessels, S. M. Ransom, I. H. Stairs, P. C. C. Freire, V. M. Kaspi, and F. Camilo, “A Radio Pulsar Spinning at 716 Hz,” in *American Astronomical Society Meeting Abstracts #207*, vol. 207 of *American Astronomical Society Meeting Abstracts*, p. 209.07, June 2006.

[67] L. Burderi, A. Possenti, M. Colpi, T. Di Salvo, and N. D’Amico, “Neutron Stars with Submillisecond Periods: A Population of High-Mass Objects?,” , vol. 519, pp. 285–290, July 1999.

[68] A. Watts *et al.*, “Probing the neutron star interior and the Equation of State of cold dense matter with the SKA,” *PoS*, vol. AASKA14, p. 043, 2015.

[69] C. Cutler and L. Lindblom, “The effect of viscosity on neutron star oscillations,” , vol. 314, pp. 234–241, Mar. 1987.

[70] D. J. Hegyi, “The Damping of Differential Rotation in the Cores of Neutron Stars,” in *Eighth Texas Symposium on Relativistic Astrophysics* (M. D. Papagiannis, ed.), vol. 302 of *Annals of the New York Academy of Sciences*, p. 528, Dec. 1977.

[71] S. L. Shapiro, “Differential Rotation in Neutron Stars: Magnetic Braking and Viscous Damping,” , vol. 544, pp. 397–408, Nov. 2000.

[72] M. Shibata and K. ō. Uryū, “Simulation of merging binary neutron stars in full general relativity: Γ=2 case,” , vol. 61, p. 064001, Mar. 2000.

[73] G. B. Cook, S. L. Shapiro, and S. A. Teukolsky, “Spin-up of a rapidly rotating star by angular momentum loss - Effects of general relativity,” , vol. 398, pp. 203–223, Oct. 1992.

[74] N. D. Lyford, T. W. Baumgarte, and S. L. Shapiro, “Effects of Differential Rotation on the Maximum Mass of Neutron Stars,” , vol. 583, pp. 410–415, Jan. 2003.

[75] S. Weinberg, *Gravitation and Cosmology: Principles and Applications of the General Theory of Relativity.* July 1972.

[76] N. Aghanim *et al.*, “Planck 2018 results. VI. Cosmological parameters,” 2018.

[77] A. Masood-ul Alam, “Proof that static stellar models are spherical,” *General Relativity and Gravitation*, vol. 39, pp. 55–85, 01 2007.

[78] W. D. Arnett and R. L. Bowers, “A Microscopic Interpretation of Neutron Star Structure,” *Astrophys. J. Suppl.*, vol. 33, pp. 415–436, 1977.

[79] V. R. Pandharipande, “Dense neutron matter with realistic interactions,” *Nuclear Physics A*, vol. 174, pp. 641–656, Oct. 1971.

[80] V. R. Pandharipande, “Hyperonic matter,” *Nuclear Physics A*, vol. 178, pp. 123–144, Dec. 1971.

[81] J. B. Hartle and T. Dray, “Gravity: An Introduction to Einstein’s General Relativity,” *American Journal of Physics*, vol. 71, pp. 1086–1087, Oct. 2003.

[82] J. M. Bardeen, “A Variational Principle for Rotating Stars in General Relativity,” , vol. 162, p. 71, Oct. 1970.

[83] J. M. Bardeen, “Rapidly rotating stars, disks, and black holes.,” in *Black Holes (Les Astres Occlus)* (C. Dewitt and B. S. Dewitt, eds.), pp. 241–289, 1973.

[84] J. M. Bardeen and R. V. Wagoner, “Relativistic Disks. I. Uniform Rotation,” , vol. 167, p. 359, Aug. 1971.

[85] F. Galeazzi, S. Yoshida, and Y. Eriguchi, “Differentially-rotating neutron star models with a parametrized rotation profile,” , vol. 541, p. A156, May 2012.

[86] A. Bauswein and N. Stergioulas, “Semi-analytic derivation of the threshold mass for prompt collapse in binary neutron-star mergers,” , vol. 471, pp. 4956–4965, Nov. 2017.

[87] A. Komar, “Covariant Conservation Laws in General Relativity,” *Physical Review*, vol. 113, pp. 934–936, Feb. 1959.

[88] S. M. Carroll, *Spacetime and geometry. An introduction to general relativity.* 2004.

[89] S. Bonazzola and G. Maschio, “Models of Rotating Neutron Stars in General Relativity,” in *The Crab Nebula* (R. D. Davies and F. Graham-Smith, eds.), vol. 46 of *IAU Symposium*, p. 346, 1971.

[90] S. Bonazzola and J. Schneider, “An Exact Study of Rigidly and Rapidly Rotating Stars in General Relativity with Application to the Crab Pulsar,” , vol. 191, pp. 273–290, July 1974.

[91] O. Benhar, V. Ferrari, L. Gualtieri, and S. Marassi, “Perturbative approach to the structure of rapidly rotating neutron stars,” , vol. 72, p. 044028, Aug. 2005.

[92] K. Yagi, K. Kyutoku, G. Pappas, N. Yunes, and T. A. Apostolatos, “Effective no-hair relations for neutron stars and quark stars: Relativistic results,” , vol. 89, p. 124013, June 2014.

[93] F. Weber, ed., *Pulsars as astrophysical laboratories for nuclear and particle physics*, 1999.

[94] J. L. Friedman and N. Stergioulas, *Rotating Relativistic Stars.* Apr. 2013.

[95] J. L. Friedman, “Upper Limit on the Rotation of Relativistic Stars,” in *Millisecond Pulsars. A Decade of Surprise* (A. S. Fruchter, M. Tavani, and D. C. Backer, eds.), vol. 72 of *Astronomical Society of the Pacific Conference Series*, p. 177, 1995.

[96] J. L. Friedman, J. R. Ipser, and R. D. Sorkin, “Turning-point method for axisymmetric stability of rotating relativistic stars,” , vol. 325, pp. 722–724, Feb. 1988.

[97] K. Takami, L. Rezzolla, and S. Yoshida, “A quasi-radial stability criterion for rotating relativistic stars,” , vol. 416, pp. L1–L5, Sept. 2011.

[98] S. Bonazzola, J. Frieben, and E. Gourgoulhon, “Spontaneous symmetry breaking of rapidly rotating stars in general relativity: influence of the 3D-shift vector,” , vol. 331, pp. 280–290, Mar. 1998.

[99] E. Zhou, A. Tsokaros, L. Rezzolla, R. Xu, and K. Uryū, “Uniformly rotating, axisymmetric and triaxial quark stars in general relativity,” *Phys. Rev.*, vol. D97, no. 2, p. 023013, 2018.

[100] N. Stergioulas, T. A. Apostolatos, and J. A. Font, “Non-linear pulsations in differentially rotating neutron stars: mass-shedding-induced damping and splitting of the fundamental mode,” , vol. 352, pp. 1089–1101, Aug. 2004.

[101] I. A. Morrison, T. W. Baumgarte, and S. L. Shapiro, “Effect of Differential Rotation on the Maximum Mass of Neutron Stars: Realistic Nuclear Equations of State,” , vol. 610, pp. 941–947, Aug. 2004.

[102] C. Breu and L. Rezzolla, “Maximum mass, moment of inertia and compactness of relativistic stars,” , vol. 459, pp. 646–656, June 2016.

[103] N. Stergioulas and J. L. Friedman, “Comparing models of rapidly rotating relativistic stars constructed by two numerical methods,” , vol. 444, pp. 306–311, May 1995.

[104] S. Bonazzola, E. Gourgoulhon, M. Salgado, and J. A. Marck, “Axisymmetric rotating relativistic bodies: A new numerical approach for ’exact’ solutions,” , vol. 278, pp. 421–443, Nov. 1993.

[105] S. Bonazzola, E. Gourgoulhon, and J.-A. Marck, “Numerical approach for high precision 3D relativistic star models,” , vol. 58, p. 104020, Nov. 1998.

[106] S. M. C. Arnowitt, R.; Deser, “Dynamical structure and definition of energy in general relativity,” *Physical Review (Series I)*, vol. 116, 1959.

[107] E. Gourgoulhon, P. Haensel, R. Livine, E. Paluch, S. Bonazzola, and J. A. Marck, “Fast rotation of strange stars,” *Astron. Astrophys.*, vol. 349, p. 851, 1999.

[108] E. Gourgoulhon, P. Grandclément, J.-A. Marck, J. Novak, and K. Taniguchi, “LORENE: Spectral methods differential equations solver.” Astrophysics Source Code Library, Aug. 2016.

[109] T. Nozawa, N. Stergioulas, E. Gourgoulhon, and Y. Eriguchi, “Construction of highly accurate models of rotating neutron stars - comparison of three different numerical schemes,” , vol. 132, pp. 431–454, Nov. 1998.

[110] F. Weber, R. Negreiros, and P. Rosenfield, “Neutron star interiors and the equation of state of superdense matter,” 06 2007.

[111] E. R. Most, L. R. Weih, L. Rezzolla, and J. Schaffner-Bielich, “New Constraints on Radii and Tidal Deformabilities of Neutron Stars from GW170817,” *Physical Review Letters*, vol. 120, p. 261103, June 2018.

[112] A. Drago, A. Lavagno, G. Pagliara, and D. Pigato, “The scenario of two families of compact stars,” *The European Physical Journal A*, vol. 52, p. 40, Feb 2016.

[113] V. A. Ambartsumyan and G. S. Saakyan, “The Degenerate Superdense Gas of Elementary Particles,” , vol. 4, p. 187, Oct. 1960.

[114] D. Lonardoni, A. Lovato, S. Gandolfi, and F. Pederiva, “Hyperon Puzzle: Hints from Quantum Monte Carlo Calculations,” *Physical Review Letters*, vol. 114, p. 092301, Mar. 2015.

[115] D. Blaschke, H. Grigorian, and D. N. Voskresensky, “Cooling of neutron stars. Hadronic model,” , vol. 424, pp. 979–992, Sept. 2004.

[116] K. G. Elshamouty, C. O. Heinke, G. R. Sivakoff, W. C. G. Ho, P. S. Shternin, D. G. Yakovlev, D. J. Patnaude, and L. David, “Measuring the Cooling of the Neutron Star in Cassiopeia A with all Chandra X-Ray Observatory Detectors,” , vol. 777, p. 22, Nov. 2013.

[117] K. A. Maslov, E. E. Kolomeitsev, and D. N. Voskresensky, “Solution of the hyperon puzzle within a relativistic mean-field model,” *Physics Letters B*, vol. 748, pp. 369–375, Sept. 2015.

[118] M. H. Johnson and E. Teller, “Classical Field Theory of Nuclear Forces,” *Physical Review*, vol. 98, pp. 783–787, May 1955.

[119] H.-P. Duerr, “Relativistic Effects in Nuclear Forces,” *Physical Review*, vol. 103, pp. 469–480, July 1956.

[120] J. D. Walecka, “A theory of highly condensed matter.,” *Annals of Physics*, vol. 83, pp. 491–529, 1974.

[121] T. Klähn, D. Blaschke, S. Typel, E. N. E. van Dalen, A. Faessler, C. Fuchs, T. Gaitanos, H. Grigorian, A. Ho, E. E. Kolomeitsev, M. C. Miller, G. Röpke, J. Trümper, D. N. Voskresensky, F. Weber, and H. H. Wolter, “Constraints on the high-density nuclear equation of state from the phenomenology of compact stars and heavy-ion collisions,” , vol. 74, p. 035802, Sept. 2006.

[122] A. R. Bodmer, “Collapsed Nuclei,” , vol. 4, pp. 1601–1606, Sept. 1971.

[123] E. Witten, “Cosmic separation of phases,” , vol. 30, pp. 272–285, July 1984.

[124] J. A. et al., “Experimental and theoretical challenges in the search for the quark–gluon plasma: The star collaboration’s critical assessment of the evidence from rhic collisions,” *Nuclear Physics A*, vol. 757, no. 1, pp. 102 – 183, 2005. First Three Years of Operation of RHIC.

[125] S. Benić, D. Blaschke, D. E. Alvarez-Castillo, T. Fischer, and S. Typel, "A new quark-hadron hybrid equation of state for astrophysics. I. High-mass twin compact stars," , vol. 577, p. A40, May 2015.

[126] M. G. Alford, G. F. Burgio, S. Han, G. Taranto, and D. Zappalà, "Constraining and applying a generic high-density equation of state," , vol. 92, p. 083002, Oct. 2015.

[127] A. Drago and G. Pagliara, "The scenario of two families of compact stars," *The European Physical Journal A*, vol. 52, p. 41, Feb 2016.

[128] G. F. Burgio, A. Drago, G. Pagliara, H.-J. Schulze, and J.-B. Wei, "Are small radii of compact stars ruled out by GW170817/AT2017gfo?," *The Astrophysical Journal*, vol. 860, p. 139, jun 2018.

[129] H. Huber, F. Weber, M. K. Weigel, and C. Schaab, "Neutron Star Properties with Relativistic Equations of State," *International Journal of Modern Physics E*, vol. 7, pp. 301–339, 1998.

[130] H. Xiang and G. Hua, "Δ excitation and its influences on neutron stars in relativistic mean field theory," , vol. 67, p. 038801, Mar. 2003.

[131] Y. Chen, Y. Yuan, and Y. Liu, "Neutrino mean free path in neutron star matter with Delta isobars," *Phys. Rev.*, vol. C79, p. 055802, 2009.

[132] T. Schurhoff, S. Schramm, and V. Dexheimer, "Neutron stars with small radii – the role of delta resonances," *Astrophys. J.*, vol. 724, pp. L74–L77, 2010.

[133] M. Prakash, M. Prakash, J. M. Lattimer, and C. J. Pethick, "Rapid cooling of neutron stars by hyperons and Delta isobars," *Astrophys. J.*, vol. 390, p. L77, 1992.

[134] S. Weissenborn, I. Sagert, G. Pagliara, M. Hempel, and J. Schaffner-Bielich, "Quark Matter in Massive Compact Stars," , vol. 740, p. L14, Oct. 2011.

[135] B. e. a. Abbott, "Gw170817: Observation of gravitational waves from a binary neutron star inspiral," *Physical Review Letters*, vol. 119, 10 2017.

[136] B. P. Abbott, R. Abbott, T. D. Abbott, F. Acernese, K. Ackley, C. Adams, T. Adams, P. Addesso, R. X. Adhikari, V. B. Adya, and et al., "Multi-messenger Observations of a Binary Neutron Star Merger," , vol. 848, p. L12, Oct. 2017.

[137] A. Drago, G. Pagliara, S. Popov, S. Traversi, and G. Wiktorowicz, "The Merger of Two Compact Stars: A Tool for Dense Matter Nuclear Physics," *Universe*, vol. 4, p. 50, Mar. 2018.

[138] B. P. Abbott *et al.*, "Properties of the binary neutron star merger GW170817," *Phys. Rev.*, vol. X9, no. 1, p. 011001, 2019.

[139] E. Annala, T. Gorda, A. Kurkela, and A. Vuorinen, "Gravitational-Wave Constraints on the Neutron-Star-Matter Equation of State," *Physical Review Letters*, vol. 120, p. 172703, Apr. 2018.

[140] M. Hanauske, K. Takami, L. Bovard, L. Rezzolla, J. A. Font, F. Galeazzi, and H. Stöcker, "Rotational properties of hypermassive neutron stars from binary mergers," *Phys. Rev.*, vol. D96, no. 4, p. 043004, 2017.

[141] H. Falcke and L. Rezzolla, "Fast radio bursts: the last sign of supramassive neutron stars," , vol. 562, p. A137, Feb. 2014.

[142] A. Drago and G. Pagliara, "Merger of Two Neutron Stars: Predictions from the Two-families Scenario," , vol. 852, p. L32, Jan. 2018.

[143] A. Bauswein, O. Just, H.-T. Janka, and N. Stergioulas, "Neutron-star Radius Constraints from GW170817 and Future Detections," , vol. 850, p. L34, Dec. 2017.

[144] O. Gottlieb, E. Nakar, T. Piran, and K. Hotokezaka, "A cocoon shock breakout as the origin of the γ-ray emission in GW170817," , vol. 479, pp. 588–600, Sept. 2018.

[145] D. Lazzati, R. Perna, B. J. Morsony, D. Lopez-Camara, M. Cantiello, R. Ciolfi, B. Giacomazzo, and J. C. Workman, "Late Time Afterglow Observations Reveal a Collimated Relativistic Jet in the Ejecta of the Binary Neutron Star Merger GW170817," *Physical Review Letters*, vol. 120, p. 241103, June 2018.

[146] A. Drago, G. Pagliara, and S. Traversi, "A multi-messenger analysis of neutron star mergers," , vol. 89, p. 236, 2018.

[147] L. Rezzolla, B. Giacomazzo, L. Baiotti, J. Granot, C. Kouveliotou, and M. A. Aloy, "The Missing Link: Merging Neutron Stars Naturally Produce Jet-like Structures and Can Power Short Gamma-ray Bursts," , vol. 732, p. L6, May 2011.

[148] M. H. P. M. van Putten, G. M. Lee, M. Della Valle, L. Amati, and A. Levinson, "On the origin of short GRBs with extended emission and long GRBs without associated SN," , vol. 444, pp. L58–L62, Oct. 2014.

[149] L. Rezzolla and P. Kumar, "A Novel Paradigm for Short Gamma-Ray Bursts With Extended X-Ray Emission," , vol. 802, p. 95, Apr. 2015.

[150] B. D. Metzger, G. Martínez-Pinedo, S. Darbha, E. Quataert, A. Arcones, D. Kasen, R. Thomas, P. Nugent, I. V. Panov, and N. T. Zinner, "Electromagnetic counterparts of compact object mergers powered by the radioactive decay of r-process nuclei," , vol. 406, pp. 2650–2662, Aug. 2010.

[151] N. et al., "The Electromagnetic Counterpart of the Binary Neutron Star Merger LIGO/Virgo GW170817. III. Optical and UV Spectra of a Blue Kilonova from Fast Polar Ejecta," , vol. 848, p. L18, Oct. 2017.

[152] C. et al., “The Electromagnetic Counterpart of the Binary Neutron Star Merger LIGO/Virgo GW170817. II. UV, Optical, and Near-infrared Light Curves and Comparison to Kilonova Models,” , vol. 848, p. L17, Oct. 2017.

[153] C. et al., “The Electromagnetic Counterpart of the Binary Neutron Star Merger LIGO/Virgo GW170817. IV. Detection of Near-infrared Signatures of r-process Nucleosynthesis with Gemini-South,” , vol. 848, p. L19, Oct. 2017.

[154] D. Radice, A. Perego, F. Zappa, and S. Bernuzzi, “GW170817: Joint constraint on the neutron star equation of state from multimessenger observations,” *The Astrophysical Journal*, vol. 852, p. L29, jan 2018.

[155] A. Perego, D. Radice, and S. Bernuzzi, “AT 2017gfo: An Anisotropic and Three-component Kilonova Counterpart of GW170817,” *Astrophys. J.*, vol. 850, no. 2, p. L37, 2017.

[156] A. Drago and G. Pagliara, “Merger of two neutron stars: Predictions from the two-families scenario,” *The Astrophysical Journal*, vol. 852, p. L32, jan 2018.

[157] A. Drago and G. Pagliara, “Combustion of a hadronic star into a quark star: the turbulent and the diffusive regimes,” *Phys. Rev.*, vol. C92, no. 4, p. 045801, 2015.

[158] S. Fujibayashi, K. Kiuchi, N. Nishimura, Y. Sekiguchi, and M. Shibata, “Mass Ejection from the Remnant of a Binary Neutron Star Merger: Viscous-radiation Hydrodynamics Study,” , vol. 860, p. 64, June 2018.

[159] N. I. Shakura and R. A. Sunyaev, “Black holes in binary systems. Observational appearance.,” , vol. 24, pp. 337–355, 1973.

[160] J. Heyvaerts, S. Bonazzola, M. Bejger, and P. Haensel, “Luminosity of a quark star undergoing torsional oscillations and the problem of -ray bursts,” *Astronomy and Astrophysics*, vol. 496, 11 2008.

[161] L. Rezzolla, E. R. Most, and L. R. Weih, “Using Gravitational-wave Observations and Quasi-universal Relations to Constrain the Maximum Mass of Neutron Stars,” , vol. 852, p. L25, Jan. 2018.

[162] J. Heyvaerts, S. Bonazzola, M. Bejger, and P. Haensel, “Luminosity of a quark star undergoing torsional oscillations and the problem of -ray bursts,” *Astronomy and Astrophysics*, vol. 496, 11 2008.

[163] S. L. Shapiro and S. A. Teukolsky, *Black holes, white dwarfs, and neutron stars: The physics of compact objects*. 1983.

[164] C. Cuofano, S. Dall’Osso, A. Drago, and L. Stella, “Generation of strong magnetic fields by r-modes in millisecond accreting neutron stars: Induced deformations and gravitational wave emission,” *Phys. Rev. D*, vol. 86, p. 044004, Aug 2012.

[165] A. Rowlinson, P. T. O'Brien, B. D. Metzger, N. R. Tanvir, and A. J. Levan, "Signatures of magnetar central engines in short GRB light curves," , vol. 430, pp. 1061–1087, Apr. 2013.

[166] B. Margalit and B. D. Metzger, "Constraining the Maximum Mass of Neutron Stars From Multi-Messenger Observations of GW170817," *Astrophys. J.*, vol. 850, no. 2, p. L19, 2017.

[167] J. D. Kaplan, C. D. Ott, E. P. OConnor, K. Kiuchi, L. Roberts, and M. Duez, "THE INFLUENCE OF THERMAL PRESSURE ON EQUILIBRIUM MODELS OF HYPERMASSIVE NEUTRON STAR MERGER REMNANTS," *The Astrophysical Journal*, vol. 790, p. 19, jun 2014.